Schweizerische Eidgenossenschaft
Confédération suisse
Confederazione Svizzera
Confederaziun svizra

Federal Department of the Environment, Transport, Energy and Communications DETEC

Swiss Federal Office of Energy SFOE
Energy Research and Cleantech Division

Final report dated 10.02.2023

RESEMO, Reservoir sedimentation, management and operation at the case study reservoir Solis

Stauraumverlandung, -management und -betrieb am Fallbeispiel Stausee Solis

Source: ©VAW 2019

Versuchsanstalt für Wasserbau,
Hydrologie und Glaziologie

Date: 10.02.2023

Location: Bern

Publisher:
Swiss Federal Office of Energy SFOE
Energy Research and Cleantech
CH-3003 Bern
www.bfe.admin.ch

Co-financing:
Elektrizitätswerk der Stadt Zürich (ewz)
Albulastrasse 110, 7411 Sils i.D.
www.ewz.ch

Subsidy recipients:
ETH Zürich
Versuchsanstalt für Wasserbau, Hydrologie und Glaziologie (VAW)
Hönggerbergring 26
CH-8093 Zürich
www.vaw.ethz.ch

Authors:
Dr. Ismail Albayrak, ETH Zürich, albayrak@vaw.baug.ethz.ch
Mohammadreza Maddahi, ETH Zürich, maddahim@vaw.baug.ethz.ch
Prof. Dr. Robert Boes, ETH Zürich, boes@vaw.baug.ethz.ch

SFOE project coordinators:
Dr. Michael Moser, michael.moser@bfe.admin.ch
Dr. Klaus Jorde, klaus.jorde@kjconsult.net

SFOE contract number: SI/501785-01

Zusammenfassung

Speicher und Reservoire leisten einen wichtigen Beitrag zur Wasserbewirtschaftung, z.B. zur Stromerzeugung mittels Wasserkraftnutzung, werden aber durch Speicherverlandung mittel- bis langfristig beeinträchtigt. Sedimentumleitstollen (SBT) stellen eine wirkungsvolle Massnahme gegen die Speicherverlandung dar. Ihre Effizienz hängt jedoch weitgehend vom Speicherbetrieb ab. Am Solis-Stausee im Kanton Graubünden wurde 2012 ein SBT in Betrieb genommen, um das kontinuierliche Fortschreiten des Verlandungskörpers in Richtung Sperre zu stoppen. Dieses Forschungsprojekt zielt darauf ab, die Hydraulik, Sedimenttransport-, Erosions- und Ablagerungsprozesse im Solis-Reservoir zu untersuchen, um die Wechselbeziehung zwischen diesen Parametern zu analysieren und möglicherweise Optimierungsmaßnahmen hinsichtlich der Wirksamkeit des SBT bei der Sedimentdurchleitung abzuleiten.

Im Oktober 2018, August 2019, September 2020, bzw. November 2021 wurde je eine Feldmesskampagne im Speicher Solis durchgeführt. 3D-Strömungsgeschwindigkeiten und die Bathymetrie wurden mit einem Acoustic Doppler Current Profiler (ADCP) in eng beieinander liegenden Querprofilen entlang des Stausees vermessen. An verschiedenen Stellen im Stausee wurden Schwebstoffe und Sedimentablagerungen entnommen. Bathymetrische Daten aus den Messkampagnen sowie Betriebsdaten inkl. Bathymetriemessungen des Betreibers von 2018 bis 2021 wurden analysiert und verglichen.

Die Auswirkungen von zwei ein- bzw. fünfjährlichen Hochwassern im Jahr 2019 und eines weiteren einjährlichen Hochwassers im Jahr 2020 auf die Sedimentation des Reservoirs wurden messtechnisch erfasst und die Auswirkungen verschiedener SBT- und Stauraumbetriebsarten (in Bezug auf den Reservoirwasserspiegel) auf den SBT-Bypass-Wirkungsgrad bewertet. Zu diesem Zweck wurden die Sedimentbilanzen und der jährliche Bypass-Wirkungsgrad für die drei Zeiträume zwischen den Messkampagnen berechnet. Zur Berechnung der Sedimentbilanz wurden die zu- und abfließenden Sedimentmengen mit installierten Trübungsmessgeräten und Geophonen gemessen und unter Verwendung bekannter Sedimenttransportformeln sowie unter Anwendung von Annahmen zur Abdeckung eines Bereichs von Partikelgrößen geschätzt.

Die Ergebnisse zeigen, dass die für die Berechnung der Sedimentbilanz getroffenen Annahmen gut mit den gemessenen Veränderungen der Bathymetrie übereinstimmen, mit Abweichungen von weniger als 15% für die Zeiträume von 2018 bis 2019 und 2020 bis 2021. Für die relativ trockene Periode von 2019 bis 2020 betrug die Differenz 28 %, was für Studien zur Sedimentforschung immer noch akzeptabel ist. Von Oktober 2018 bis November 2021 wurden netto knapp 50'000 m^3 Sedimente im Stausee abgelagert, während durch den Betrieb des SBT bei niedrigem Reservoirwasserspiegel ein Gesamtvolumen von gut 200'000 m^3 umgeleitet wurde. Diese ausgetragenen Sedimentmengen hätten den Stauseegrund um rund 1 m angehoben. Die Ergebnisse zeigen, dass der Wirkungsgrad des Sedimentumleitstollens von 17% ohne SBT auf 88% mit dem SBT im Betrieb angestiegen ist. Es wurde festgestellt, dass der Wirkungsgrad des SBT-Bypasses in hohem Maße von der Höhe des Wasserspiegels des Stausees abhängt. Für hohe Wirkungsgrade zwischen 70 % und 250 % sollte der Mindest-*Wasserspiegel* um 813 müM liegen. Der Betrieb des SBT mit einem Mindest-*Wasserspiegel* von mehr als 814 müM wird nicht empfohlen, da der Wirkungsgrad unter 20 % abfällt. Ein Stauspiegel von 816 müM entspricht dem Absenkziel des Reservoirs, bei dem der Betrieb der an den Speicher Solis angeschlossenen Wasserkraftwerke noch möglich ist. Diese Ergebnisse zeigen, dass der SBT vom Typ B mit einem Einlaufbauwerk im Speicher unter Druckabfluss einerseits die Sedimentation stoppen kann, andererseits aber sogar zu einer Erhöhung des aktiven Speichervolumen führen kann, sofern er unter optimalen Bedingungen betrieben wird.

Der Betreiber hat die Geschiebeleitwand am Einlaufbauwerk des SBT Anfang 2021 entfernt. Die Entfernung der Leitwand könnte die Sedimentation in Zone 3 zwischen dem SBT-Einlass und der Talsperre erhöhen und den Wirkungsgrad des SBT verringern. Daher werden weitere Studien empfohlen, um die Auswirkungen der Entfernung der Leitwand auf die Verlandung des Solis-Stausees zu bewerten.

Die Ergebnisse dieses Projekts dienen dem verbesserten Betrieb des SBT und Reservoirs im Hinblick auf die Abnahme der Verlandungsraten und einer längeren Nutzungsdauer des Speichers Solis. Darüber hinaus sollen sie einen Beitrag zur nachhaltigen Nutzung der Wasserkraft, zur Verbesserung des Sedimentmanagements an Stauseen und zur Umsetzung der Schweizer Energiestrategie 2050 leisten.

Résumé

Les réservoirs permettent l'exploitation des ressources d'eau, par exemple du potentiel hydroélectrique, mais ils sont exposés à la sédimentation à moyen et à long terme. Les galeries de dérivation des sédiments (SBT) sont une mesure efficace contre la sédimentation des réservoirs. Cependant, leur efficacité dépend en grande partie de l'exploitation des réservoirs. Une SBT a été mise en service en 2012 au réservoir de Solis dans le canton des Grisons pour arrêter la progression continue du corps d'aggradation des sédiments vers le barrage. Ce projet de recherche vise à étudier l'hydraulique, le transport des sédiments, ainsi que les processus d'érosion et d'alluvionnement dans le réservoir de Solis pour analyser l'interrelation entre ces paramètres et potentiellement en déduire des mesures d'optimisation en termes d'efficacité de contournement des sédiments par la SBT.

Quatre campagnes de mesures sur le terrain ont été menées en octobre 2018, août 2019, septembre 2020 et novembre 2021. Les vitesses d'écoulement en 3D et la bathymétrie ont été mesurées avec un profileur de courant Doppler acoustique (ADCP) sur des sections transversales étroitement espacées le long du réservoir de Solis. Les sédiments en suspension et les dépôts de sédiments ont été échantillonnés à différents endroits du réservoir. Les données bathymétriques des campagnes ainsi que les données de l'exploitation de 2018 à 2021 y inclus des données bathymétriques de l'exploitant ont été analysées et comparées.

Les effets de deux crues avec des périodes de retour d'un an et de cinq ans en 2019 et d'une autre crue avec une période de retour d'un an en 2020 sur la sédimentation du réservoir ont été capturé et les effets des différents modes de fonctionnement du SBT et du réservoir (en termes de niveau d'eau du réservoir) sur l'efficacité de dérivation de la SBT ont été évalués. Pour ce faire, les bilans sédimentaires et l'efficacité annuelle de la dérivation du réservoir ont été calculés pour les trois périodes entre les campagnes de mesures sur le terrain. Pour calculer le bilan sédimentaire, les volumes de sédiments entrants et sortants ont été mesurés à l'aide de turbidimètres et de géophones installés et estimés en utilisant des équations de transport de sédiments bien connues et en appliquant des hypothèses pour couvrir une gamme de tailles de particules.

Les résultats montrent que les hypothèses faites pour les calculs du bilan sédimentaire sont en bon accord avec les changements de bathymétrie, avec des différences inférieures à 15% pour les périodes de 2018 à 2019 et 2020 à 2021. Pour la période relativement sèche de 2019 à 2020, la différence était de 28%, ce qui est encore acceptable pour les études de recherche sur les sédiments. D'octobre 2018 à novembre 2021, un volume net d'environ 50'000 m^3 de sédiments s'est déposé dans le réservoir, tandis que le fonctionnement du SBT à faible niveau d'eau a permis de contourner un volume total d'environ 200'000 m^3. Ces volumes de sédiments contournés auraient pu augmenter le niveau du lit du réservoir de 1 m. Les résultats montrent que l'efficacité de la dérivation du réservoir

est passée de 17% sans SBT à 88% avec la SBT en fonctionnement. Les résultats soulignent que l'efficacité de la dérivation par la SBT dépend fortement du niveau d'eau du réservoir pendant l'exploitation de la SBT. Pour des valeurs d'efficacité élevées entre 70% et 250%, le niveau d'eau minimum du réservoir devrait être autour de 813 m d'altitude. Le fonctionnement de la SBT avec un niveau d'eau minimum de plus de 814 m d'altitude n'est pas recommandé, car l'efficacité tombe à moins de 20%. Le niveau d'eau de 816 m d'altitude correspond au niveau de rabattement du réservoir auquel les centrales hydroélectriques alimentées par le réservoir de Solis peuvent encore être exploitées. Ces résultats indiquent qu'une SBT de type B avec prise d'eau dans le réservoir ne se contente pas seulement d'arrêter la sédimentation, mais peut même aider à regagner le volume actif du réservoir, s'il fonctionne dans des conditions optimales d'exploitation du réservoir.

L'exploitant a démonté le mur de guidage du charriage au début de 2021. Le retrait du mur de guidage peut augmenter la sédimentation dans la zone 3 entre l'entrée de la SBT et le barrage et diminuer l'efficacité de la SBT. Par conséquent, d'autres études sont nécessaires pour évaluer les effets de la suppression du mur de guidage sur la sédimentation du réservoir Solis.

Les résultats de ce projet contribuent à l'amélioration des régimes d'exploitation d'une SBT et du réservoir en ce qui concerne la réduction des taux de l'ensablement et la prolongation de la durée de vie du réservoir. En outre, ils devraient contribuer à une utilisation durable de l'énergie hydraulique, fournir une base pour améliorer la gestion des sédiments dans les réservoirs et à la réalisation de la Stratégie Energétique Suisse 2050.

Summary

Reservoirs allow to make better use of water resources, e.g. to produce electricity from hydropower, but are subject to sedimentation. Sediment Bypass Tunnels (SBTs) are effective measures against reservoir sedimentation for certain types of reservoirs. However, their efficiency largely depends on reservoir operation. A SBT at the Solis reservoir in the canton of Grisons was commissioned in 2012 to stop the continuous progression of the sediment aggradation body towards the dam. This research project aims at investigating the hydraulics, sediment transport, erosion and deposition processes in the Solis reservoir to analyze the interrelation between these parameters and potentially deduce optimization measures in terms of sediment bypassing efficiency through the SBT.

Four field measurement campaigns were conducted in the Solis reservoir in October 2018, August 2019, September 2020 and Novermber 2021, respectively. 3D flow velocities were measured and bathymetry was mapped using an Acoustic Doppler Current Profiler (ADCP) at densely spaced cross-sections along the reservoir. Suspended sediments and sediment deposits were sampled at different locations in the reservoir. Bathymetric data from the campaigns as well as the operator's data from 2018 to 2021 were analyzed and compared. The effects of two floods with one-year and five-year return periods in 2019 and a one-year return period flood in 2020 on the reservoir sedimentation were captured and the effects of different SBT and reservoir operation modes (in terms of reservoir water level during SBT operation) on the SBT bypass efficiencies were evalauted. To do so, sediment balances and annual reservoir bypass efficiency were calculated for the three periods between the field campaigns. To calculate sediment balances, in- and outflow sediment volumes were measured with installed turbidimeters and geophones and estimated by using well-known sediment transport equations and applying assumptions to cover a range of particle sizes.

The results show that the assumptions made for sediment balance calcualtions are in a good aggreement with the bathymetry changes, with differences of less than 15% for periods from 2018 to 2019 and 2020 to 2021. For the relatively dry period from 2019 to 2020, the difference was 28%,

which is still acceptable for sediment research studies. From October 2018 to November 2021, a net volume of almost 50'000 m^3 of sediments was deposited in the reservoir, while running the SBT at low reservoir water level allowed to bypass a total volume of some 200'000 m^3. These bypassed volumes of sediments could have led to an increase of the reservoir bed level by 1 m. The results reveal that the reservoir bypass efficiency has increased from 17% without a SBT to 88% with the SBT in operation. It was found that the SBT bypass efficiency is highly dependent on the reservoir water level during SBT operation. For high bypassing efficiencies between 70% and 250%, the minimum water level *WL* should be around 813 m asl. Operation of the SBT with a minimum *WL* above 814 m asl is not recommended, because the bypassing efficiency drops to less than 20%. A *WL* of 816 m asl corresponds to the reservoir drawdown level at which the hydropower plants fed from the Solis reservoirs can still be operated. These results indicate that a type B SBT with intake in the reservoir under submerged flow such as in Solis enables to stop sedimentation on the one hand, but can even increase the active reservoir storage on the other hand, if it is operated under optimal conditions with sufficiently low reservoir *WL*.

The operator removed the guiding wall at the SBT intake at the beginning of 2021. The removal of the guiding wall may increase sedimentation in zone 3 between the SBT inlet and the dam and decrease the SBT efficiency. Therefore, more studies are required to evaluate the effects of the bedload guiding wall on sedimentation of the Solis reservoir.

The findings of this project contribute to improved SBT and reservoir operation regimes with regard to decreasing the sedimentation rates and extending the reservoir lifetime. Furthermore, they are expected to contribute to sustainable use of hydropower, to provide a basis for improving sediment management at reservoirs, and to the realization of the Swiss Energy Strategy 2050.

Main findings

- **Solis SBT bypassed around 200'000 m^3 of sediments around the reservoir to the downstream river reach during the study period between 2018 and 2021.**
- **The sediment bypass efficiency increased from 17% without SBT to 88% with the SBT during the study period, resulting in a considerable extension of the Solis reservoir life.**
- Reservoir operation has a high impact on the bypass efficiency of the type B Solis SBT.
- **The reservoir water level of 813 m asl results in high bypass efficiencies of the Solis SBT of up to 250%.**
- A reservoir water level above 814 m asl is not recommended for SBT operation because of low bypass efficiencies of less than 20%.
- **If operated in an optimal way, the efficiency of a type B SBT can be similar to those of type A SBTs.**
- Accurate and continuous measurement of suspended sediment and bedload transport as well as operational, hydraulic and annual bathymetry data are important to better understand sediment transport, erosion and deposition processes in reservoirs and to determine optimal operational conditions of reservoir and SBT.
- The study results indicate that SBTs are effective measures against reservoir sedimentation.
- The effect of the guiding wall removal on the bypass efficiency of the Solis SBT should be investigated in future.

Contents

Abbreviations

ADCP	Acoustic Doppler Current Profiler
BE	Bypass Efficiency
BFE	Swiss Federal Office of Energy
BL	Bed Load
DEM	Digital Elevation Model
DF	Desilting Factor
DGPS	Differential Global Positioning System
ewz	Electric Power Stations of the city of Zurich
FOEN	Swiss Federal Office for the Environment
GCD	Geomorphic Change Detection
HPP	Hydropower Plant
LD	Laser Diffraction
LISST	Laser In-Situ Scattering and Transmissometry
PSD	Particle Size Distribution
RTK-GPS	Real Time Kinetic Global Positioning System
SBT	Sediment Bypass Tunnel
SFOE	Swiss Federal Office of Energy
SPGS	Swiss Plate Geophone Sensor
SSC	Suspended Sediment Concentration
SSL	Suspended Sediment Load
TIN	Triangular Irregular Network
TL	Total Load
UTM	Universal Transverse Mercator
VAW	Laboratory of Hydraulics, Hydrology and Glaciology
WL	Water Level
WSL	Swiss Federal Institute for Forest, Snow and Landscape Research

1 Introduction

1.1 Background information and current situation

Sedimentation is a major issue for many reservoirs, particularly those with glaciated catchments. Several reservoirs in the Swiss Alps have large sedimentation rates. Reservoir sedimentation causes numerous operational problems and may threaten the envisaged service life in severe cases like the Solis Reservoir in the canton of Grisons. From 1986 to 2008, less than 50% of the reservoir storage capacity was lost due to reservoir sedimentation (Figure 1). To reduce the sedimentation problem in this reservoir, a Sediment Bypass Tunnel (SBT) was constructed and commissioned in 2012. SBTs are considered as an efficient and environmentally compatible sediment routing technology. In general, their performance can be quantified by the bypass efficiency (*BE*, expressed by the ratio of bypassed sediment volume to inflow sediment volume) or by the reservoir lifetime enhancement (expressed by the prolongation of reservoir lifetime, which is defined as the ratio of reservoir capacity to mean annual sediment load effectively depositing in the reservoir). Albayrak et al. (2019) and Boes et al. (2021) reported that the *BE* values of Solis, Pfaffensprung, Runcahez and Palagnedra SBTs are 31, 98, 83 and 95%, respectively. The former states that the *BE* depends on various parameters such as hydrology, sediment transport characteristics, design, and operating conditions of the reservoir and the SBT. Sediment transport processes within a reservoir are governed by bed shear stresses, which are controlled by the reservoir water level and the local velocities. Therefore, reservoir operation and management are of prime importance to achieve higher sediment bypass efficiencies and hence reduce sedimentation.

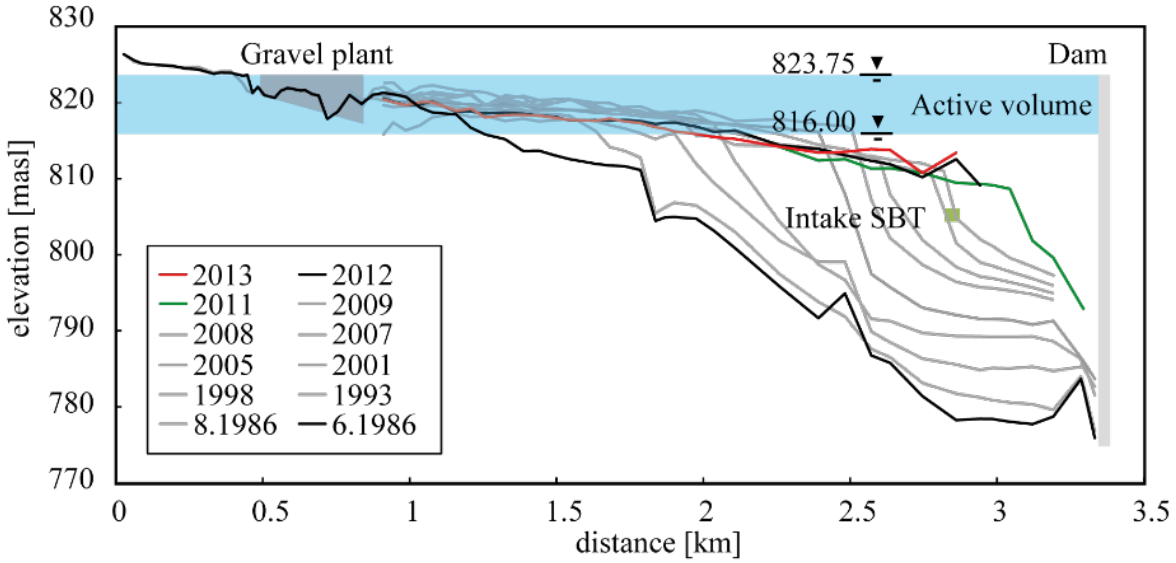

Figure 1: Temporal and spatial evolution of the aggradation body since the commissioning of the Solis Reservoir in 1986 and location of the SBT intake structure put into operation in 2012 (Müller-Hagmann, 2017).

1.2 Purpose of the project

In this project, we aim at a better understanding of the nexus between reservoir sedimentation and management and at determining optimal operating conditions. To achieve these goals, we conducted field measurements in the Solis Reservoir to acquire important data of bathymetry, velocity, and sediment transport between 2018 - 2021. The project makes additional use of bed load measurements

using a Swiss Plate Geophone Sensor (SPGS) installed in the SBT, being part of another SFOE project conducted by VAW (contract number SI/501609-01).

1.3 Objectives

The objectives of the present field study at the Solis Reservoir are to:

- use various techniques based on acoustic, geophone and laser to measure velocities, bathymetry, bed load transports, and suspended sediment in the Solis Reservoir and SBT,
- acquire and provide hydraulic data for numerical modelling,
- better understand sediment transport and deposition processes in reservoirs under different operation conditions,
- quantify the impacts of reservoir operation on sedimentation and SBT efficiency,
- contribute to the optimization of reservoir operation and sustainable use of hydropower,
- provide a basis for improving sediment management at reservoirs,
- assess the effects of reservoir sedimentation in a Swiss reservoir with an SBT,
- contribute to the realization of the Swiss Energy Strategy 2050.

In contrast to many studies worldwide, the present project investigates reservoir sedimentation processes and management in a reservoir equipped with an SBT. The findings will give an insight into the bypass efficiency of the SBT affected by the reservoir operation and will provide a basis to further improve it by an optimized operation management.

2 Description of facility

2.1 Solis Reservoir

The Solis Reservoir located in the Swiss Alps, commissioned in 1986, is fed by the Albula and Julia Rivers and by the tailrace water of the hydropower plant (HPP) Tiefencastel (Figure 2). Initially, the total storage volume was 4.07×10^6 m^3, with an active volume of 1.46×10^6 m^3. The stored water is turbined in the HPPs Sils and Rothenbrunnen (design discharge of 22 and 25 m^3/s, respectively) before being released into the Albula and Hinterrhein Rivers, respectively. After twenty-two years of operation, 50% of the reservoir storage capacity was lost due to reservoir sedimentation (Müller-Hagmann, 2017). By reservoir drawdowns in 2006 and 2008 the settled material was partially relocated from the active to the dead storage. Assuming a constant aggradation rate, the hydropower generation would have been increasingly affected, and without the mentioned sediment relocation actions the aggradation body was expected to have reached the dam by 2012, which would have endangered the operational safety of the dam (Auel et al., 2011).

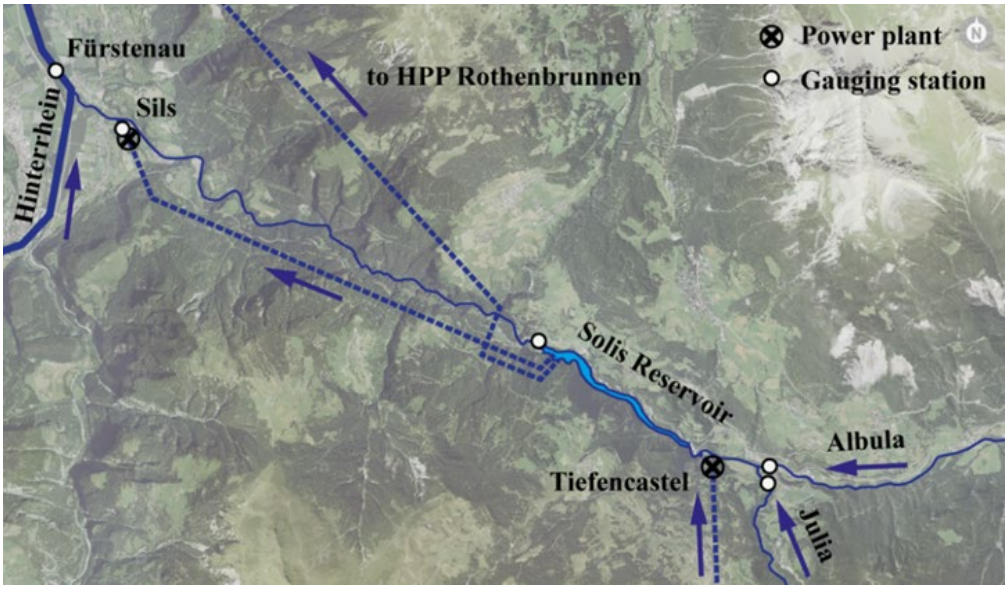

Figure 2: Overview of the Solis Reservoir, the HPP scheme and the gauging stations of the FOEN and ewz (based on map.geo.admin.ch, Müller-Hagmann, 2017)

2.2 Solis sediment bypass tunnel

To reduce the further progression of the sediment aggradation body towards the dam, and to restore the interrupted sediment transport in the downstream river system, a one-kilometer long SBT was constructed and commissioned in 2012 (Figure 3). More details are given by Oertli and Auel (2015). SBTs in general and the Solis SBT in particular have been a research focus at VAW in terms of tunnel hydraulics, sediment transport and hydroabrasive wear of SBT inverts for more than ten years (Auel, 2014; Facchini, 2017; Müller-Hagmann, 2017; Demiral Yüzügüllü, 2021).

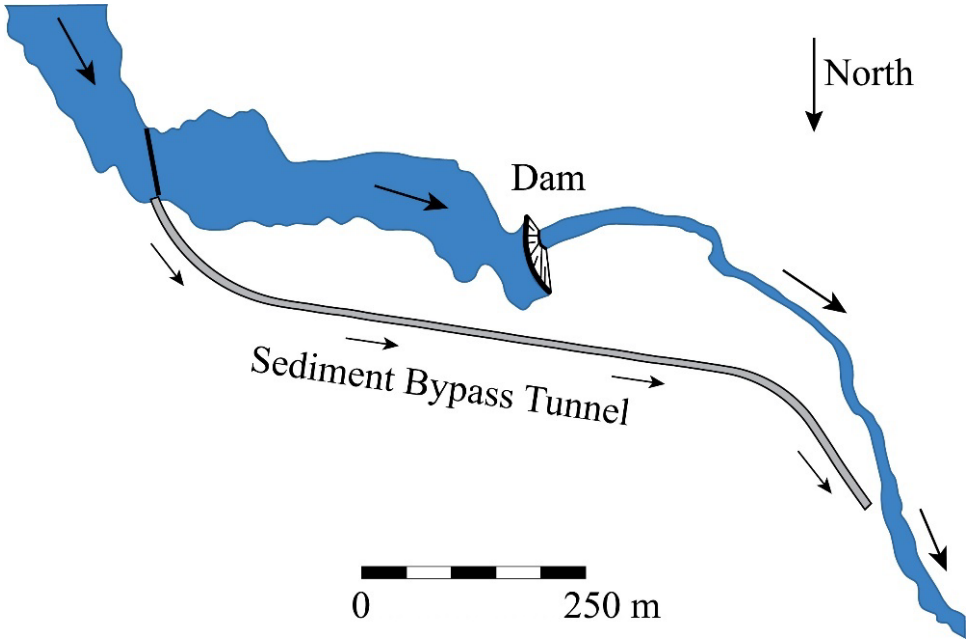

Figure 3: Plan view of Solis SBT.

3 Procedures and methodology

To reach the goals of the project, (i) sediment properties and suspended sediment concentrations (SSC) were determined at different discharges along the reservoir, (ii) sediment transport and deposition were quantified at different locations of the reservoir, (iii) flow velocities as well as bed shear stress along the reservoir were calculated, and (iv) volumes of incoming sediments to the reservoir and outgoing sediments from the SBT were calculated within a period of four years (2018 - 2021).

These procedures were conducted using different devices, computational analyses, and assumptions. In the following, first the description of the instruments is presented, the analytical equations are presented, and the classification of the sediments and the methods to calculate inflow and outflow sediments to/from the reservoir are presented.

3.1 Methodology

3.1.1 Instruments

Acoustic Doppler Current Profiler (ADCP) for hydraulic and bathymetry monitoring

Reservoir bathymetry and 3D flow velocities were measured using a high resolution ADCP mounted on a remote-control boat (Figure 4a). A Differential Global Positioning System (DGPS) was used to measure ADCP positions in 2018. The GPS system was replaced by a new Real-time Kinematic GPS (RTK-GPS) in 2019, 2020 and 2021 campaigns (Figure 4b). The measurement results show that the RTK-GPS provides more accurate measurements of altitude in addition to longitude and latitude positions. The types of the ADCP and boat are River Pro 1200 kHz including a piston style four-beam transducer with a 5th independent 600 kHz vertical beam and Q-Boat supplied by Teledyne Marine, USA, respectively. The ADCP enables to measure reservoir water depths up to 160 m and velocities up to 25 m below the water surface. From the velocity fields, the bed shear stresses are determined along the reservoir at several cross-sections.

During the measurements, the water level (*WL*) fluctuated, and differed in each field campaign. It is assumed that the *WL* was horizontal along the reservoir and hence the operator data of *WL* were used to correct any errors from the RTK-GPS measurements. The bed elevations of areal measurement points can be calculated by subtracting the measured *WL* from the measured ADCP water depths. With the periodic bathymetric measurements, the sediment erosion and deposition volumes affected by the reservoir and SBT operations were determined from the differences in the bed elevations. For each measurement campaign, the bathymetry was obtained from a point based triangular irregular network (TIN) using ArcGIS. The method of interpolation to form these triangles is the delaunay triangulation method. With this method, the minimum interior angle of all triangles was maximized and long and thin triangles were avoided as much as possible. For calculation of erosion/deposition volumes, the TINs were converted into rasters. Then, the volume and depth changes for different measurement periods were calculated by subtracting the values of pixels. The errors of bathymetry measurements were stemmed from two sources. The first source of error consists in *WL* fluctuations. This error was determined as the maximum change of water level between each reading. The second error was caused by the ADCP vertical beam accuracy, which corresponds to ± 1% of the water depth. (http://www.teledynemarine.com/Lists/Downloads/riverpro_datasheet_lr.pdf). Therefore, the total error varied along the reservoir and during the measurements. To account for these errors, a Geomorphic Change Detection (GCD) tool was used to calculate the volumes of erosion/deposition sediments.

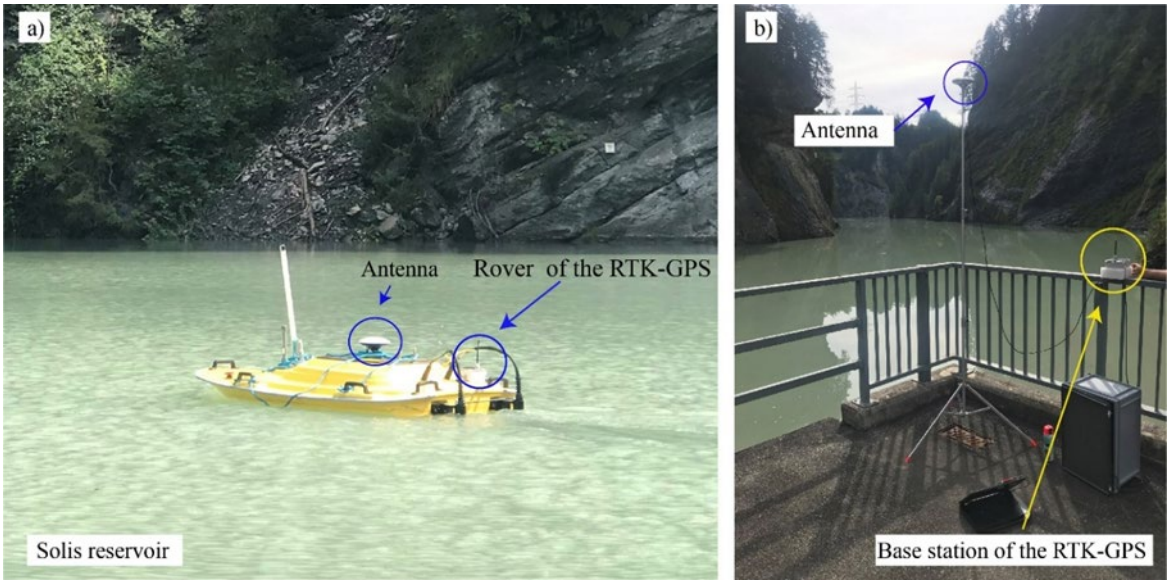

Figure 4: a) Remote controlled Q-Boat housing the ADCP and RTK-GPS and b) base station of the RTK-GPS.

River bottom sediment sampler, Niskin bottle sampler, and Laser in-situ Scattering and Transmissometry (LISST) for sediment monitoring

During four field measurement campaigns in 2018, 2019, 2020 and 2021 samples of suspended and deposited sediment were collected at various water depths and several locations along the reservoir using a Niskin bottle sampler and a river bottom sediment sampler, respectively (Figure 5a and b). The collected bottles and bed samples in 2018 field measurement campaign are presented in the Appendix. At the sediment sampling locations, the flow velocities were continuously measured up to 10 - 15 minutes at the middle of the corresponding cross-section. Collected suspended and deposited sediment samples were analysed in the laboratory to determine *SSC* and Particle Size Distribution (*PSD*). Based on particle sizes collected at each location, three methods were used to obtain *PSD* in laboratory. The first method was dry or wet sieving of dried residuals which is mainly for sand and coarser particles. In these methods, the percentages of particle mass passing through a series of sieves with decreasing mesh sizes was determined by weighing. Sieving was considered as the primary technique for particles larger than 62 µm, while wet sieving was possible down to 20 µm (Felix, 2017). The third method is the laser diffraction (LD). *PSD*s were obtained from light intensities scattered at various angles. Smaller particles caused scattering at larger angles. The LD has been widely used in laboratories since the 1970 to characterize powders (e.g., cement). In this study, a stationary laser diffractometer (LA-950 manufactured by Horiba) at the Geotechnical Institute of ETH Zürich was used to determine *PSD* of particles smaller than 3 mm. This instrument has a nominal size-measuring range of 0.01 µm to 3 mm.

The mineralogical composition and hardness of the sediment particles in the Solis reservoir were analysed in the laboratory in the scope of our parallel BFE project on sediment bypass tunnels (SI/501609-01).

In addition to the Niksin bottle sampler, a LISST instrument was also used in the 2021 field campaign to measure *SSC*. LISST can measure a dense *SSC* profile in the water column. The construction of LISST instruments and the mathematical approach used in the data treatment and analysis are described in Agrawal and Pottsmith (2000). The LISST model used in this measurement was LISST-100X with a typical range from 1 – 800 mg/l for a standard 50 mm optical path (actual range depends

on grain size) (https://www.sequoiasci.com/product/lisst-100x/). The effective upper limit of SSC to be measured by the LISST-100X depends on the *PSD* and can lie well above 800 mg/l for sand (Felix 2017).

Swiss Plate Geophone System (SPGS) for bedload transport monitoring

The SPGS is a robust device allowing for continuous bedload transport monitoring in rivers and torrents with high flow velocities. The SPGS is submersible and consists of an elastically bedded steel plate mounted flush to the channel bed. The plate is equipped with a geophone sensor (GS-20DX, manufactured by “Geospace Technologies”, Houston, Texas), encased by a waterproof aluminium housing. The length, width and thickness of the plate corresponding to streamwise, transversal and vertical directions are 36 cm, 50 cm, and 1.5 cm, respectively. The sensor does not directly measure bedload transport, but records the vibration signal of the geophone plate, i.e., the vertical plate oscillations induced by impingement of passing particles (Turowski et al., 2013; Wyss, 2016). The minimum threshold detection particle size amounts to approximately d = 10 - 20 mm (Morach, 2011; Rickenmann et al., 2012; Wyss, 2016; Wyss et al., 2016a, b; Koshiba et al., 2018). The number of impulses ‘Imp’ above the threshold value correlates linearly with bedload mass m (Rickenmann et al., 2012). The linear relation coefficient K_b between the number of impulses and bedload mass is used to estimate the sediment mass transport rate and is defined as:

$$q_b = \frac{1}{K_b}\mathrm{Imp} \qquad \text{[kg/s/m]} \qquad (1)$$

where q_b is the unit mass bedload transport rate (kg/s/m), Imp is the unit impulse rate (1/s/m), and K_b is a calibration coefficient (1/kg).

A 15m-long SGPS with 30 steel plates of which 15 are equipped with geophones was installed by WSL in River Albula close to the official BAFU gauging station for bedload transport monitoring. The calibration of the SPGS was conducted and the calibration coefficient of K_b = 11.8 was provided by Rickenmann et al. (2020) for d > 9.5 mm.

Another SPGS with 8 geophones was installed with an angle of 10° against the flow direction at the outlet of the SBT to monitor bedload transport in the SBT (Figure 5c). Details of the calibration of these geophones are presented in another parallel BFE project on sediment bypass tunnels (SI/501609-01). Here, the summary of calibration is presented.

The calibration coefficient K_b is affected by signal interference induced by impact overlaps related to high sediment transport rates (Wyss, 2016; Dhont et al., 2017; Koshiba et al., 2018). The probability of this interference can be determined by z_p, defined as the ratio of the total signal envelope time exceeding the impulse counting threshold to the total bedload sampling duration T (Wyss et al., 2016c):

$$z_p = \frac{\sum \Delta t_i}{T} \qquad \text{[-]} \qquad (1)$$

At $z_p \leq 0.01$, the signals of impinging particles rarely overlap and do not significantly affect the measurements, so that the bedload analysis is expected to deliver accurate results. However, with increasing z_p, the effect of signal overlaps increases and causes a certain signal saturation, biasing bedload estimations particularly for $z_p > 0.1$ (Wyss, 2016). Therefore, for accurate bedload estimation, a functional relationship between K_b and z_p should be used, which reads (Albayrak et al., 2022).

$$K_b = 6.6 \cdot z_p^{-0.15} \qquad \text{[1/kg]} \qquad (3)$$

Using Eqs. (1) and (3), SPGS signals are converted to mass bedload transport rate in kg/s.

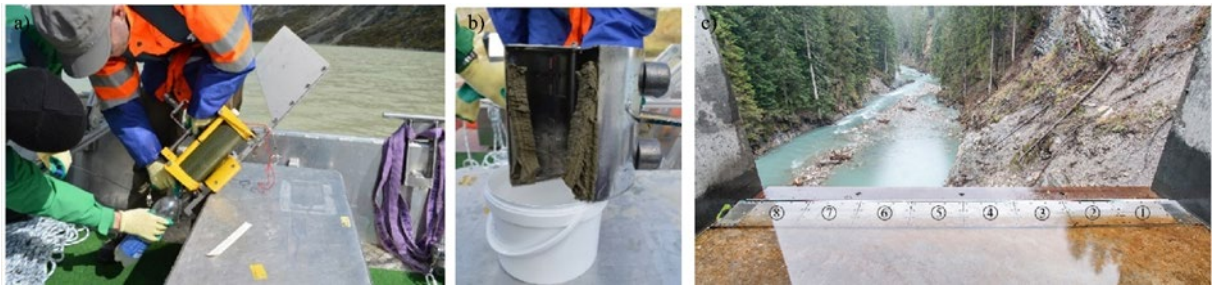

Figure 5: a) Niskin bottle sampler, b) river bottom sediment sampler and c) SPGS at the Solis SBT outlet.

Turbidimeter for suspended sediment transport monitoring

The presence of solid particles in water leads to a reduction of transparency, i.e., turbidity. For turbidity measurements, a collimated beam of visible or near infrared light (wavelength 0.3 to 1 µm) is sent into a sample volume and light is scattered by the particles. Based on this principle, suspended sediment transport was monitored by means of turbidimeters (Turbimax W CUS41 manufactured by Endress + Hauser, Reinach, Switzerland) installed in the Albula, tailrace channel of the HPP Sils and outlet of SBT. The signal transmitter (Liquisys M CUM22) from the same company transmits the signal to a data logger. Particles larger than 0.25 – 1.0 mm were found to have little impact on the turbidity (Campbell and Spinrad, 1987; Black and Rosenberg, 1994). Therefore, particles with a diameter of less than 0.5 mm can be monitored using turbidimeters (Müller-Hagmann, 2017).

Among numerous techniques to monitor suspended sediment transport, turbidimeters are relatively inexpensive, easy to handle and the most suitable for application in high-speed flows as in SBTs. However, they have some limitations: (i) the detection sediment diameter is small (less than 0.5 mm), (ii) they need a site-specific calibration, since particle size, shape, composition, and color affect the measurements, and it is mandatory to include samples of a large discharge range to calibrate each sensor (Gippel 1995; Teixeira et al. 2016), and (iii) air bubble correction of transmitters needed to be changed from 3% to 100% to extend the measurement range beyond turbidities of 350 FNU.

These limitations caused unrealistic turbidity measurements at the Albula gauging station from the turbidimeter installation until November 2012 and from December 2014 to July 2015; and in the tailwater of the HPP Sils until March 2013. Furthermore, some settings of the turbidimeters installed at the Solis SBT were changed to improve the measurement accuracy since 2015, so that a new calibration curve for these turbidimeters in SBT were needed. However, no calibration has been conducted so far. Therefore, the data of turbidimeters from four SBT operations in 2013 and 2014 were only used to find the effect of *WL* on concentration of inflowing suspended sediments from the Albula and outflowing suspended sediments from the SBT and because of no calibration of the turbidimeters, the data from 2015 until now could not be used. This is explained in detail in section 3.1.3.

3.1.2 Hydraulic parameters

The total sediment load (*TL*) includes suspended sediment load (*SSL*) and bedload (*BL*). The incipient motion of bed load is related to the bed shear velocity, u_{*_b}, which is a fictitious velocity representing the bed shear stress in velocity unit. It is used to calculate the non-dimensional Shields parameter. There are two methods used herein to calculate shear velocity. The first method is based on the energy line slope and applied for non-uniform flows as present in the reservoirs:

$$u_{*b} = \sqrt{\frac{\tau_b}{\rho}} = \sqrt{gR_hS_e} \qquad \text{[m/s]} \qquad (4)$$

where τ_b is the bed shear stress, ρ is the water density, g is the gravitational acceleration, $R_h = A/P$, is the hydraulic radius with A = wetted area and P = wetted perimeter, and S_e is the energy line slope.

The second method to calculate shear velocity is based on the logarithmic Prandtl-Karman type streamwise velocity distribution known as log-law (Nezu and Nakagawa, 1993):

$$\frac{u}{u_{*b}} = \frac{1}{\kappa}\ln\left(\frac{z}{z_0}\right) \qquad \text{[-]} \qquad (5)$$

where u is the streamwise velocity at water depth z, κ is the von Karman constant equal to 0.40, and z_0 is the zero-velocity level from the channel bed which can be calculated for smooth, transitionally, and rough bed, respectively, as:

$$z_0 = 0.11\frac{\nu}{u_*} \qquad \text{[m]} \qquad (6)$$

$$z_0 = 0.11\frac{\nu}{u_*} + 0.033k_s \qquad \text{[m]} \qquad (7)$$

$$z_0 = 0.033k_s \qquad \text{[m]} \qquad (8)$$

where ν is the kinematic viscosity of water and k_s is Nikuradse's equivalent sand roughness height. It must be noted that this method is only applicable for velocity profiles with logarithmic distribution and in the inner region of the boundary layer.

The threshold between *SSL* and *BL* transport depends on the particle size and hydraulic conditions. Sediments are transported in suspension when the turbulence eddies overcome the settling velocity of the particles (Prosser and Rustomji, 2000). The transition from saltation (bedload) to suspension mode occurs when the vertical component of turbulence intensity, w_{rms} (root-mean-square rms) is equal or larger than the particle settling velocity (Francis and Bagnold, 1973; Abbott and Francis, 1977; Bose and Dey, 2013). The settling velocity, V_s, is determined using Eq. (9):

$$V_s = \frac{\left(s_g - 1\right)gd^2}{C_1\nu + \left(0.75C_2\left(s_g - 1\right)gd^3\right)^{0.5}} \qquad \text{[m/s]} \qquad (9)$$

where s_g is the specific gravity of sediments, which is equal to 2.65, d is the particle diameter, and C_1 and C_2 are constants with values of 20 and 1.1, respectively, for natural sands (Felix, 2017). Figure 6 shows the relation between particle diameter and settling velocity. Table 1 also shows the settling velocity of different particles.

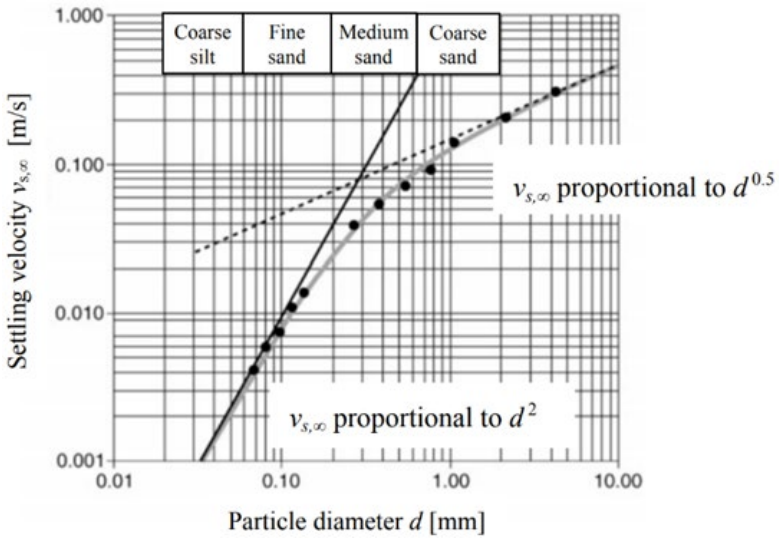

Figure 6: Settling velocity of river sediments as a function of their diameter (Felix, 2017, Ferguson and Church, 2004)

Table 1: The settling velocity of suspended sediments with different diameters.

Particles	Diameter (μm)	Settling velocity (m/s)
Clay	< 2	< 3.24×10^{-6}
Fine silt	2 – 6.3	3.24×10^{-6} - 3.2×10^{-5}
Medium silt	6.3 – 20	3.2×10^{-5} – 0.00032
Coarse silt	20 – 63	0.00032 – 0.0029
Fine sand	63 – 200	0.0029 – 0.021
Medium sand	200 – 630	0.021 – 0.082
Coarse sand	630 – 2000	0.082 – 0.18
Fine gravel	2000 – 6300	0.18 – 0.35
Medium gravel	6300 – 20000	0.35 – 0.62
Coarse gravel	20000 – 63000	0.62 – 1.11
Cobble	> 63000	> 1.11

The universal vertical turbulence intensity equation for 2D open-channel flows is (Nezu and Nakagawa, 1993):

$$\frac{w_{rms}}{u_{*b}} = 1.27 \exp\left(-\frac{z}{h}\right) \qquad [-] \qquad (10)$$

where h is the flow depth. The vertical turbulence intensity near the bed region, i.e. at $z/h = 0$, is $w_{rms} = 1.27u_{*b}$. Therefore, by determining the bed shear velocity at different inflowing discharges, w_{rms} values and corresponding settling particles were calculated at different locations along the reservoir.

3.1.3 Sediment classification and transport

Sediment classification

To determine sediment balance and bypass efficiencies of the SBT, the inflow and outflow sediment transport rates were measured by means of direct measurements using SPGS and turbidimeters, and estimated using the empirical equations. For this purpose, the sediments are categorised into three groups based on their size because of the limitation of our measuring systems (turbidimeters and SPGS) (Figure 7). There is no exact threshold sediment diameter between *BL* and *SSL,* and it varies based on hydraulic conditions. In river engineering applications, this threshold is often assumed to 1 mm (Maniak, 2010). As sediment transport conditions in the SBT is different from rivers, Müller-Hagmann (2017) assumed particles larger than 22 mm to be transported as bedload; these particles can be detected by the SPGS. Therefore, this size class is denoted as BL_{22}.

Particles with a diameter of less than 0.5 mm are in suspension mode and can be monitored using turbidimeters and are denoted herein as “fine suspended sediments” (SSL_{fine}).

The size class between 0.5 mm and 22 mm is supposed to be detected neither by the SPGS nor by the turbidimeters. Sediments in this size range are assumed to be transported in suspension mode in the SBT with clearly supercritical flow (Müller-Hagmann, 2017). But in the Albula River, only particles from 0.5 mm to 1 mm are assumed to be in suspension mode and the rest, from 1 mm to 22 mm, are transported as bedload (based on the typical threshold size in river engineering projects). In this study, the size class between 0.5 mm and 22 mm is denoted as “coarse suspended sediment” (SSL_{coarse}) (similar to Müller-Hagmann, 2017). As SSL_{coarse} cannot be detected by neither the SPGS nor the turbidimeters, it was derived based on assumptions.

The methodologies to determine the sediment inflow and outflow of the Solis Reservoir for the three particle size classes are presented in the following subsections.

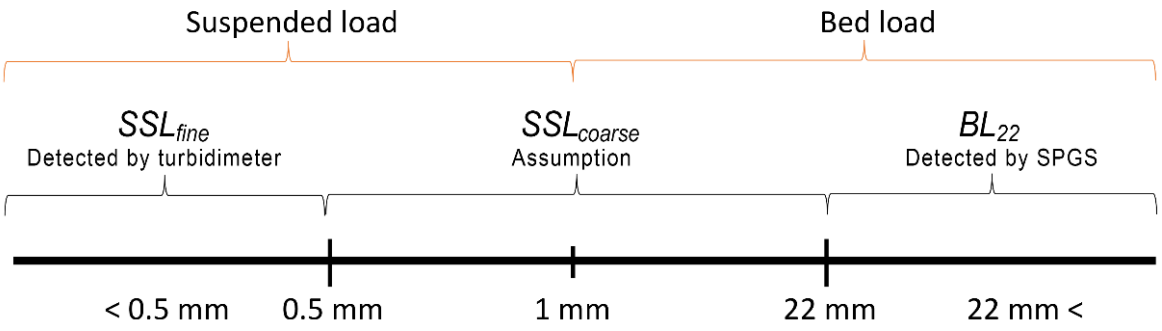

Figure 7: Sediment classifications used in this study.

General sediment inflow and outflow transport

Figure 8 shows inflow and outflow BL_{22}, SSL_{coarse} and SSL_{fine} to / out of the Solis Reservoir.

The inflow sediments to the reservoir are:

a) BL_{22}:

- BL_{22} coming from Julia River and HPP Tiefencastel is neglected because of the desilting effect of the upstream Marmorera and Tinizong reservoirs (Müller-Hagmann, 2017).
- The main source of inflow BL_{22} is the Albula River, which is measured by means of SPGS and empirical equations (explained in the following subchapters).

b) SSL_{coarse}:

- SSL_{coarse} in Julia River and HPP Tiefencastel is neglected because of the desilting effect of the upstream reservoirs (Müller-Hagmann, 2017).
- The main source of inflow SSL_{coarse} is the Albula River, which is calculated by assumptions (explained in the following subchapters).

c) SSL_{fine}:

- SSL_{fine} in Julia River is neglected because of the desilting effect of the upstream reservoirs and of the fact that the river reach downstream of the Tinizong reservoir is a residual flow stretch (Müller-Hagmann, 2017).
- SSL_{fine} from HPP Tiefencastel is estimated to 4'800 m^3/year, which is around 4% of the yearly total sediment inflow to the reservoir (more details on how to calculate this volume is presented in the Appendix and Müller-Hagmann, 2017).
- The main source of inflow SSL_{fine} is the Albula River, which was calculated using an *SSC-Q* equation (explained in the following subchapters).

The outflowing sediments from the reservoir are presented as:

a) BL_{22}:

- 31'400 m^3/year of sediments are annually excavated on average from the reservoir head which consist of BL_{22} (50%) and SSL_{coarse} (50%). Therefore, the volume of BL_{22} excavated from the reservoir is 15'700 m^3 (Müller-Hagmann, 2017).
- No BL_{22} is transported through the dam outlets and HPPs Sils and Rothenbrunnen.
- The main way of transporting BL_{22} is through the SBT, which is measured by the SPGS at the outlet of the SBT.

b) SSL_{coarse}:

- 15'700 m^3 of SSL_{coarse} is excavated from the reservoir head (Müller-Hagmann, 2017).
- No SSL_{coarse} is transported through the dam outlets and HPPs Sils and Rothenbrunnen due to the desilting effect of the Solis Reservoir.
- SSL_{coarse} is mainly transported out of the reservoir through the SBT which is a portion of inflow SSL_{coarse} by the Albula (explained in next subchapters)

c) SSL_{fine}:

- SSL_{fine} transported through dam outlets and HPPs Sils and Rothenbrunnen was 16'300 m^3/year on average which is around 14% of the yearly total incoming sediments to the reservoir (more details on how to calculate this volume is presented in the Appendix and Müller-Hagmann, 2017).
- The main passage of outflowing SSL_{fine} is through the SBT which is calculated based on the relation between inflowing fine sediment concentration and reservoir water level obtained from operations in 2013 and 2014 (explained in the following subchapters).

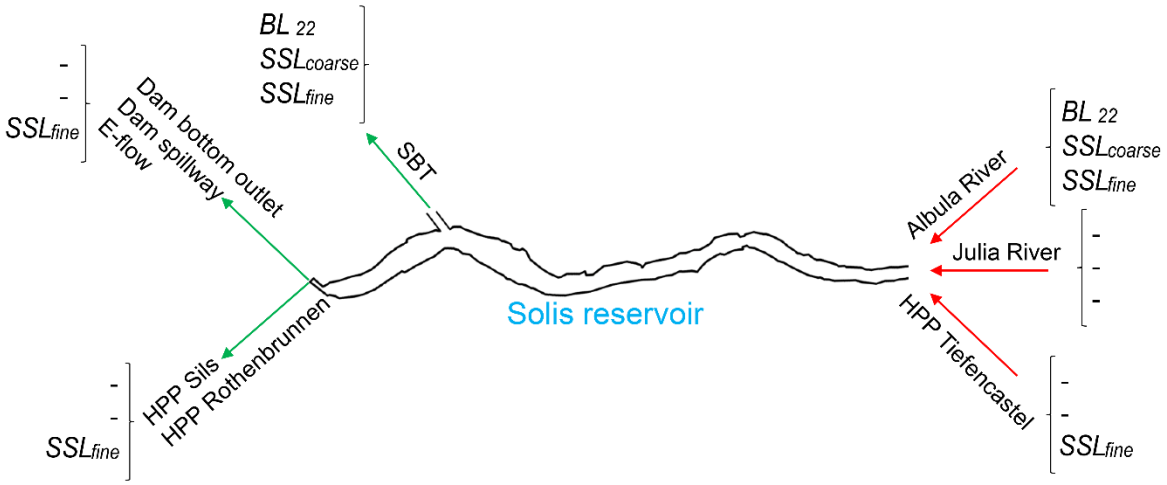

Figure 8: A schematic showing inflowing and outflowing sediments to Solis Reservoir.

To calculate the sediment balance in the Solis Reservoir, we consider a large amount of sediment inflow from the Albula River and most of the outflow through the SBT. The following shows how we calculated or measured them.

Bed load transport to the reservoir (by Albula)

The bedload transport in the Albula was determined by two methods:

(i) measurements using the SPGS in Albula, Eq. (1), with a calibration coefficient of K_b = 11.8, provided by Rickenmann et al. (2020), to convert recorded Imp to bedload transport rates.

(ii) estimations using empirical bedload equations, which were compared with mean annual bedload volumes from 1987 to 2006 by Müller-Hagmann (2017).

Müller-Hagmann (2017) showed that the transport equations of Smart and Jaeggi (1983) (SJ) and Rickenmann (2001) (RM) led to similar estimates of annual bedload volumes from 1987 to 2006 in the Solis Reservoir. The proposed equations of SJ and RM are:

$$q_s^* = 4\frac{\rho_s R_s U}{(s-1)}\left(\frac{d_{90}}{d_{30}}\right)^{0.2} S^{1.6}\left(1-\frac{\theta_c}{\theta}\right) \qquad \text{[kg/(s.m)]} \qquad (11)$$

$$q_v^* = 2.5\mathrm{Fr}^{1.1}\cdot\sqrt{\theta}\times(\theta-\theta_c) \qquad \text{[-]} \qquad (12)$$

where q_s^* is the specific gravimetric bedload transport capacity and q_v^* is the dimensionless volumetric transport rate per unit width; ρ_s is the particle density equal to 2'650 kg/m^3, R_s is the hydraulic radius related to the bed, U is the cross-sectional average streamwise velocity, s is the specific density of sediments which is the ratio of sediment density to water density, equal to 2.65, d_x denotes the particle size equal to a sieve size with x percent of particles passing, S is the channel slope which is 0.0088 at the Albula gauging station, θ_c is the critical Shields parameter, Fr is the Froude number, and θ is the Shields parameter calculated as:

$$\theta = \frac{R_h S}{(s-1)d_{50}} \qquad \text{[-]} \qquad (13)$$

Assumptions and correction factors were included by Müller-Hagmann (2017) to simplify Eq. (11) and (12) and avoid overestimation of bedload transport rates as follows:

- the channel at the location of the Albula gauging station is trapezoidal with side wall slopes of 1, channel width of 18.75 m and longitudinal bed slope of 0.0088,
- d_{30}, d_{50} and d_{90} in Albula station are 0.03 m, 0.06 m and 0.3 m, respectively,
- the hydraulic radius as a function of discharge is given by Müller-Hagmann (2017) for Albula as:

$$R_s = 0.1028 Q^{0.5546} \quad \text{[m]} \quad (14)$$

- The critical Shields parameter as a function of the angle of repose, φ, of the sediment material (with $\varphi = 45^{\circ}$) is:

$$\theta_c = 0.05\left[\cos\left(\tan^{-1}(S)\right)\right]\left(1-\frac{S}{\tan\varphi}\right) = 0.049 \quad \text{[-]} \quad (15)$$

- Rickenmann (2005) developed a formula with a reduced slope S' to account for energy dissipation induced by large immobile boulders in steep channels and for moderate roughness as:

$$S' = 0.083\frac{S}{S^{0.35}}\left(\frac{h}{d_{90}}\right)^{0.33} \quad \text{[-]} \quad (16)$$

- Marti (2006) indicated the bedload transport effective channel width, b', which is generally not equal to the channel width, b, as:

$$b' = 1.19 b \cdot \exp\left[-0.6\frac{b^{0.65}\cdot d_{50}^{0.25}\cdot S^{0.3}\cdot g^{0.18}}{Q^{0.36}}\right] \quad \text{[m]} \quad (17)$$

- The flow depth at different discharges is presented as:

$$h = 0.1819\left(\sqrt{Q+4.913}-2.22\right) \quad \text{[m]} \quad (18)$$

Therefore, the simplified SJ and RM methods to calculate volumetric bedload transport capacities [m³/s] are presented as:

$$Q_v^* = 4\frac{R_s\cdot U}{(s-1)}\cdot 1.05 S'^{1.6}\cdot\left(1-\frac{\theta_c}{\theta}\right)\cdot b' \quad \text{[m³/s]} \quad (19)$$

$$Q_v^* = 2.5\,\mathrm{Fr}^{1.1}\cdot\sqrt{\theta}\cdot(\theta-\theta_c)\cdot\sqrt{(s-1)\cdot g\cdot d^3}\cdot b' \quad \text{[m³/s]} \quad (20)$$

It must be noted that the above-mentioned equations allow to calculate the total bedload in the Albula River (particles larger than 1 mm). The relation between *BL* (based on a 1 mm grain size threshold) and BL_{22} (on the basis of 22 mm grain size) depends on the *PSD* and is assumed to be roughly $BL_{22} \approx 2/3BL$ for the Solis *PSD* in the Albula (Müller-Hagmann, 2017). Note that bedload transport is subjected to large fluctuations due to its intermittent character. Its estimation includes model uncertainties and measurements errors so that the bedload estimation error can amount to ± 50% or even more (Müller-Hagmann, 2017).

Bedload transport out of the reservoir (from SBT)

The bedload can be released from the reservoir mainly by the SBT. The outflow transport rates were indirectly measured by the SPGS. The measured 'Imp' by SPGS is converted to transport rate using Eq. (1). The coefficient K_b in Eq. (1) is calculated using Eqs. (2) and (3) (details are presented in another BFE project report on sediment bypass tunnels (SI/501609-01)).

Fine suspended sediment transport into the reservoir (by Albula)

The mass of fine suspended sediment (SSL_{fine}) results from summing up the product of the instantaneous fine suspended sediment concentration (SSC_{fine}) [mg/l] and discharge Q [m³/s] over n time steps Δt [s]:

$$SSL_{fine} = \sum_{i=1}^{n} SSC_{fine_i} \cdot Q_i \cdot \Delta t \qquad \text{[g]} \qquad (21)$$

The instantaneous SSC_{fine} in the Albula was determined based on an SSC_{fine}-Q rating curve applied to the hydrograph. This rating curve was calibrated using 274 bottle samples (SSC_B) collected in 1993, 2010 and 2011 in the Albula, among which 169 data points were skipped because of error in discharge measurements (Müller-Hagmann, 2017). By applying least square fitting to the remaining 105 data points using a power fit, the solid black line in Figure 9 was obtained by Müller-Hagmann (2017). In Figure 9, SSC_B = SSC_{fine}. However, this SSC_B-Q rating curve is based on the bottle samples collected at discharges up to 40 m³/s (Figure 9). Therefore, the equation may yield wrong estimates at discharges above 40 m³/s. During the field visit on 12th June 2019, we collected two bottle samples at Q_{Albula} = 100 m³/s, corresponding to 5-year flood. The measured SSC was around 4 g/l. Adding this point to the data points from FOEN, a new SSC_B-Q equation was obtained (Eq. 22, dashed black line in Figure 9). Figure 9 shows that the previous equation (solid line) underestimates the SSC_{fine} values at higher discharges. Therefore, the new Eq. (22) is used in this study to estimate inflow SSL_{fine} in the Albula for all discharges.

$$SSC_{fine} = 0.02Q^{2.651} \qquad \text{[mg/l]} \qquad (22)$$

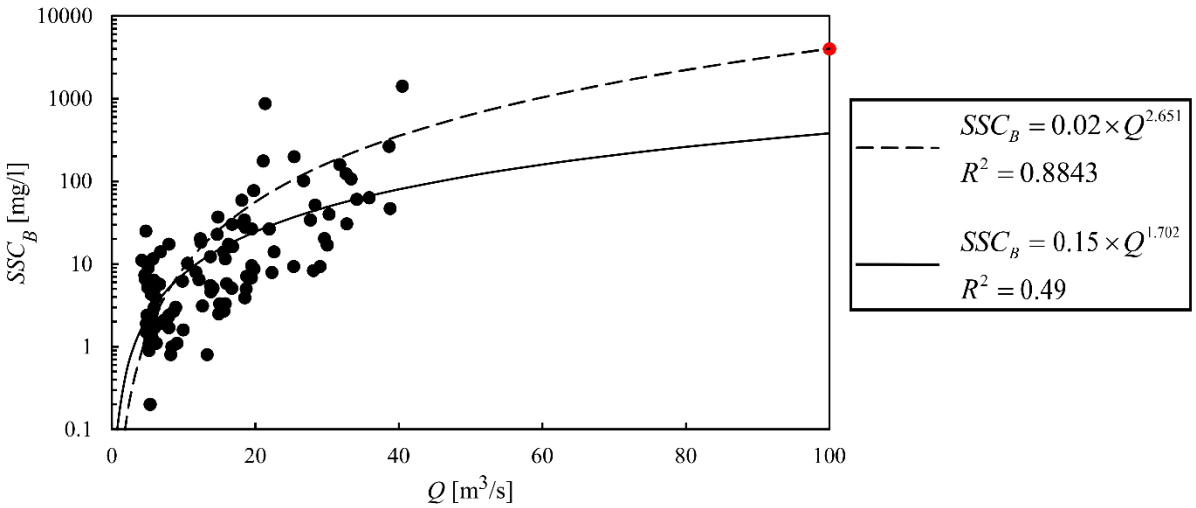

Figure 9: New SSC_{fine}-Q correlation (dashed line) using bottle samples collected by FOEN (black dots) and VAW (red dot). The solid line is Eq. (22) proposed by Müller-Hagmann, 2017 for discharges lower than 40 m³/s.

Fine suspended sediment transport out of the reservoir (by SBT)

The main passage of outflow SSL_{fine} is through the SBT. The turbidity of fine suspended sediment in the SBT is continuously monitored by two turbidimeters. With a calibration curve, turbidity data can be converted into mass concentration values. However, as the turbidimeter on the right side of the SBT was broken and the setting of the left turbidimeter was changed and no calibration was conducted with the new setting, the SSL_{fine} in the SBT could not be calculated from the turbidity data. Therefore, assumptions are required to calculate the outflowing fine suspended sediments from the SBT. The outflow SSL_{fine} is calculated by the inflow SSC_{fine} measured based on Eq. (22) and Figure 9. During three periods of SBT operations in 2013 and 2014, the SSC_{fine} was measured by turbidimeters in both the SBT and at the Albula gauging station (Figure 10). Turbidimeters at both locations were the same type with the same settings and linear calibration curves, therefore the ratio of FNU_{SBT} / FNU_{Albula} is equal to the ratio of SSC_{SBT} / SSC_{Albula}. The time interval of turbidimeter recordings in the Albula and SBT was 1-hour and 1-min, respectively. Based on reservoir *WL* during SBT operations, the ratio of SSC_{SBT} / SSC_{Albula} was calculated. Figure 11 shows hourly ratios of turbidimeter values in the SBT and Albula River versus *WL* during SBT operations in 2013 and 2014. During these three events, the SBT was in operation for around 33 hours in total. The average *WL* was calculated for each hour of operation and plotted versus the ratio of SSC_{fine} in the SBT and Albula River, respectively. The three red points in Figure 11 belong to the first SBT operation after its construction. Therefore, on the one hand, the bed armouring was weaker at this operation and there were a lot of loose fine sediments deposited at the inlet of the SBT from previous years. On the other hand, these three points belong to the time when the FNU values in the Albula reduced, but the Albula discharge did not change (Figure 10a). Subsequently, the FNU values in the SBT did not change, while the *WL* was constant. Therefore, these three red points are not considered here. For *WL* lower than 816 m asl, the big blue rectangle in Figure 11, the ratio of outflow to inflow fine sediment turbidity is assumed to be around 2. This implies that the SBT does not only convey the incoming SSL_{fine}, but also the previously deposited SSL_{fine} out of the reservoir. By increasing *WL* to more than 820 m asl, the small blue rectangle in Figure 11, this ratio decreases to 0.25, showing that most inflowing SSL_{fine} from the Albula are trapped in the reservoir and only a small portion is transported through the SBT. Based on Figure 10 and Figure 11, the outflow SSL_{fine} from the SBT is calculated as follows: when *the WL* is not considerably lowered during SBT operations, the ratio of SSC_{fine} in the SBT to SSC_{fine} in the Albula is assumed to be 0.25. When the *WL* is lowered to around 814 m asl, this ratio is 2. SSC_{fine} in the Albula is also calculated by Eq. (22). After calculation of SSC_{fine} in the SBT, the SSL_{fine} is calculated as:

$$SSL_{fine} = \sum_{i=1}^{n} \frac{SSC_{fine_i} \cdot Q_{\mathrm{SBT}_i} \cdot \Delta t}{\rho_s} \qquad [\mathrm{g/l}] \qquad (23)$$

It must be noted that the duration of all the SBT operations in 2013 and 2014 was below 16 hours Studies show that the *SSC* reduces over time during reservoir flushing through dam bottom outlets (Moridi and Yazdi, 2017; Panthi et al. 2022). In Solis reservoir, when the *WL* is lowered to around 813 m asl, the reservoir is flushed from the inlet of the reservoir to the location of the SBT inlet. Therefore, it is expected that the outflowing *SSC* reduces over time. As a result, the ratio of SSC_{SBT} / SSC_{Albula} tends to 1 in long operations with *WL* of around 813 m asl. Therefore, it is assumed that the ratio SSC_{SBT} / SSC_{Albula} ≈2 for the first 2 days of the SBT operation, and from the third day of the SBT operation, this ratio is 1, because the fine sediment deposited in the reservoir will be eroded and the erosion capacity will reduce in time. There were two events with SBT operation longer than 2 days with *WL* of around 813 m asl. The first operation was in June 2019 with a duration of around 7 days. Therefore, the average ratio for this operation is judged to be around 1.25. The second long SBT operation was in June 2021 with a duration of around 4 days. The average ratio for this operation is

considered to be 1.5. The duration of the rest of SBT operations with *WL* of around 813 m asl was less than 2 days, therefore the ratio of 2 is used to calculate the outflowing SSC_{fine} from the SBT. The results based on these assumptions are compared to results of bathymetry measurements in the results and discussion section (chapter 4).

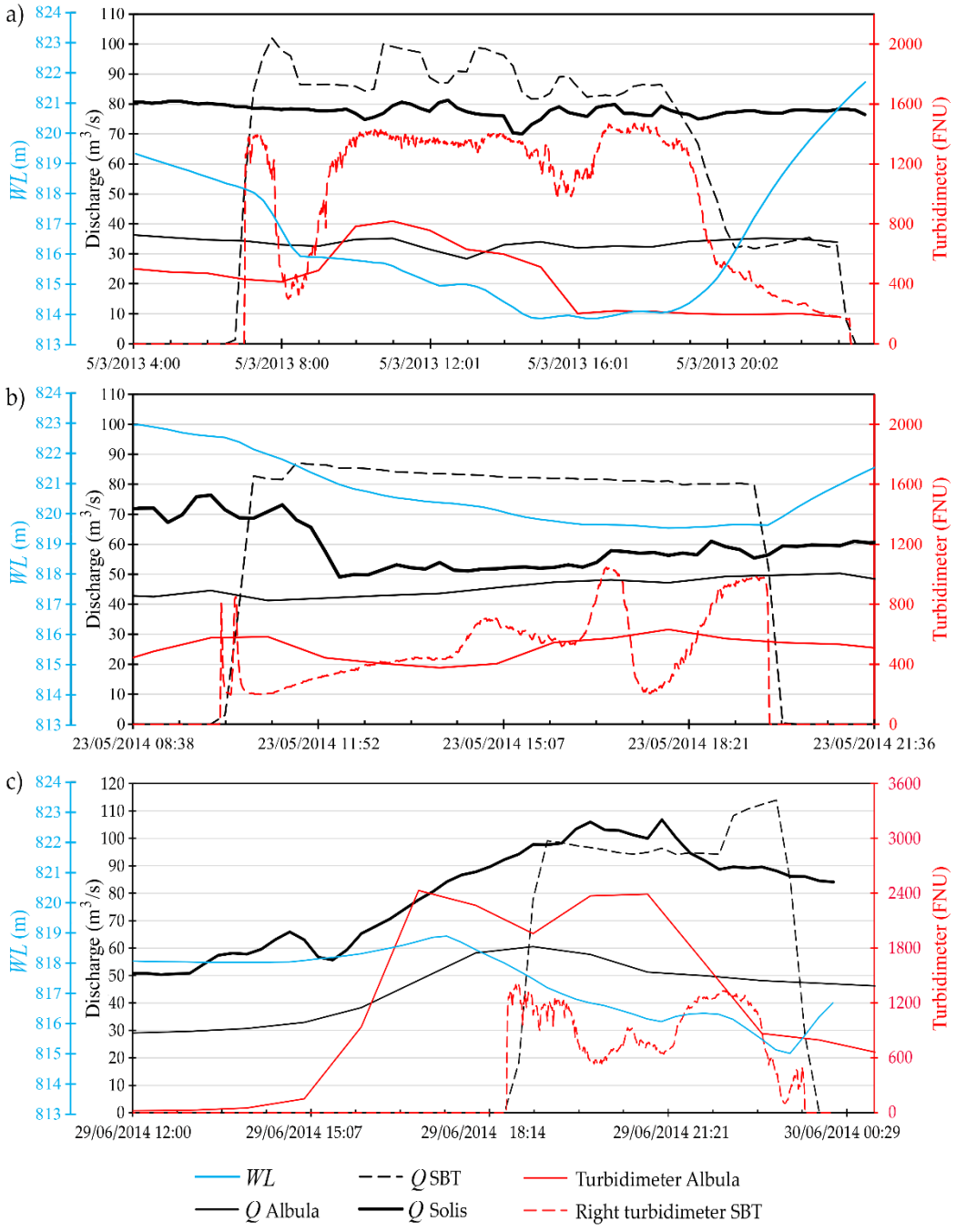

Figure 10: SSC_{fine} measurements using turbidimeters during SBT operations in 2013 (a) and 2014 (b and c).

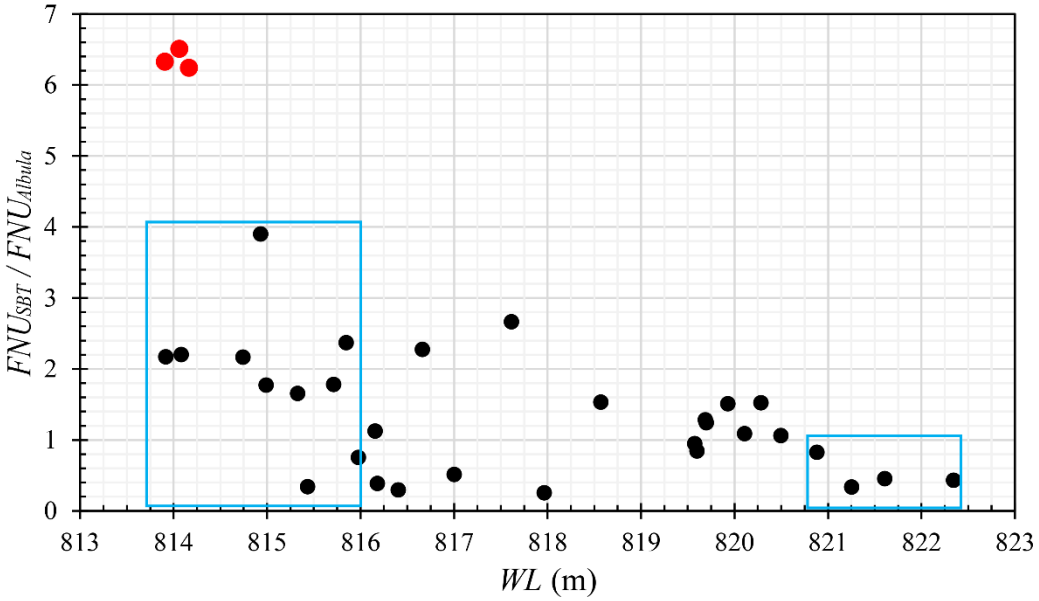

Figure 11: Ratio of turbidimeter values in the SBT and Albula River versus *WL* during SBT operations in 2013 and 2014. The duration of all operations was less than 16 hours. The red dots belong to the first SBT operation, after construction of the SBT, when the bed armoring was weaker at this operation and there were a lot of loose fine sediments deposited at the inlet of the SBT from previous years, on one hand. On the other hand, the red dots belong to the time when the *FNU* values in Albula reduced, but the Albula discharge did not change. Subsequently, the *FNU* in SBT did not change, while the *WL* was constant.

Coarse suspended sediment into the reservoir (by Albula)

The coarse suspended sediment inflow into the Solis Reservoir originates from the Albula River. The transport of coarse suspended sediment in the Albula River is neither detectable by the SPGSs nor by the turbidimeter. Therefore, the estimation of the SSL_{coarse} in the Albula was done as follows.

The coarse suspended sediment mass in the Albula was estimated by assuming a volumetric ratio of BL_{22} / TL = 0.25 (Müller-Hagmann, 2017), where TL is the total sediment load. This assumption is in line with the value for the Albula reported by Rickenmann et al. (2017). The SSL_{coarse} was computed using the following equation based on the determined BL_{22} and SSL_{fine}:

$$SSL_{coarse} = TL - BL_{22} - SSL_{fine} = 3BL_{22} - SSL_{fine} \quad [m^3] \quad (24)$$

Coarse suspended sediment out of the reservoir (by SBT)

The outflow of coarse suspended sediment is released by the SBT. Since no direct measurement was available for SSL_{coarse} in the SBT, it is assumed that the ratio of Albula inflow SSL_{coarse} to outgoing SSL_{coarse} is equal to the average of the ratios for BL_{22} and SSL_{fine}. These ratios and corresponding SSL_{coarse} were calculated for each event. After the inflow and outflow BL_{22} and SSL_{fine} have been calculated for the Albula River and SBT, respectively, the outflow SSL_{coarse} is determined as:

$$\left(SSL_{coarse}\right)_{SBT} = \left(SSL_{coarse}\right)_{Albula} \cdot \frac{1}{2}\left[\left(\frac{BL_{SBT}}{BL_{Albula}}\right)_{22} + \left(\frac{SSL_{SBT}}{SSL_{Albula}}\right)_{fine}\right] \quad [m^3] \quad (25)$$

3.2 Field measurement campaigns

Four measurement campaigns were conducted in the Solis Reservoir in October 2018, August 2019, September 2020 and November 2021 (Table 2). In the first measurement campaign in 2018, on the first day, the velocities and bathymetry of the reservoir at 55 locations along the reservoir were measured (black dots in Figure 12). On the following day, cross-sectional flow velocities were measured at 8 cross sections with 8 to 10 repetitions, called transects (the locations of measurements is shown in Figure 13 and Table 3). At the centre of each cross section, stationary measurements (continuous flow velocity measurements) were conducted over 10 to 15 minutes. Furthermore, suspended and deposited sediments were sampled at those locations (Figure 13 and Table 3). At three more locations (locations 8, 10 and 11), only deposited samples were collected; neither suspended samples were taken nor cross sections measured in these locations.

In the second, third and fourth measurement campaigns (2019, 2020 and 2021), the bathymetry measurement was conducted differently by densely steering the boat in a manner of zig-zags between the shores of the reservoir (Figure 12). With this technique, the number of measurement points and the resolution were increased, while the required measurement time reduced compared to the bathymetry measurements in the previous year. The interpolation error was also reduced, especially close to the shores and in bends. During the measurement campaigns in 2019, 2020 and 2021, sediment sampling, cross-sectional (up to 10 transects) and stationary velocity (10 to 15 minutes) measurements were conducted at approximately same locations as in the first measurement campaign in 2018. Additional cross sections and suspended load sampling were conducted in location 11 close to the dam. No deposited sediment samples were taken from stations 8 and 10 in 2019 and 2020.

In 2021, similar to 2018, 2019 and 2020, between 3 and 5 bottle samples of suspended sediment were collected from different depths as well as one sample from the sediment deposits at each location along the reservoir (approximately similar locations as shown in Figure 13). In 2021, we additionally measured *SSC* distributions in the water column, i.e., from the water surface to the reservoir bottom, at each measurement location (Figure 13) using LISST-100 X. The collected bottle samples were analysed to determine *SSC*, which were compared with those measured with LISST.

Reservoir and SBT monitoring data from 2018 to the beginning of 2022 is obtained. The analyses of the velocity, bathymetry and LISST data and sediment samples from four different measurement campaigns are presented and the project was completed according to the timetable in Table 2.

For better evaluation of the bypassing efficiency, the bathymetry measurements conducted by the operator from 25 - 27 June 2019 are also used. Although those measurements were conducted at predefined cross sections and not in zigzag, they were performed a few days after the SBT operation at a reduced *WL*. Comparing the differently acquired data provided better information about the operation of the SBT during floods.

Table 2: Project schedule.

	2018	2019				2020				2021				2022	
Quarter	4	1	2	3	4	1	2	3	4	1	2	3	4	1	2
Field measurements in Solis reservoir - ADCP - Sediment sampling - Reservoir operation monitoring - SBT operation monitoring	X			X				X					X		
Data analysis - Velocity fields - Turbulence and bed shear analysis - Bathymetry - Sediment analysis - Backscatter signal analysis in relation to suspended sediment transport* - Bottom tracking signal analysis in relation to bed load transport* - Sedimentation and reservoir operation analysis - SBT efficiency analysis	X	X		X	X	X	X		X	X			X	X	X

* because of low *SSC* and no *BL* during our measurements, we could not find the correlation between the backscatter and bottom tracking signals and sediments. For this task we recommend continued measurements with installation of a fixed ADCP at the inflow of the reservoir.

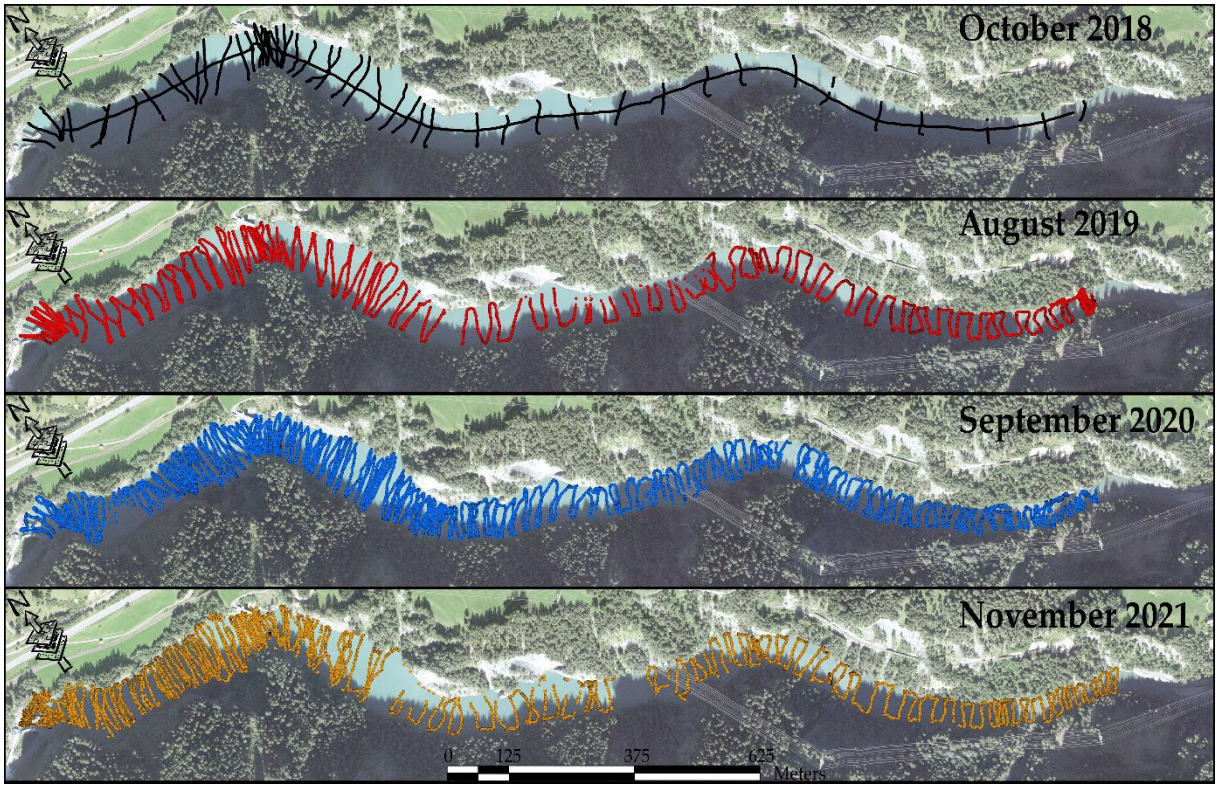

Figure 12: Bathymetry measurement locations in Solis reservoir in different field campaigns.

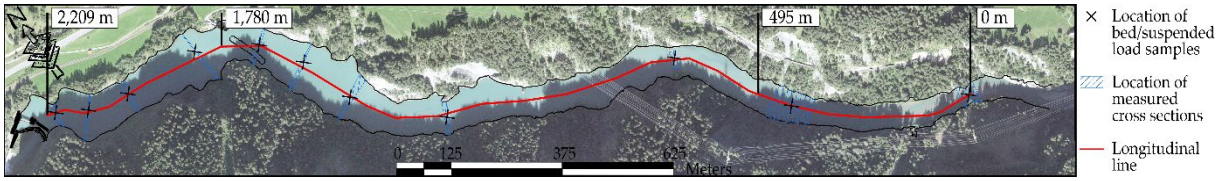

Figure 13: Velocity and sediment sampling locations in Solis Reservoir. The crosses refer to the sediment sampling and stationary velocity (10 to 15 minutes) measurements locations in 2018, 2019, 2020, and 2021. The dashed blue area shows cross-sectional (up to 10 transects) locations which slightly differ in each field campaign.

Table 3: Velocity and sediment sampling locations in 2018, 2019, 2020, and 2021. The naming of each station during measurement days is presented in the Appendix. ST = Station.

Distance	2018			2019			2020			2021		
	Cross sectional meas.	Bedload samples	Bottle samples	Cross sectional meas.	Bedload samples	Bottle samples	Cross sectional meas.	Bedload samples	Bottle samples	Cross sectional meas.	Bedload samples	Bottle samples
0 m	A	ST 1	ST 1	A	ST 1	ST 1	A	ST 1	ST 1	A	ST 1	ST 1
420 m	B	ST 2	ST 2	B	ST 2	ST 2	B	ST 2	ST 2	B	ST 2	ST 2
700 m	C	ST 3	ST 3	C	ST 3	ST 3	C	ST 3	ST 3	C	ST 3	ST 3
1235 m	D	ST 4	ST 4	D	ST 4	ST 4	D	ST 4	ST 4	D	ST 4	ST 4
1460 m	E	ST 5	ST 5	E	ST 5	ST 5	E	ST 5	ST 5	E	ST 5	ST 5
1590 m	F	ST 6	ST 6	F	ST 6	ST 6	F	ST 6	ST 6	F	ST 6	ST 6
1695 m	G	ST 7	ST 7	G	ST 7	ST 7	G	ST 7	ST 7	G	ST 7	ST 7
1840 m	-	-	-	-	-	-	-	-	-	H	ST 8	ST 8
2015 m	I	ST 9	ST 9	I	ST 9	ST 9	I	ST 9	ST 9	I	ST 9	ST 9
2110 m	-	ST 10	-	-	-	-	-	-	-	J	ST10	ST 10
2190 m	-	ST 11	-	K	ST 11	ST 11	K	ST 11	ST 11	-	ST 11	ST 11

4 Results and discussion

This section is divided into five parts. First hydrology and hydraulic data are presented. Second, the inflow and outflow sediments are specified. Third, bathymetry changes and the volumes of deposition/erosion between each measurement are presented. Then the sediment analysis is elaborated, and finally the calculation of sediment balance and SBT efficiency are given.

4.1 Hydrology and hydraulics

The Solis Reservoir is fed by the Albula and Julia Rivers and the tailrace water of HPP Tiefencastel (Figure 2). Figure 14 shows the 15-min discharge data of reservoir inflow and SBT outflow as well as the reservoir water level measured by ewz in 2018, 2019, 2020, and 2021.

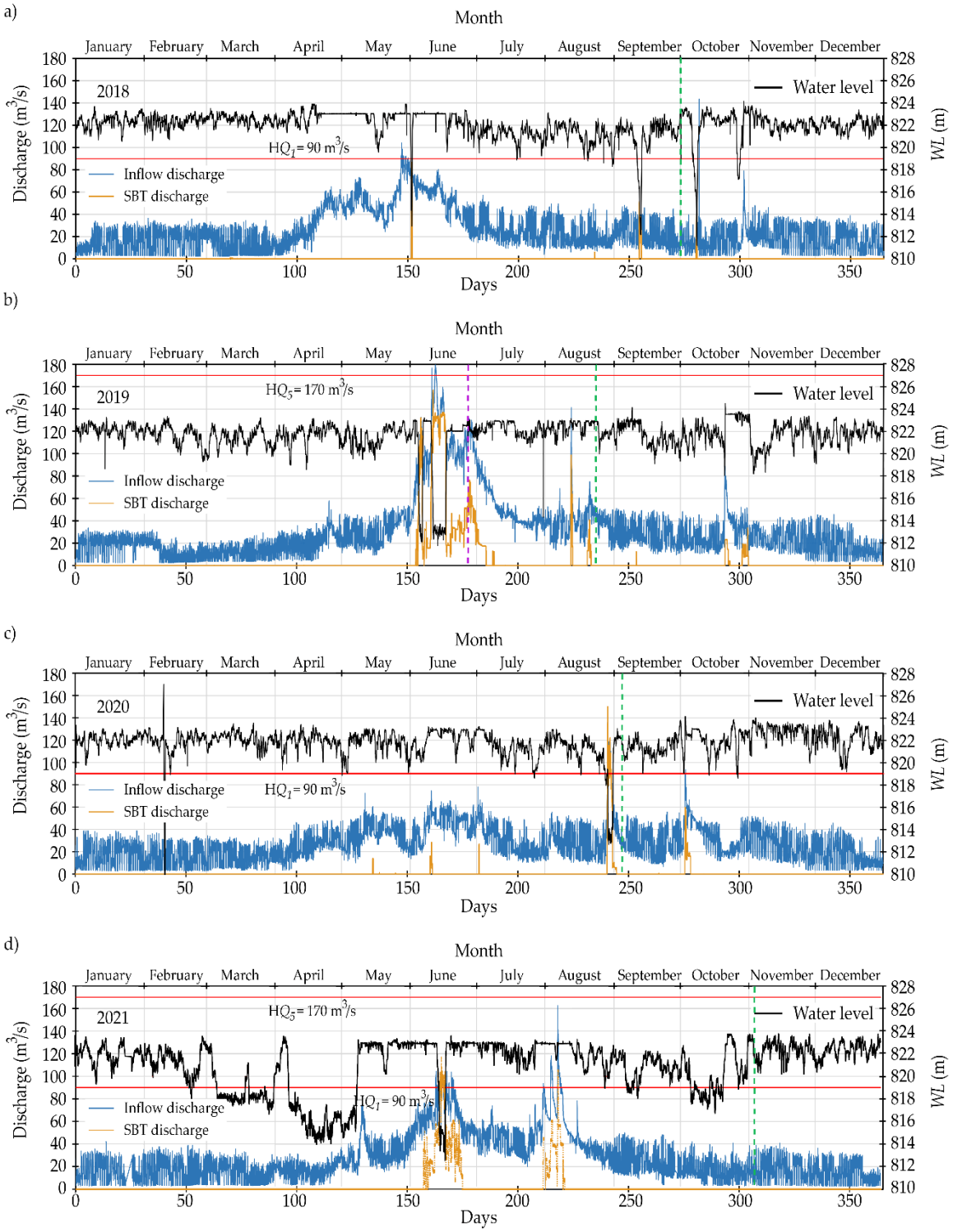

Figure 14: Time series of 15-min inflow and SBT discharges and reservoir water level in Solis reservoir in 2018 (a), 2019 (b), 2020 (c), and (d) 2021 (source: ewz). Field campaign dates: dashed green line (ETH), dashed purple line (operator).

In 2018, the inflow discharge stayed steady around 20 m^3/s during the first 100 days of the year and then increased up to HQ_1 = 90 m^3/s, i.e., a flood with a one-year return period, on 28th May 2018. After this peak, the discharge gradually decreased until the end of the year 2018 except for a few small interim peaks. The SBT operated on 1st June 2018 with mean and 15-min peak discharges of $Q_{SBT,mean}$ = 62 m^3/s and $Q_{SBT,peak}$ = 87 m^3/s, respectively. The second SBT operation was on 12th and 13th September, with $Q_{SBT,mean}$ = 30 m^3/s and $Q_{SBT,peak}$ = 52 m^3/s, and finally on 8th October with $Q_{SBT,mean}$ = 23 m^3/s and $Q_{SBT,peak}$ = 41 m^3/s (Figure 14a). During these operations, the reservoir water level was reduced from the daily mean value of about 822 m to about 813, 812, and 811m asl (above sea level, asl), respectively (Figure 14a). In general, the operator undercut the originally targeted water level of 816 m asl during SBT operation. Overall, there was no major flood discharge in 2018 and the SBT was in operation only three times with relatively low discharges. Therefore, no major sediment accumulation in the reservoir is expected to have occurred in 2018.

In the first 100 days of 2019, the mean inflow discharge was similar to that of 2018 (Figure 14b). However, between 5th June and 1st July 2019, the discharge stayed above a flood with a one-year return period of HQ_1 = 90 m^3/s and reached 183 m^3/s, which is higher than a five-year flood of HQ_5 = 171 m^3/s on 12th June. Before, during and after this flood period (3rd June and 5th July), the SBT was continuously in operation at varying reservoir water levels (with a minimum of 812 m asl) and with a peak mean 15-min discharge of $Q_{SBT,peak} \approx$ 157 m^3/s (i.e. approaching the design discharge of $Q_{SBT,design} \approx$ 170 m^3/s), bypassing large amounts of sediment around the dam for 37 days (as a qualitative information, see the photos in Figure 15). After this flood event, the SBT was in operation four times with relatively low average discharges Q_{SBT} < 47 m^3/s and high water levels of around 822 m asl (Figure 14b).

In the first 100 days of 2020, the inflow discharge was also similar to 2018 and 2019 and then mostly increased, peaking at 136 m^3/s, i.e., above HQ_1 = 90 m^3/s, on 29th August 2020 (Figure 14c). The SBT was in operation between 29th August and 2nd September at a reservoir water level of around 813 m asl with a peak 15-min discharge of $Q_{SBT,peak} \approx$ 150 m^3/s. The second SBT operation was from 3rd to 6th October, when the maximum inflow discharge of the reservoir reached about 90 m^3/s. The reservoir water level at this operation was 820 m asl with a peak 15-min SBT discharge of $Q_{SBT,peak} \approx$ 60 m^3/s.

In the first 120 days of 2021, the inflow discharge was also similar to 2018, 2019, and 2020 and then mostly increased, peaking at around 162 m^3/s, on 8th August 2021 (Figure 14d). There is no recorded information about SBT discharge in that year by operator. Looking at the sensors installed in the SBT by VAW, the SBT gates opened two times in 2021, from 8th to 25th June and 1st to 11th August. In the first SBT operation, the maximum inflow discharge into the reservoir reached 104 m^3/s, slightly higher than HQ_1 = 90 m^3/s, on 14th June. The minimum water level reduced to around 813 m asl with a peak discharge of $Q_{SBT,peak} \approx$ 117 m^3/s in the SBT. In the second operation in August 2021, the reservoir inflow discharge reached 162 m^3/s, but the reservoir level was kept around 823 m. The peak 1-min SBT discharge was $Q_{SBT,peak} \approx$ 106 m^3/s, which is slightly lower than for the previous operation.

Overall, the bathymetry and sediment transport data in 2019 and 2020 are of prime interest to evaluate the SBT bypass efficiency. In contrast, there was no flood event above the one-year flood in 2018, and hence the SBT had been in operation for a shorter total period than in 2019 and 2020 (Figure 14). In 2021, the reservoir inflow discharge increased to almost a five-year flood, but the SBT bypass efficiency was low due to shorter periods of SBT operation concomitant with high *WL* values .

Figure 15: a) Solis reservoir and SBT inlet and b) SBT outlet during larger than five-year flood on 12th June 2019.

Figure 16 shows the interpolated depth averaged velocity magnitude (in a horizontal plane) along the reservoir measured at each field campaign. In all campaigns, the velocity at the inlet of the reservoir is high and decreases along the reservoir due to an increase of flow depth and width of the reservoir. The highest velocities were measured in 2019 and 2020. The highest inflowing discharge to the reservoir was around 53 m^3/s in 2019 followed by 32 m^3/s in 2020, 27 m^3/s in 2018, and 15 m^3/s in 2021. Although inflow discharges during the 2018 and 2020 field measurement campaigns were approximately similar, the velocity distribution is different due to different *WL* and reservoir bed morphology. The velocity at the inlet of the reservoir was much higher in 2020 than in 2018. The reason for that is the fact that the reservoir *WL* in the 2020 measurement campaign was around 1 m below the 2018 values (Figure 17), and there was a sediment accumulation on the right bank of the reservoir inlet, see black area in Figure 16.

Figure 17 shows the water levels in the Solis reservoir during the field campaigns and the effective measurement periods. Although there were large fluctuations during the whole measurement day (from 12:00 AM to 11:59 PM), the water level was approximately constant during the measurement periods, except for the measurements before noon on 3 November 2021 (black lines in Figure 17).

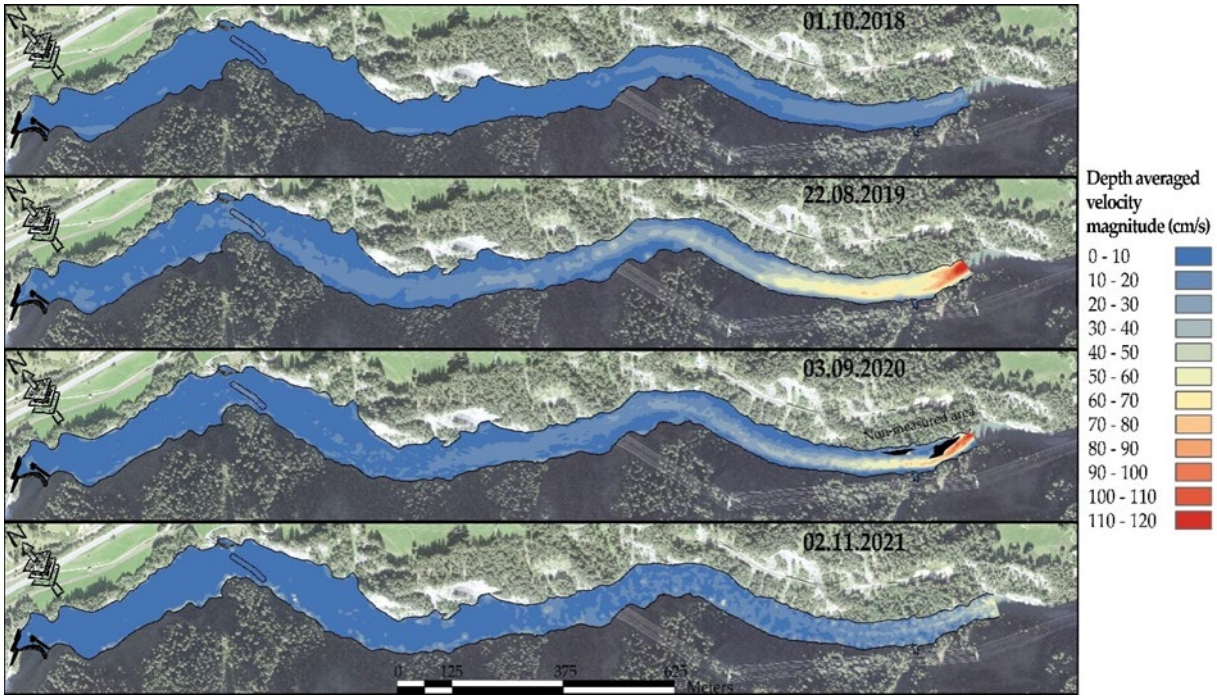

Figure 16: Interpolated depth averaged velocity magnitude along the Solis Reservoir in the four field measurement campaigns.

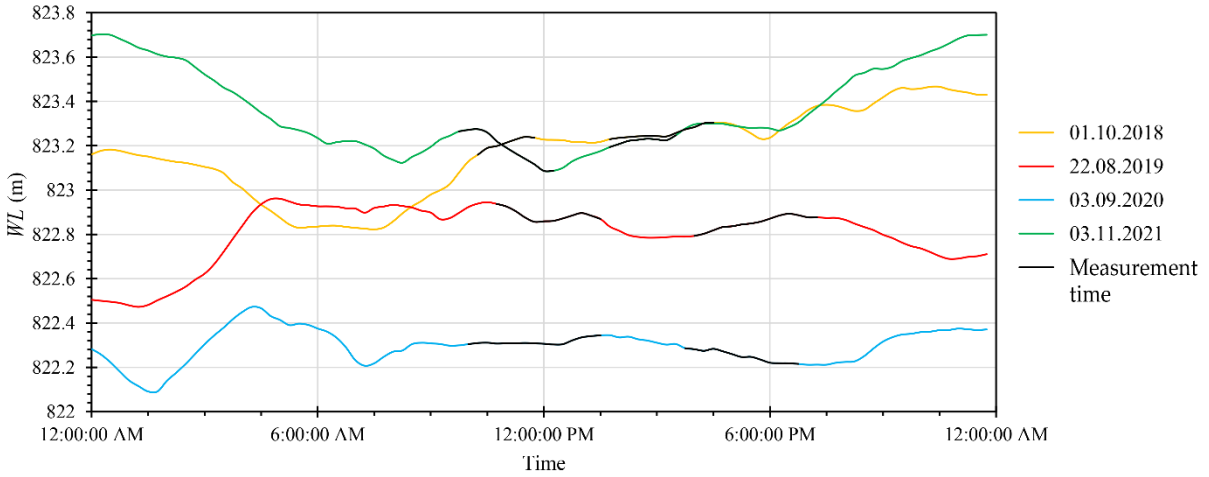

Figure 17: Fluctuations of *WL* during the field campaigns. The black lines show the fluctuations during the effective measurement periods.

Figure 18 shows cross-sectional velocity distributions at the inlet of the reservoir, i.e. location A according to Table 3 and Figure 13, for different field campaigns. The location of cross-sections in the campaigns does not exactly match and the maximum distance between them is around 40 m. At the inlet of the reservoir, because of the narrow channel width, sedimentation causes large changes in the bathymetry from year to year as depicted in Figure 18. The measured locations in 2019 and 2021 had larger widths, while the location in 2020 had the shortest width.

Figure 18a shows the measured cross section in 2018. It was in a mild bend; therefore, the approach flow accelerates to the right bank. There was also a secondary current at the left bank which is typical for trapezoidal channel. The velocity distribution shows that the higher velocity is passing from the

right bank with low velocity to the left bank. This area and the velocity distribution show the potential of sediment deposition at the left side with erosion in the right channel portion, during low discharges. Therefore, the *PSD* in the left channel is finer than the right channel.

In 2019, the cross-sectional velocity was measured 18 m downstream of the measured location in 2018. From 2018 to 2019 a large flood occurred; therefore, many sediments were eroded from the inlet of the reservoir. Due to finer sediments in the left bank, this area was eroded more than the right bank, therefore, Figure 18b shows that the left bank in 2019 is deeper than the right bank. Deformation of the bed topography changed velocity distribution. As a result, higher velocity passed from the centre of the channel, instead of the right bank and secondary currents separated at this location towards the right and left bank. The secondary cell at the right bank was because of the bend and the one in the left bank is because of the deep part in left channel as well as return flow at this location. Low velocity at left bank shows the potential location for sediment deposition in low discharges.

Figure 18c shows the deposition at the left bank from 2019 to 2020. Although cross section is measured 26 m upstream, lower velocity at the left channel caused sediment deposition at this area. There was a sedimentation patch on the left side of the measurement location in 2020. Due to low *WSE* in 2020, the sedimentation patch was non-submerged. Figure 18c shows the sedimentation patch at the left side of the measured cross section. This causes that the flow with high velocity pass from the right bank. It shows that faster velocity is passing from right bank, with a strong secondary current which is generated from the right bank to the centre of cross section. This higher velocity at right side as well as strong secondary current, causes bed erosion at this location.

Figure 18d shows the cross section measured in 2021, 15 meters upstream of the location of 2020. It shows that higher discharges with higher *WSE* caused erosion from left bank, with fined *PSD*, from 2020 to 2021. This resulted that the higher velocity pass from the centre of the channel width, with secondary flows tend to deeper part at right bank.

Overall, the velocity distributions are affected by the topographical changes at the inlet location and dynamically change year by year.

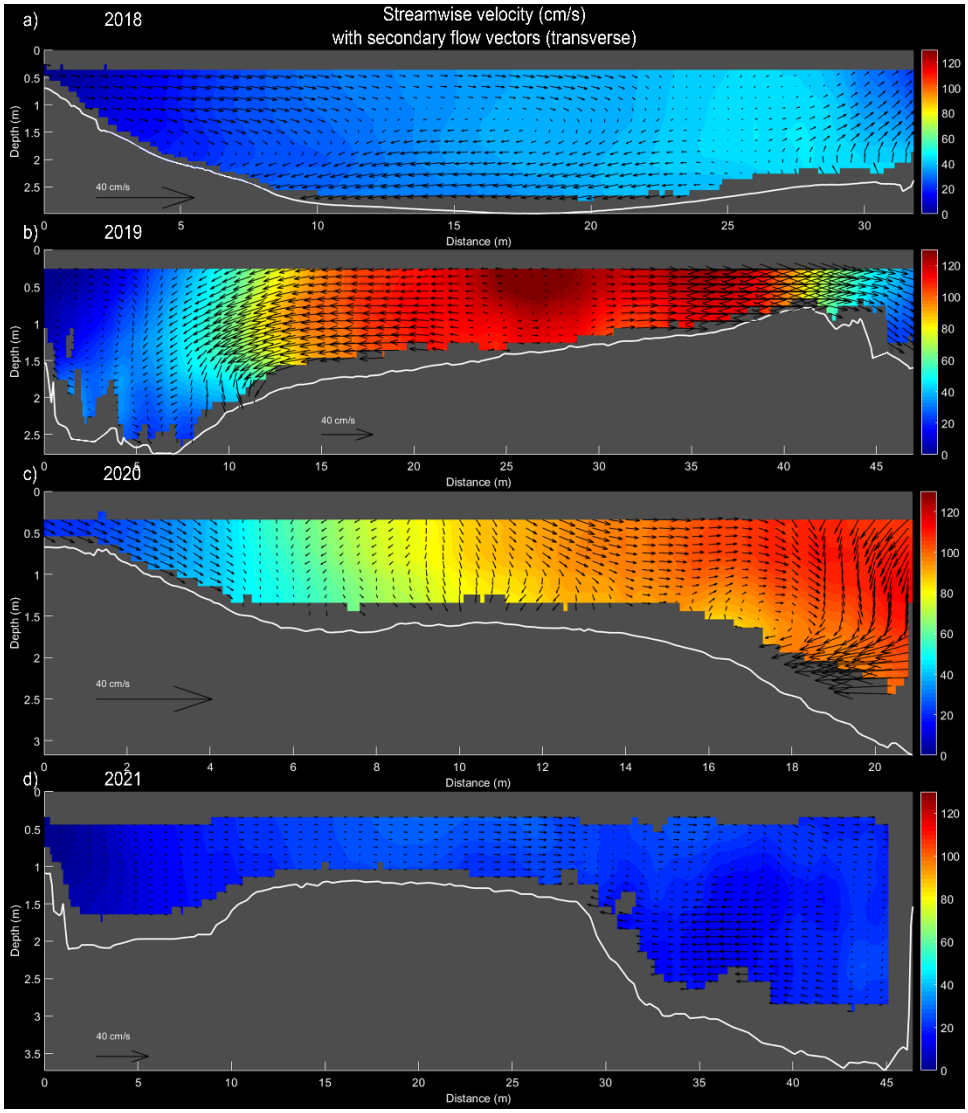

Figure 18: Velocity fields at location A with view in downstream direction. The background is the streamwise velocity and the vectors show transverse and vertical secondary currents.

Figure 19 shows the velocity field measured at location C (based on Table 3 and Figure 13), where the old dam was located (Figure 20). It is 700 m downstream of the inlet of the reservoir. Similar to cross section A, Figure 19 shows that changes of the flow discharge and *WL*, as well as locations of deposition patches in the reservoir change the velocity field. In 2018, the higher velocity is near the bed, which causes erosion of small particles, based on shear velocity, while in 2020 the higher velocity is in the regions near the water surface. This velocity distribution is also confirmed by stationary measurements of velocity in almost the centre of the channel for durations of 5 - 10 minutes (Figure 21). Figure 19 also shows that the secondary flow patterns differ over the years. The reasons are i) different operational conditions (in terms of *WL*, inflowing discharge and outflowing discharge) and ii) changes of bed morphology due to erosion/deposition in the location of the cross sections.

Velocity fields at other locations in the reservoir are presented in Appendix. Similar to cross sections A and D, velocity distributions at those locations are affected by reservoir discharge, *WL,* and bed morphology.

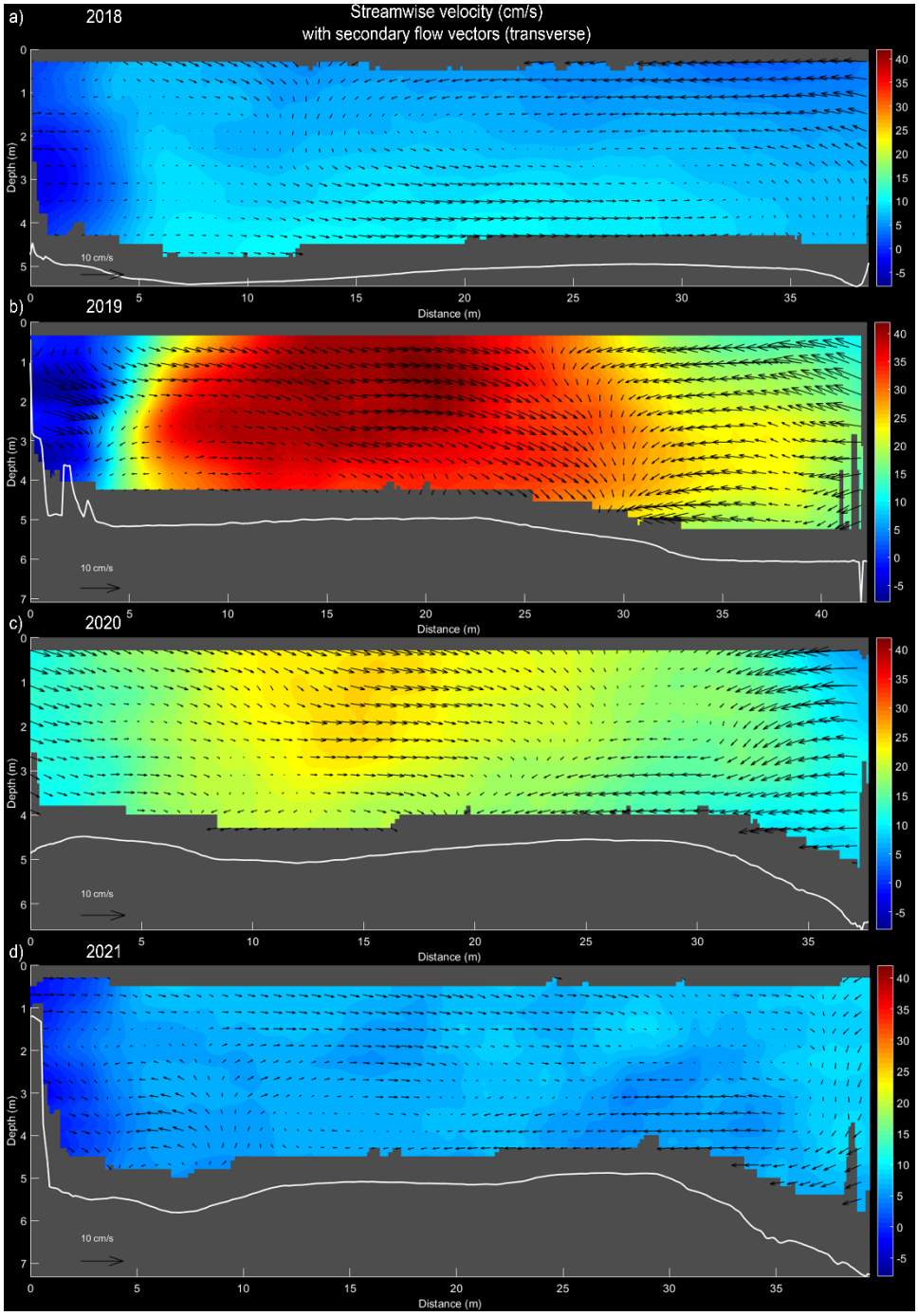

Figure 19: Velocity fields at location C with view in downstream direction. The background is the streamwise velocity and the vectors show transverse and vertical secondary currents.

Figure 20: Location of the old dam, 700 m downstream of the reservoir inlet where cross sections C were measured (photo by ewz).

In addition to cross sectional measurements, stationary measurements were also conducted at the centre of each cross section over the flow depth. Figure 21 shows streamwise time-averaged velocity profiles normalized with the corresponding maximum flow velocity (u_{max}) in different years. These velocity profiles match well with cross sectional velocity fields. The velocity profiles follow the log-law distribution with increasing velocity from the bed to the water surface at locations A, B and C near the reservoir inlet depending on the inflow discharge and *WL*. The velocity profiles differ from the log-law with almost zero velocity near the water surface and a jet-like high velocity near the bed Just before and after the guiding wall towards the dam, i.e. at locations 1695 m before the guiding wall and 1840 m, 2015 m, 2110 m and 2190 m after the guiding wall. Furthermore, at some locations, the surface flow velocity becomes negative because of the effect of boat movement, wind, or backwater effect. In general, the flow passing over the guiding wall plunges into the reservoir, creating a jet-like velocity profile, and follows the reservoir bathymetry with a steep slope until the dam (Figure 21).

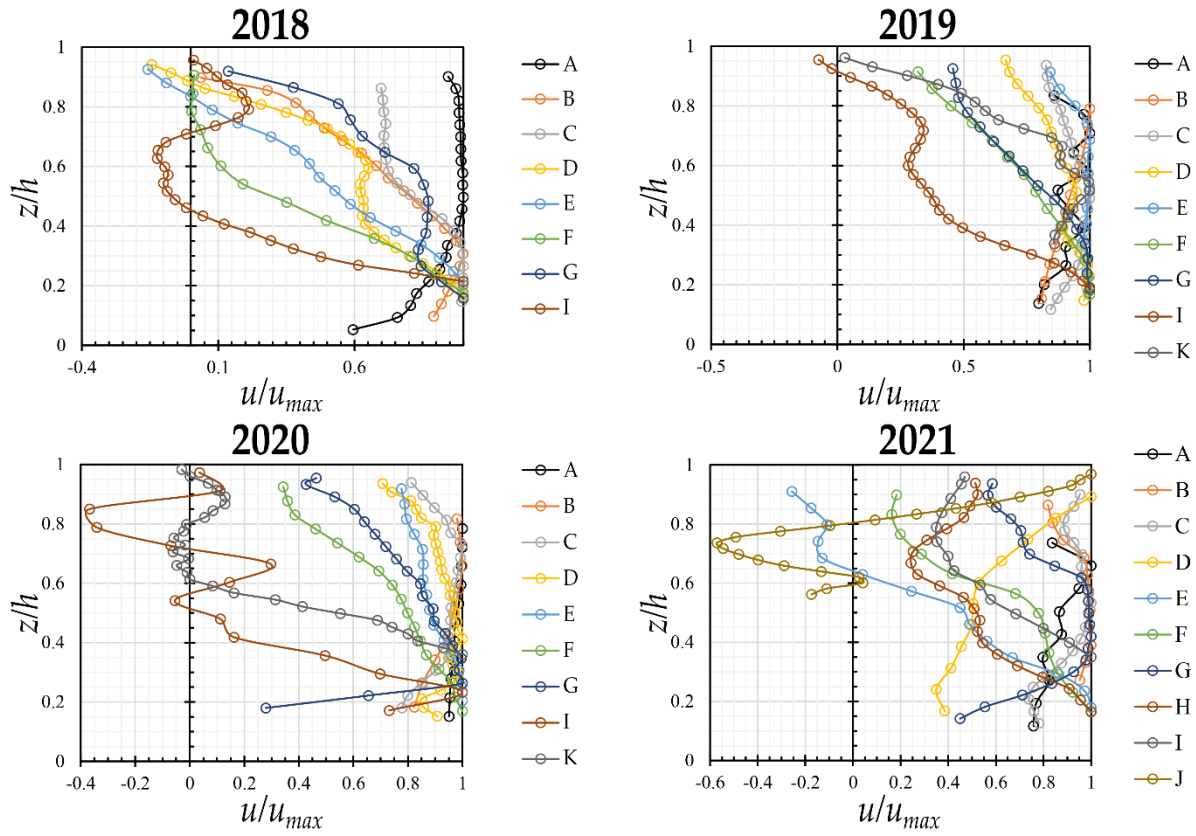

Figure 21: Velocity profiles at the centre of each cross section measured by stationary ADCP.

Figure 22 shows the streamwise time-averaged velocity profiles and corresponding low-lag fits at locations A, B and C for all yearly measurements. From the log-fits, the shear (friction) velocities were calculated at those locations. When the discharge is above 32 m^3/s in the years 2019 and 2020, the log-fit applies at locations A, B and C, i.e. until 700 m from the inlet into the reservoir (Figure 22). At a lower discharge of 27 m^3/s in 2018, the velocity profile follows the log-law at location A. In the 2021 field campaign with a discharge of 15 m^3/s, although a logarithmic distribution could be fitted to the data, the coefficient of determination R^2 is low at location A; therefore, the calculated shear velocity might be quite erroneous. It must be noted that the R^2 value in Figure 22 is based on the inner layer of the flow where the log-law is valid (green line in Figure 22).

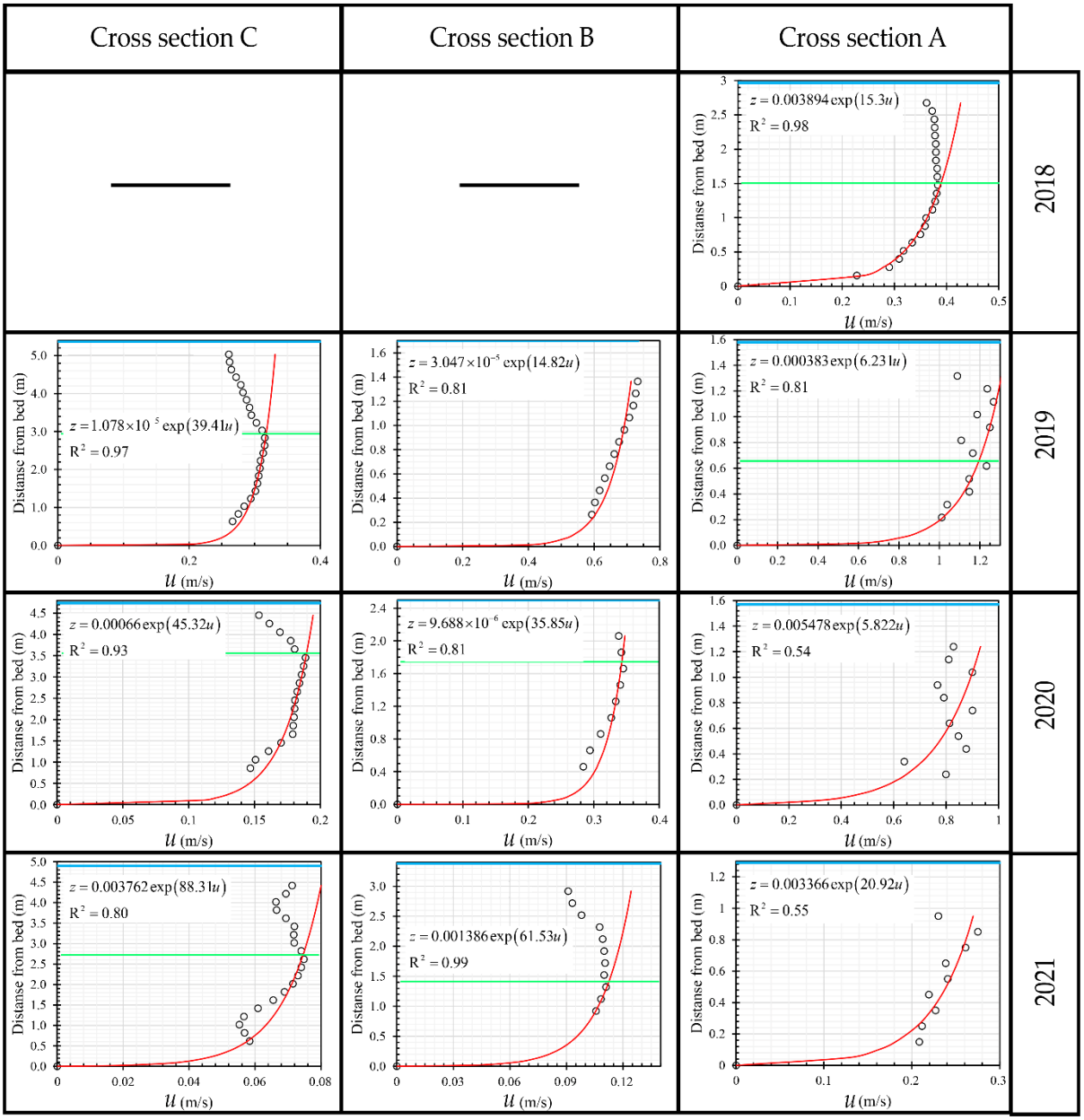

Figure 22: Calculation of shear velocties based on logarithmic velocity distributions; the green horizontal line denotes the upper location where the log-law is applied.

The energy line method (Nezu and Nakagawa, 1993) was also used to calculate shear velocities along the whole reservoir where log-fits do not apply. Table 4 shows calculated shear velocities using both logarithmic law and energy line, for the inflow discharges during the field measurements. The calculated shear velocity matches well with most of the values obtained from using log-law fits. As seen in Figure 22 the shear velocities calculated using velocity profiles do not have a perfect fit and hence the difference in the shear velocities between the log-law and energy line may be explained by these uncertainties.

Table 4: Calculation of shear velocities (m/s) using log-law and energy slope methods.

2190 (near dam) K	2110 J	2015 I	1840 H	1695 G	1590 F	1460 E	1235 D	700 C	420 B	0 (inlet) A	Distance from upstream (m) Location name	
-	-	-	-	-	-	-	-	-	-	0.0261	u_* calculated by log-law	2018
-	-	0.0009	-	0.0019	0.0013	0.0015	0.0034	0.0095	0.0052	0.0255	u_* calculated by energy line (Q = 27 m^3/s)	
-	-	-	-	-	-	-	-	0.0101	0.0266	0.0642	u_* calculated by log-law	2019
0.0017	-	0.0017	-	0.0030	0.0023	0.0026	0.0041	0.0090	0.0174	0.0409	u_* calculated by energy line (Q = 53 m^3/s)	
-	-	-	-	-	-	-	-	0.0088	0.0113	0.0687	u_* calculated by log-law	2020
0.0012	-	0.0012	-	0.0026	0.0016	0.0019	0.0029	0.0091	0.0070	0.0687	u_* calculated by energy line (Q = 32 m^3/s)	
-	-	-	-	-	-	-	-	0.0045	0.0065	0.0191	u_* calculated by log-law	2021
-	0.0003	0.0006	0.0005	0.0007	0.0007	0.0009	0.0013	0.0048	0.0037	0.0114	u_* calculated by energy line (Q = 15 m^3/s)	

It must be noted that the data presented in Table 4 are based on the assumption that the discharges are constant during the whole measurement day of each campaign. To check this assumption, measured discharges along the reservoir are presented in Figure 23. The dashed lines are the discharges measured by the operator, at the time when each cross section was measured. Figure 23 shows that the values measured by the operator and the measured values by ADCP match well in all cross sections, except for cross sections downstream of the guiding wall (i.e. above 1750 m from the inlet), which are too close to the dam and the velocity is too small, due to large water depths. The reason for the deviations at these locations lies in the limitations of ADCP in low flow velocities and ADCP measured areas near the bed (Maddahi et al., 2021).

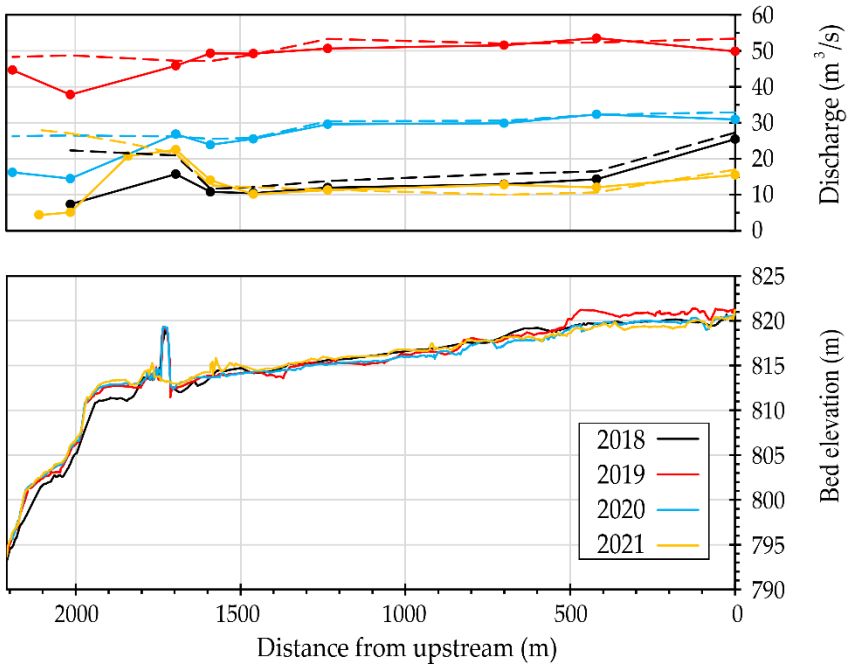

Figure 23: Discharge fluctuations along the reservoir, measured by operator (dashed lines) and by ADCP (solid lines) (top), and bed elevations along the reservoir for the respective field measurement periods.

In addition to shear velocity, the critical sediment diameters which can be transported as bedload were also determined (Table 5). The critical Shields parameter is assumed as 0.049 for movable beds in the Albula River (Müller-Hagmann, 2017). The particles with diameters larger than the calculated d_{cr} are assumed to be deposited in the cross section and particles smaller than d_{cr} will be carried by the flow to locations closer to the dam (for the discharges during field measurement campaigns). Figure 24 shows that the larger the velocity at the inlet of the reservoir, the larger particles are transported into the reservoir. Figure 24 also depicts that for all measured discharges, from 15 m³/s to 53 m³/s, particles larger than around 0.025 mm (25 μm) will be deposited in the first 1'200 m of the reservoir.

Table 5: Calculation of the critical particle diameter (µm) which can be transported with the corresponding shear velocity.

2190 (near dam) K	2110 J	2015 I	1840 H	1695 G	1590 F	1460 E	1235 D	700 C	420 B	0 (inlet) A	Distance from upstream (m) Location name	
-	-	-	-	-	-	-	-	-	-	898	d_{cr} calculated by log-law	2018
-	-	1	-	5	2	3	15	118	36	854	d_{cr} calculated by energy line (Q = 27 m^3/s)	
-	-	-	-	-	-	-	-	135	931	5417	d_{cr} calculated by log-law	2019
4	-	4	-	11	7	9	22	107	400	2197	d_{cr} calculated by energy line (Q = 53 m^3/s)	
-	-	-	-	-	-	-	-	102	169	6205	d_{cr} calculated by log-law	2020
2	-	2	-	9	3	5	11	108	65	6212	d_{cr} calculated by energy line (Q = 32 m^3/s)	
-	-	-	-	-	-	-	-	27	55	480	d_{cr} calculated by log-law	2021
-	0.1	0.5	0.3	0.7	0.7	1	2	30	19	171	d_{cr} calculated by energy line (Q = 15 m^3/s)	

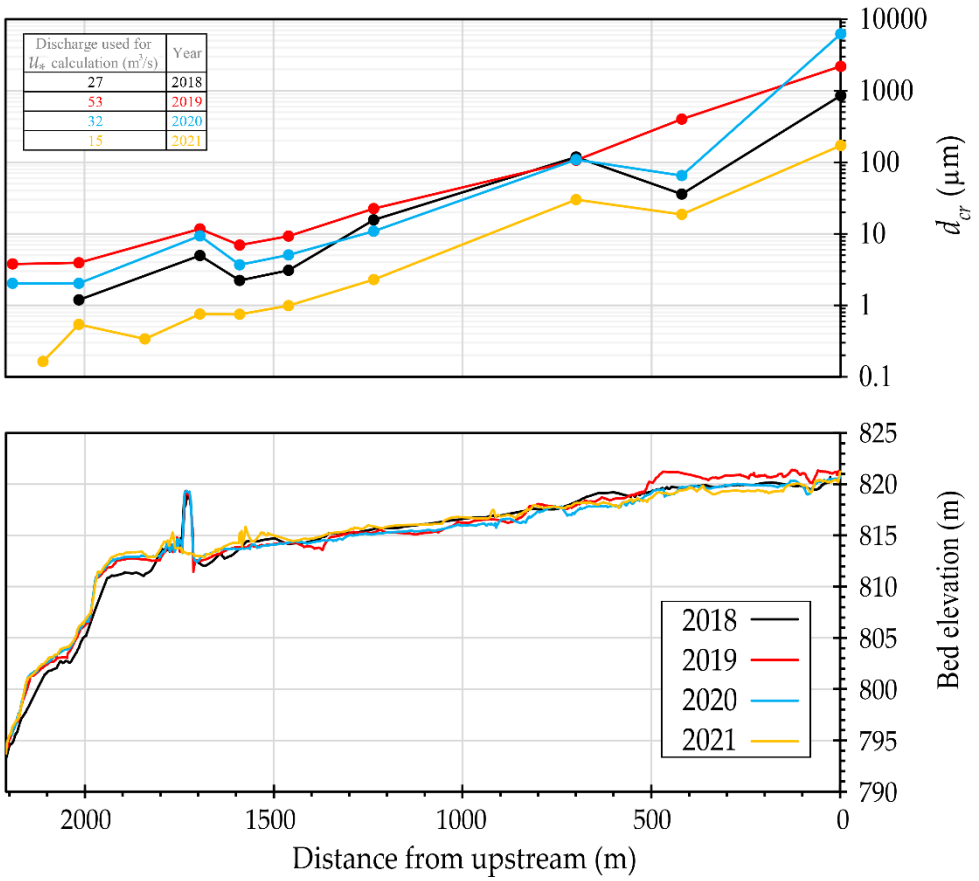

Figure 24: Fluctuations of crirtical sediment diameter along the reservoir for different discharges.

4.2 Sediment transport in Albula River

The inflow discharge to the reservoir comes from the Albula River, Julia River and HPP Tiefencastel, of which the Albula River is clearly the main sediment source. Bed load transport rates BL_{22} in the Albula River are estimated by indirect data measured using the SGPS and based on two bedload transport equations, namely, Smart and Jaeggi (1983) (SJ) and Rickenmann (2001) (RM). Figure 25 shows the discharge and BL_{22} time series from 2018 to 2021. There were no measurements from the SPGS in June, August, and September 2019, and January, February, March, and April 2020. The missing data from Albula SPGS were estimated based on the relationship between the river discharge and the bedload transport rate given by Rickenmann et al. (2020). More details on the procedures and estimated values are presented in Appendix D.

Figure 25 and Table 6 show that the SPGS measurements underestimate the volumes of BL_{22}, specially at higher discharges compared to SJ and RM estimates. The mean annual BL supply of the Albula was in the range of 40'000 m³ to 55'000 m³ (Zarn, 2009; Zarn 2010). Table 6 shows that the annual measured BL_{22} by the SPGS is much smaller than the annual supply of the Albula according to the mentioned transport formulae, which are smaller than the Zarn values because only grains above 22 mm are considered in the BL_{22} values. The differences between measured and calculated data are likely related to the effect of the flow velocity on the calibration coefficient, K_b, for the SPGS (Figure 26). The SPGS at the Albula River was calibrated during snow melt periods in May 2018, with discharges between 30 and 40 m³/s and from 45 to 60 m³/s (Nicollier et al., 2019). The measured velocities during the calibration measurements were up to 1.7 m/s and 2 m/s around 10 cm over the riverbed (Nicollier et al., 2019). Because the calibration of SPGS in the Albula was conducted at low

discharges, the obtained calibration coefficient could not accurately predict the bedload transport rates at higher discharges. For larger velocities, K_b decreases, increasing the estimated bedload mass and volume. Antoniazza et al. (2022) also stated that calculated bedload using shear stress-based equations are in excess of measured bedload mass (using SPGS) by a factor of 3 to 30.

Müller-Hagmann (2017) suggested that the average of the SJ and RM methods yields reasonable results to calculate BL_{22}. Although in Müller-Hagmann's calculations, the outputs are BL_{22}, in this study, the outputs are total BL. Then, the volume of BL_{22} is calculated as $BL_{22} = 2/3 \times BL$ (see Müller-Hagmann 2017). The average estimated annual BL_{22} based on the Rickenmann (2001) equation (BL_{22} = 25'696 m^3 → BL = 3/2 × 25'696 = 38'544 m^3) is closer to the annual BL supply of the Albula according to Zarn (2009, 2010) (40'000 m^3 to 55'000 m^3) than based on the SJ formula. Therefore, Rickenmann (2001)'s equation is used for further analysis in this study.

Table 6: Annual bedload transport (BL_{22}) calculated by different methods of Smart and Jaeggi (SJ), 1983, Rickenmann (RM), 2001 and SPGS

Year	SJ method (m^3)	RM method (m^3)	SPGS (m^3)
2018	17'115	19'181	2'664
2019	50'432	53'030	22'480
2020	5'530	6'148	1'881
2021	22'036	24'426	4'610
Total	**95'113**	**102'785**	**31'635**
Annual average	**23'778**	**25'696**	**7'909**

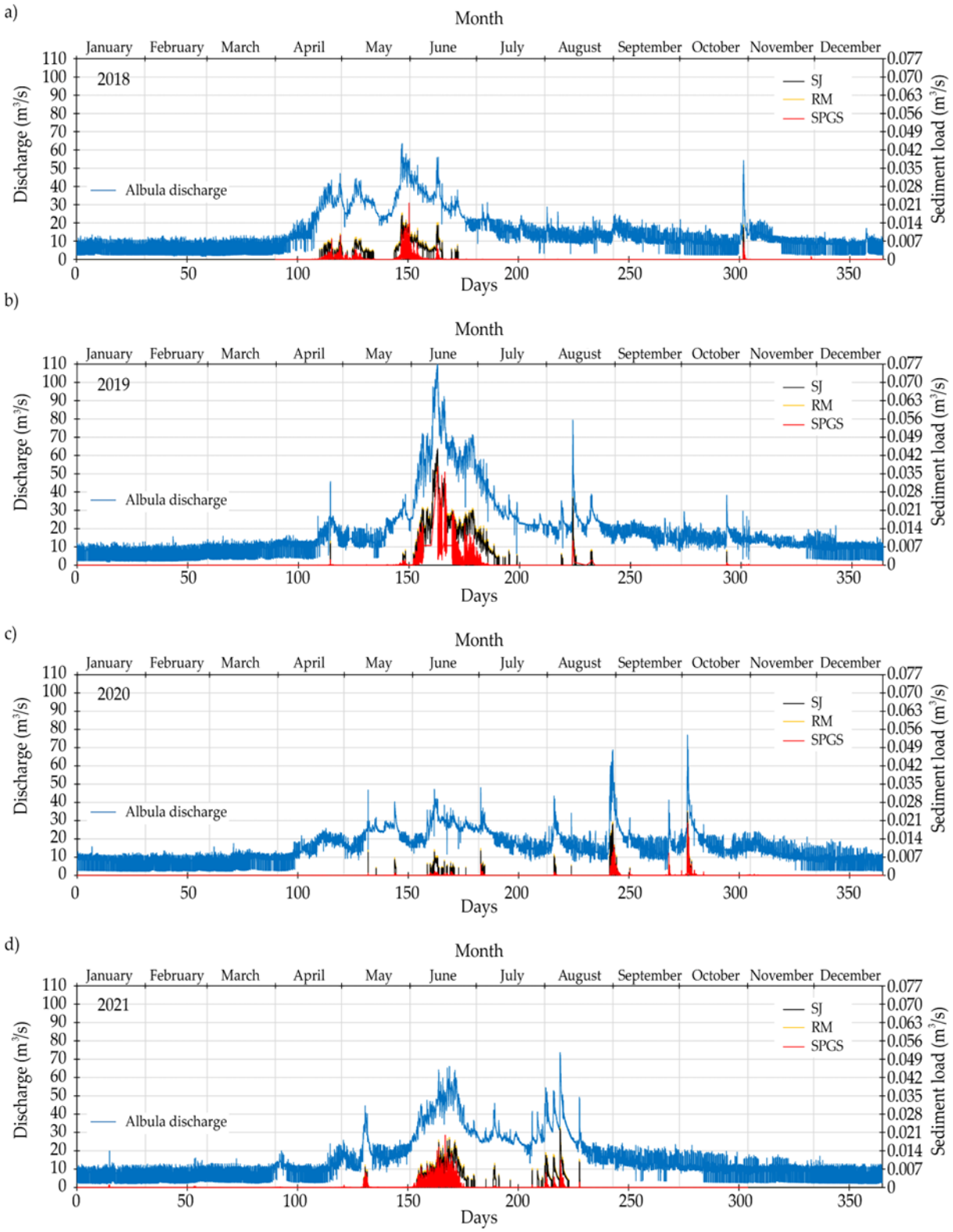

Figure 25: Hydrograph of discharge and BL_{22} transport calculated using Smart and Jaggi (1983) (black line), Rickenmann (2001) (orange line), and SPGS (red line) in a) 2018, b) 2019, c) 2020, and d) 2021.

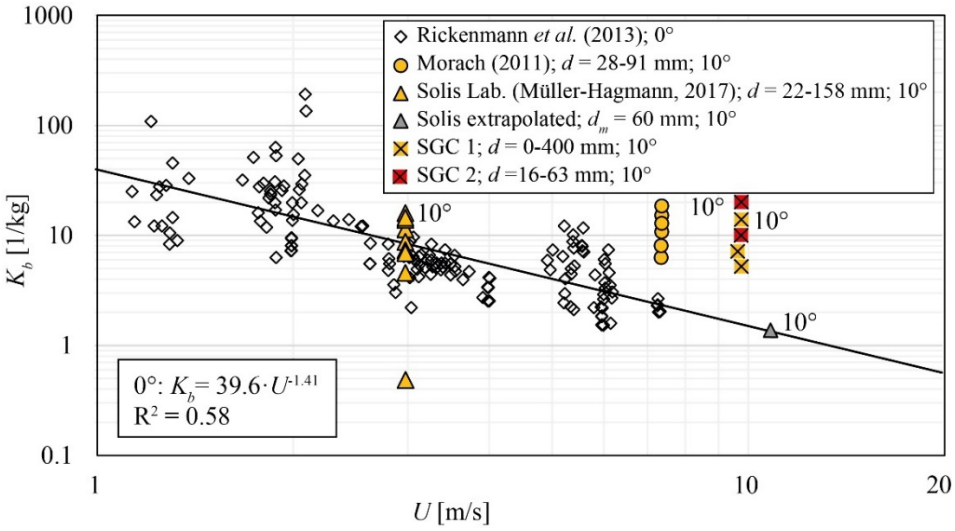

Figure 26: K_b as a function of flow velocity for different geophone inclinations and grain sizes including various data sets (SFOE project contract number SI/501609-01).

The inflow SSC_{fine} from the Albula was calculated using an *SSC*-*Q* equation (Eq. 22). The concentration was then converted to SSL_{fine} volumes by multiplying it with discharge, integrating this over time, and dividing this mass load it by the sediment density of 2'650 kg/m^3 (Eq. 23).

The inflow SSL_{coarse} was calculated based on the assumption that the total load is $TL = 4 \times BL_{22}$ (Müller-Hagmann, 2017). Then the SSL_{coarse} was calculated using Eq. (24). This equation was applied to 15-min time series data. There are three options to be considered when calculating SSL_{coarse} for time series of:

(i) low discharges with no bedload transport, but transport of suspended fines. In this case, $SSL_{coarse} = TL\ (4 \times BL_{22}) - BL_{22} - SSL_{fine}$ would become negative. Therefore, in this case, SSL_{coarse} is assumed to be 0.

(ii) moderate discharges with both transport of BL_{22} and SSL_{fine}. In these cases, SSL_{coarse} was calculated using Eq. (24).

(iii) floods when SSL_{fine} is significantly larger than BL_{22}. Then, $SSL_{coarse} = TL\ (4 \times BL_{22}) - BL_{22} - SSL_{fine}$ becomes negative. In this case, it is assumed that the calculated SSL_{fine} contains particles of less than 1 mm. Therefore, SSL_{coarse} contains particles from 1 mm to 22 mm and can be calculated as $SSL_{coarse} = BL - BL_{22}$.

The time series of BL_{22}, SSL_{coarse}, and SSL_{fine}, as well as discharge in Albula station are presented in Figure 27. The annual SSL_{fine}, SSL_{coarse} and BL_{22} and the ratio of *BL*/*SSL* is presented in Table 7. The average ratio of bedload to suspended sediment load from 2018 to 2021 is 0.52 (1:1.92) which is in the range of 1:1 to 1:2 for typical Swiss torrents (Rickenmann, 2001; Turowski et al., 2010). Only in 2020, with no flood, this ratio is 1:2.65 which is still in the range of Alpine regions (1:0.5 and 1:11 (Sommer, 1980, Lenzi and Marchi, 2000, Boes 2011)). Based on Table 7, the mean annual sediment volume in the Albula River was around 112'590 m^3 from 2018 to 2021, which is in the range of the mean annual sediment volume in the Solis Reservoir from 1986 to 2008 (111'200 m^3 given by Müller-Hagmann, 2017), verifying that our assumptions are plausible.

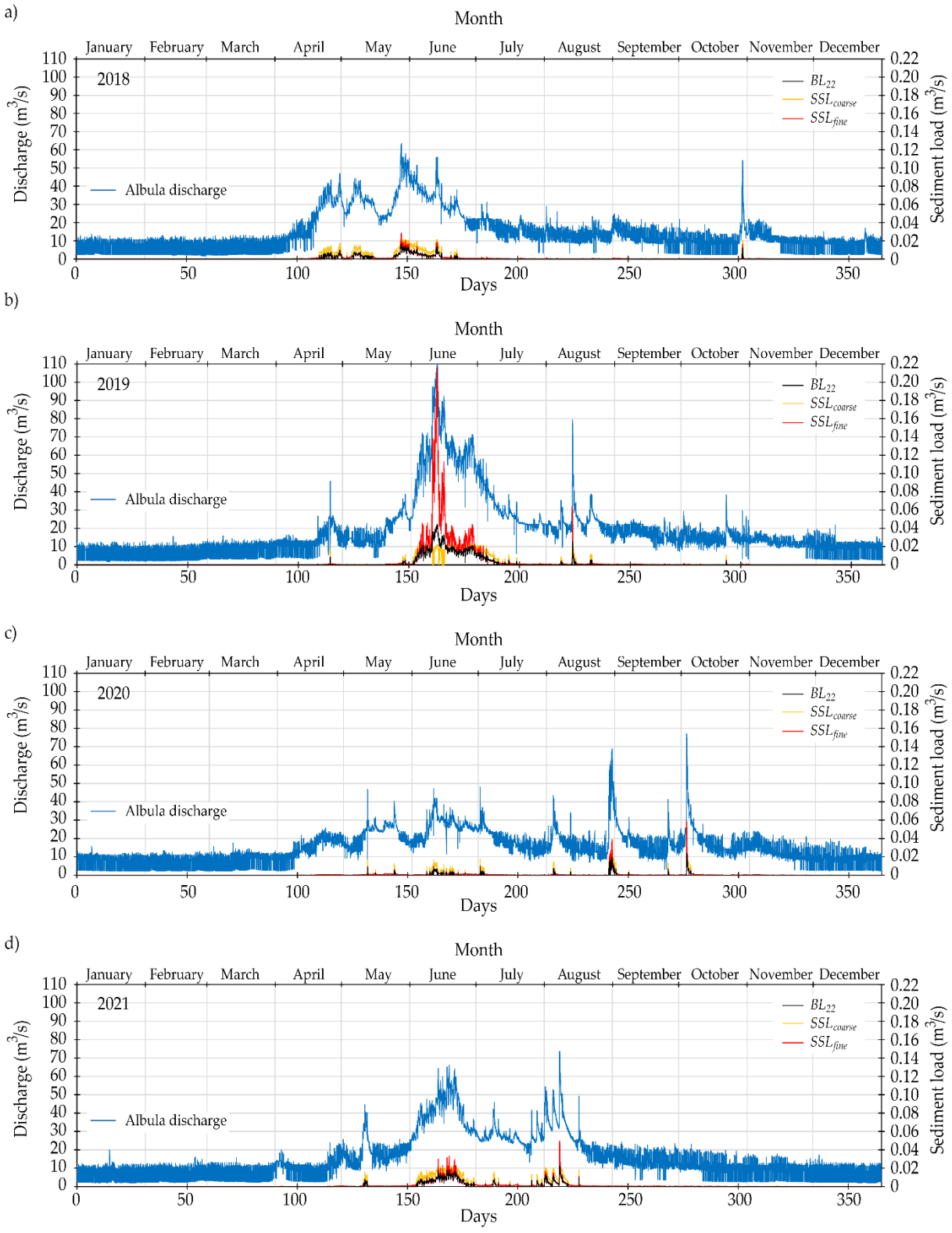

Figure 27: Hydrograph of discharge, BL_{22}, SSL_{coarse}, and SSL_{fine} in Albula River in a) 2018, b) 2019, c) 2020, and d) 2021.

Table 7: Annual sediment volumes and ratio of total bedload to suspended load in Albula River. The BL_{22} is calculated using the Rickenmann (2001) method.

Year	SSL_{fine} (m^3)	SSL_{coarse} (m^3)	BL_{22} (m^3)	**Total (m^3)**	$SSL_{<1mm}$ (m^3)	$BL_{>1mm}$ (m^3)	***BL/SSL***
2018	22'691	40'734	19'181	**82'606**	53'835	28'771	1:1.87
2019	107'690	68'907	53'030	**229'627**	150'082	79'545	1:1.88
2020	15'120	12'379	6'148	**33'647**	24'425	9'222	1:2.65
2021	30'955	49'100	24'426	**104'481**	67'842	36'639	1:1.85
Total	**176'456**	**171'120**	**102'785**	**450'361**	**296'184**	**154'177**	**1:1.92**
Annual average	**44'114**	**42'780**	**25'696**	**112'590**	**74'046**	**38'544**	**1:1.92**

4.3 Bathymetry changes

The reservoir bathymetry measured in the October 2018, August 2019, September 2020, and November 2021 campaigns are shown in Figure 28. Due to low water levels in the measurement period of 2020, there are two areas which were not submerged and hence no measurement was conducted at these areas (red areas near the reservoir inlet in Figure 28). Figure 28 also shows that the guiding wall was removed in 2021. Further measurements are required to assess the effects of guiding wall removal on sedimentation in the reservoir as well as efficiency of the SBT.

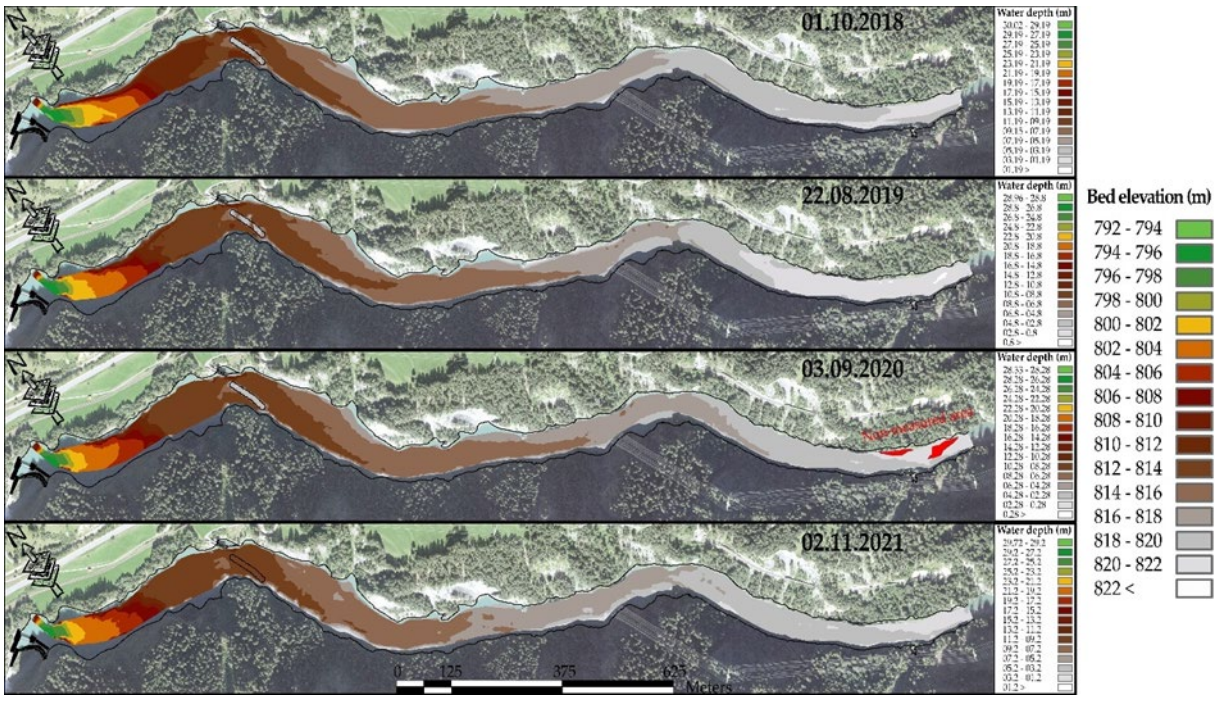

Figure 28: Bathymetry maps of Solis Reservoir in 2018, 2019, 2020 and 2021.

The volume and location of erosion/deposition in the reservoir were obtained by subtracting the new from the previous bathymetries. For this purpose, the elevation of the unmeasured locations needs to be interpolated using the measured points. The denser the measurement points, the more accurate the interpolation and final Digital Elevation Model (DEM). The size of the DEM pixels is 0.5 m × 0.5 m because of dense measured points. Smaller pixels increase the calculation time. Therefore, the resulting picture (DEM) includes pixels with dimensions of 0.5 m × 0.5 m and a unique value which shows the height of erosion/deposition at each pixel. Using the area of pixel (0.25 m^2) and height of erosion/deposition, the volume of erosion (negative)/deposition (positive) at each pixel is calculated. Figure 29 shows the DEM of the erosion/deposition between each measurement. Table 8 lists also the volumes of erosion/deposition during each year and at different zones in the reservoir. It must be noted that the values in Table 8 were recalculated, leading to very small differences to numbers given in the last annual report. The reason is that in the final calculations, the interpolated triangles were modified manually to reduce the error of interpolation. There are three different zones defined in Figure 29 and Table 8. These zones are selected for better analysis of the efficiency of the SBT and the effects of reservoir operation on sedimentation. Zone 1 is approximately the straight part of the reservoir starting from the inlet of the reservoir to 215 m upstream of the old dam. The border between zones 2 and 3 is located along the guiding wall up to the inlet of the SBT. Figure 29 shows that from October 2018 to August 2019, 63’414 ± 10'508 m^3 and 40’002 ± 7’818 m^3 of sediments were deposited and eroded in the study area, respectively. The difference between the sediment deposition and erosion results in a net sediment deposition volume of 23’412 m^3 in the reservoir in that period. Most of the sediment deposition occurred along the upstream 450 m of the reservoir (zone 1) and between the SBT inlet and the dam, i.e., along the most downstream 500 m of the reservoir (zone 3). Gravel deposition likely occurred in zone 1 during high inflow discharges with high reservoir water levels, i.e., particularly from about mid-June to beginning of July 2019, because the sediment transport capacity in the inflow region was then reduced, while there was bed load transport from upstream as the river discharges were higher than the critical discharge of 31.5 m^3/s for bedload transport (Müller-Hagmann, 2017). Deposition of finer sediment occurred in zone 3, because the bedload material such as gravel were transported through the SBT around the dam to the downstream river reach, while the suspended fines were carried with a surplus discharge exceeding the SBT discharge capacity and passing the guidance structure in front of the SBT inlet to reach the front reach of the reservoir. Because of the SBT operation in June 2019 with a significant drawdown to 813 m asl, net erosion in the reservoir took place in zone 2. The bed elevation changes between 2018 and 2019 along the longitudinal section in the centre line of the reservoir clearly show the erosion and deposition patterns (Figure 30).

For an enhanced evaluation of the reservoir operation on SBT efficiency, the bathymetry measurements conducted by the operator on 25th - 27th June 2019 were compared with our measurements in October 2018 and August 2019 (Figure 31). The operator bathymetry measurements were conducted a few days after the end of the water level drawdown to 813 m asl during SBT operation in June 2019. These measurements only included zones 2 and 3. Although the SBT was still in operation during the bathymetric measurements, the water level had risen to around 822.5 m asl, the inflow hourly discharge was between 80 and 129 m^3/s and the SBT discharge between 18 and 67.5 m^3/s (Figure 14).

The legend in Figure 31 depicts that the SBT operation at a reservoir level of 813 m asl caused 67’400 ± 9’322 m^3 of erosion in zone 2 from 1st October 2018 to 25th - 27th June 2019, while the deposition was negligeable. In zone 3, 11’443 ± 1’285 m^3 of sediment were eroded, while 13’052 ± 2’486 m^3 were deposited in this zone near the dam. It must be noted that an area within 50 m upstream of the dam was not measured due to loss of GPS signals.

Figure 31 also shows the bed level volume changes between 27th June and 22nd August 2019 when the reservoir water level was slightly fluctuating around 822 ± 1 m asl. In that period, approx. 45'762 ± 9'925 m^3 of sediment were deposited in zone 2, while the total erosion was about 10% of the deposition value. It is important to mention that sediment was also deposited in front of the SBT inlet in these two months without SBT operation. *PSD* of bed material (collected in 2019 field campaign) shows that these particles are fine sediments (Figure 38 and Figure 39). This shows that large particles were deposited in zone 1 and upstream of the reservoir inlet (no measurment), and finer particles were deposited in zone 2. Figure 31 further shows that 19'340 ± 3'790 m^3 of sediment were deposited near the dam in zone 3. In these two months in summer 2019, a total net volume of some 60'000 m^3 was deposited in zones 2 and 3 of the reservoir.

It should be noted that there was no further information on the June 2019 field campaign by the operator, therefore these values are rough calculations. To evaluate the accuracy of these volumes, inflow and outflow sediments during these periods were calculated and the results are compared with bathymetry changes. This part is presented in detail in section 4.5 of this report.

Figure 29 shows the difference plot with the sediment erosion and deposition volumes between 22nd August 2019 and 3rd September 2020. Between these dates, 23'936 ± 8'278 m^3 and 52'466 ± 6'332 m^3 of sediments were deposited and eroded in the study area, respectively. The difference between the sediment deposition and erosion results in a net sediment erosion volume of around 28'530 m^3 from the reservoir. Most of sediment erosion occurred along the first 750 m of the reservoir. From there to the SBT inlet, sediment erosion and deposition were roughly balanced. Downstream of the SBT inlet, sediment deposition was higher than erosion. These results indicate that the 4-day SBT operation under a low reservoir water level of 813 m asl between 29th August and 2nd September 2020 effectively diverted a large amount of incoming and previously deposited particles (in 2019) around the dam. As a result, after the SBT operation in 2020 the bathymetry along the first 750 m roughly returned to the bathymetry measured in 2018. This striking finding can be related to the hydrology and the SBT operation conditions in 2020 compared to 2019. In 2019, despite high to moderate inflow discharges, the reservoir water level increased from 813 m to 822.5 m asl on 19th June after bypassing a HQ_5 flood. Although the SBT was still in operation between 19th June and 9th July, due to the increased water level of 822.5 m asl, clearly above the targeted level of 816 m asl for the SBT operation, high sediment deposition occurred at the inlet of the reservoir (zones 1 and 2) and less sediment were bypassed through the SBT. On the contrary, in 2020, as the inflow discharge sharply increased at the end of August, the SBT was immediately put in operation at a low reservoir water level of 813 m asl. The inflow and SBT discharges equalled, resulting in a direct bypassing of the inflow through the SBT. In such a case, the inflow carries incoming sediment without deposition and erodes and flushes most of the sediment previously deposited.

From 3rd September 2020 to 2nd November 2021, 68'310 ± 12460 m^3 and 14'191 ± 2'969 m^3 of deposition and erosion, respectively, occurred along the reservoir, resulting in a net deposition volume of 54'119 m^3. In this period, the SBT was in operation for a few times, despite high inflows. Furthermore, the guiding wall was also removed in March 2021. This caused high volumes of sediment deposition in zone 2 and at the beginning of zone 3. Further bathymetry measurements are recommended to investigate the effect of the guiding wall removal on sediment deposition in zone 3 and efficiency of SBT.

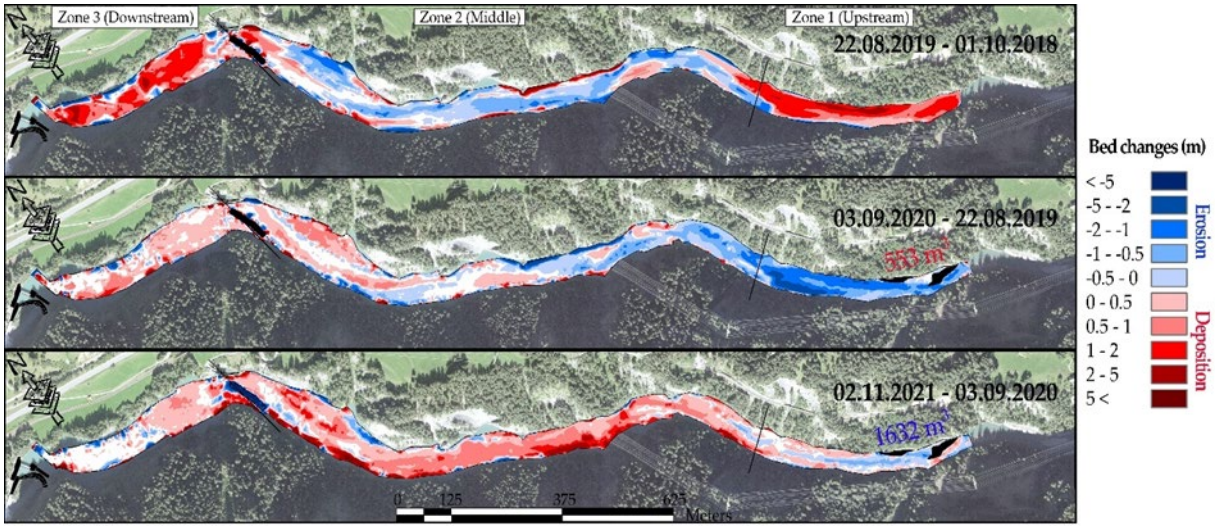

Figure 29: Annual sediment erosion and deposition in Solis Reservoir between 2018 and 2021.

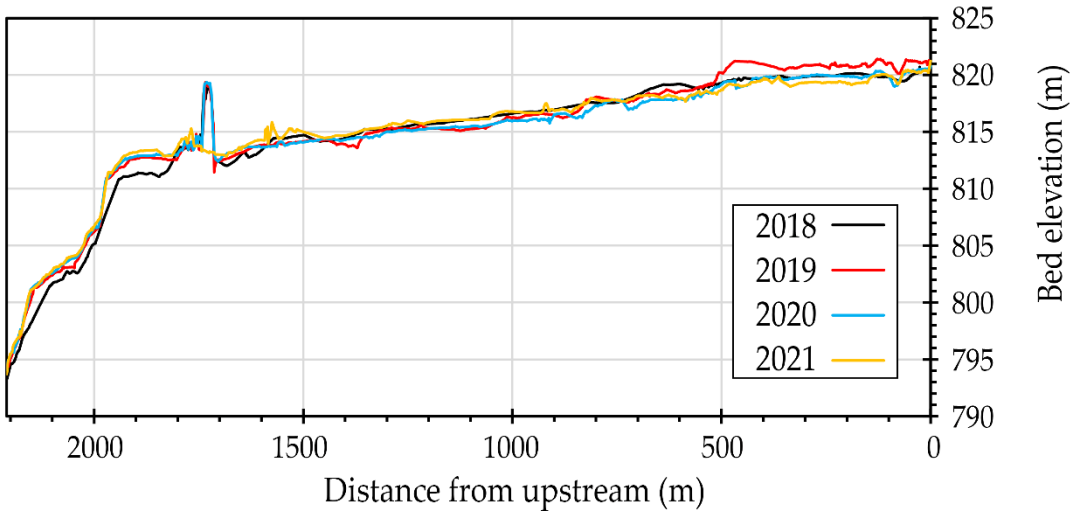

Figure 30: Longitudinal section of bed elevation changes in the center line of the Solis reservoir.

Table 8: Erosion/deposition volumes at different zones between each measurement campaign

		Zone 3 (Downstream)	Zone 2 (Middle)	Zone 1 (Upstream)	Total	**Net difference* (m^3)**
01.10.2018-22.08.2019	Erosion (m^3)	6'637 ± 1'076	31'706 ± 6'575	1'659 ± 167	40'002 ± 7'818	**+ 23'412**
	Deposition (m^3)	25'573 ± 6'141	16'923 ± 2'860	20'918 ± 1'507	63'414 ± 10'508	
	Average depth of erosion (m)	1.46 ± 0.24	0.68 ± 0.14	0.83 ± 0.08	0.77 ± 0.15	
	Average depth of deposition (m)	1.07 ± 0.26	0.81 ± 0.14	1.14 ± 0.08	1.02 ± 0.16	
22.08.2019-03.09.2020	Erosion (m^3)	2'959 ± 658	25'913 ± 4'259	23'594 ± 1'415	52'466 ± 6'332	**− 28'530**
	Deposition (m^3)	10'581 ± 4'417	13'171 ± 3'829	184 ± 32	23'936 ± 8'278	
	Average depth of erosion (m)	0.98 ± 0.22	0.71 ± 0.12	1.17 ± 0.07	0.88 ± 0.11	
	Average depth of deposition (m)	0.54 ± 0.23	0.49 ± 0.14	0.38 ± 0.07	0.55 ± 0.17	
03.09.2020-02.11.2021	Erosion (m^3)	4'631 ± 1'115	5'782 ± 1'061	3'778 ± 793	14'191 ± 2'969	**+ 54'119**
	Deposition (m^3)	12'161 ± 3'195	53'653 ± 8'596	2'496 ± 669	68'310 ± 12'460	
	Average depth of erosion (m)	1.04 ± 0.25	0.7 ± 0.13	0.4 ± 0.08	0.86 ± 0.15	
	Average depth of deposition (m)	0.76 ± 0.2	0.84 ± 0.13	0.33 ± 0.09	0.78 ± 0.14	

* Erosion in (−) and deposition is (+)

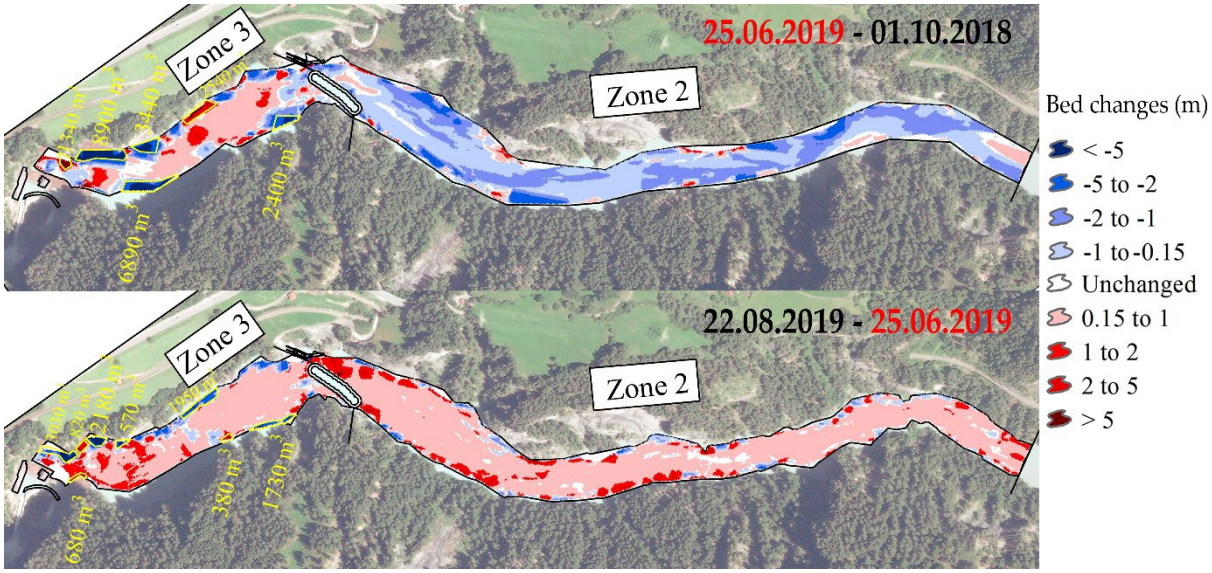

Figure 31: Sediment erosion and deposition in Solis Reservoir calculated by data from operator and ADCP (our field campaign). Blue colors show erosion and red ones show deposition. The yellow areas and volumes show larger differences between the two methods of bathymetry measurements (zig-zag measurements by VAW and cross-sectional measurements by operator). These volumes can be considered as errors of calculations and data measurements.

4.4 Sediment analysis

In this section, the sediment analysis is presented. The sediments were sampled from the bed (bed materials), and from the bottle samples at different depths (suspended materials).

4.4.1 Bed material

The bed material was collected from different locations along the reservoir, at each measurement campaign. Larger gravels existed in the upstream cross sections, cross sections 1 to 4, along the first 1'200 m of the reservoir, showing that the large particles were transported and deposited until this location. From there on, until cross section 7 which is upstream of the guiding wall, small sediment particles were deposited on the bed. In cross section 7 close to the SBT inlet and upstream of the guiding wall, larger particles, i.e. gravel, were deposited in the bed. The reason for this deposition is that these particles were carried by the flow from previous floods and could not pass the guiding wall, so deposited at this location, which shows the importance of a guiding wall to block large particles transported to the region near the dam. The collected bed materials were then analysed to determine the mineralogy of bed material as well as the effects of SBT operations on d_{50} and *PSD* at each cross section.

Figure 32 shows the mineralogy of the bed material deposited downstream of the guiding wall. This information is of prime importance for turbine and SBT abrasion studies (Felix, 2017, Demiral-Yüzügüllü, 2021). Figure 32 shows that around 33% of the minerals are Dolomite with a Mohs hardness of 4. Only 14% of the particles feature quartz minerals having the highest Mohs hardness of 7, indicating less potential for turbine and SBT invert hydroabrasion (Felix, 2017).

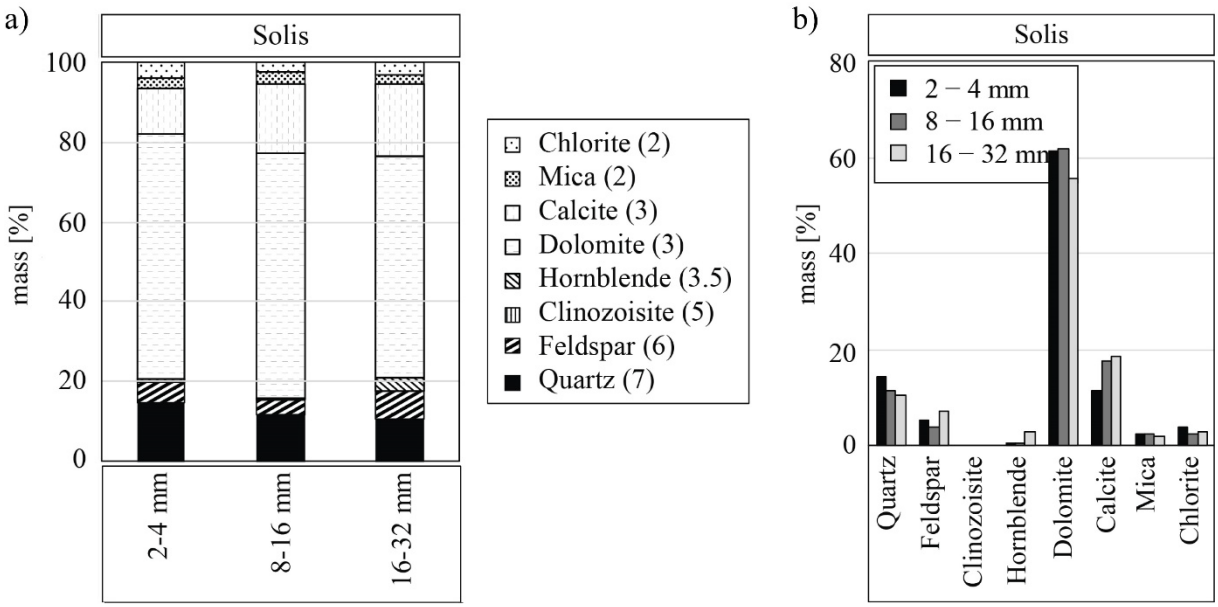

Figure 32: Mineralogical composition of the sediment transported through the Solis SBT arranged by a) sediment size and b) mineral type.

Figure 33 shows *PSD* along the reservoir in different years. The *PSD* in zone 3 (downstream of the guiding wall and close to the dam) is approximately constant during the four years of measurements, showing that only small particles (silt and clay) are passing the guiding wall, of which parts of the silt particles deposited in this zone. The *PSD* in the upstream part of the reservoir changes each year depending on the incoming floods and particularly reservoir operation. In zone 1, the particles were mainly of gravel size in 2018 while they were sandy and silty in this zone in 2019. Later, in 2020 and 2021, the *PSD* shows mostly gravel deposition in zone 1. There are two possible reasons for this difference: (i) errors in taking the bed samples (not enough samples) or (ii) effect of the operation. The device used for collecting the samples has a small opening and because of large particles in the bed, it was very difficult to collect a lot of samples at the locations in zone 1. Therefore, it is possible that the sampling device did not collect large stones in 2019 and the *PSD* tends to consist of sand particles in that year. To check if this hypothesis is true, the operational information and sediment transport from 2018 to 2019 are investigated and discussed in the next chapters. In zone 2, the *PSD* fluctuated more year by year, but still in the range of sand. Fluctuations of *PSD* in zone 2 and constant *PSD* downstream of the guiding wall in zone 3 indicate that the guiding wall has a very important role to block the larger particles at the SBT inlet before reaching the dam.

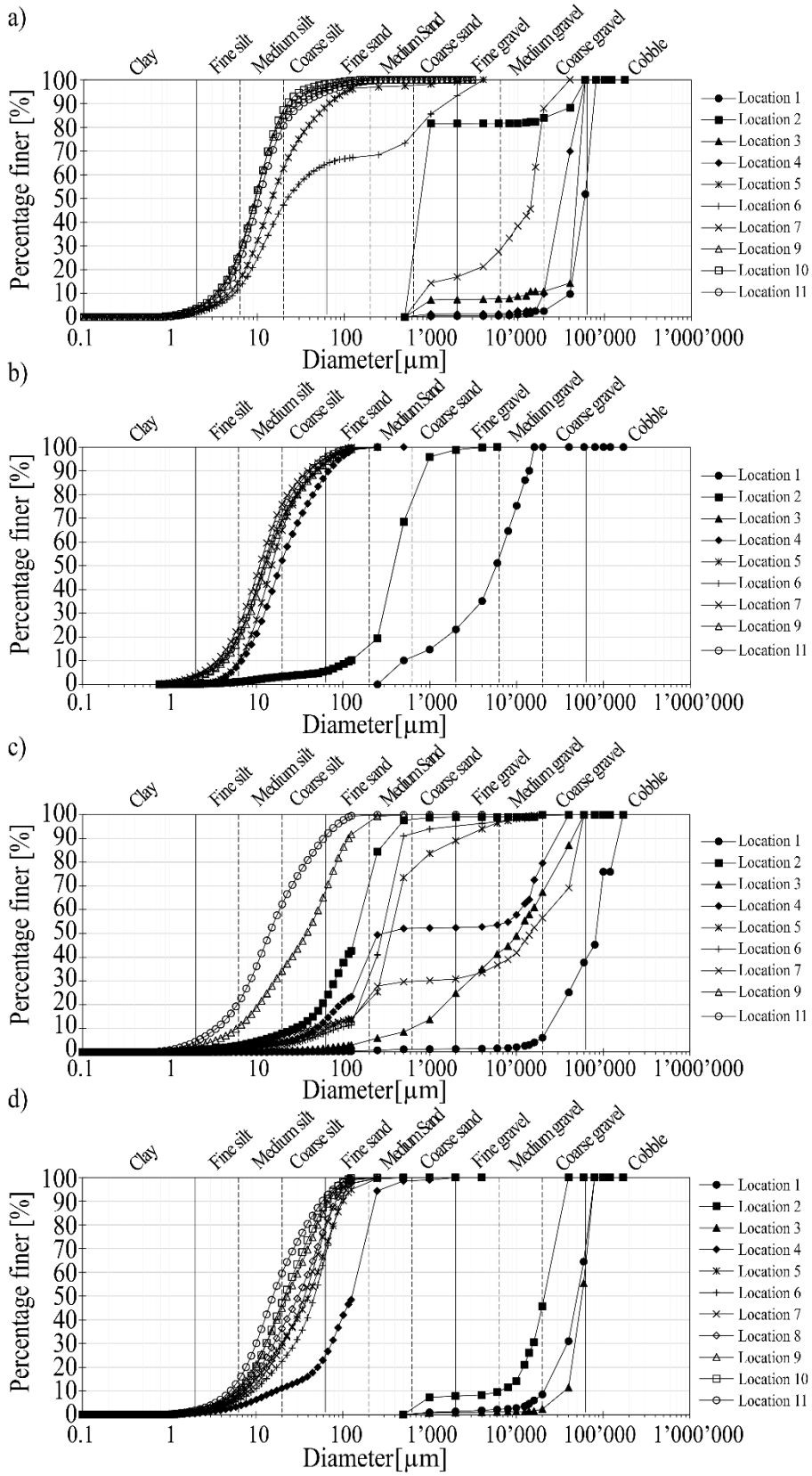

Figure 33: Particle size distribution along the Solis reservoir in a) 2018, b) 2019, c) 2020 and d) 2021.

Figure 34 shows the fluctuations of d_{50} along the reservoir in each year. Upstream of the guiding wall, the reservoir operation has a large effect on *PSD*. Fine particles (medium silt) are deposited downstream of the guiding wall. At this location, operation has a small effect on *PSD* because *WL* is high, even during high discharges. The d_{50} of the bed material close to the dam, 2'190 m downstream of the reservoir inlet, increased from 10 µm in 2018, to 16 µm in 2021. It shows that slightly larger particles passed the guiding wall, deposited on the bed and moved toward, the dam because of the gravity force due to the large bed slope. Around 200 m upstream of this location, i.e. 2'015 m downstream of the reservoir inlet, d_{50} increased from 9 µm (medium silt) in 2018 to 38 µm (coarse silt) in 2020, and then decreased to 23 µm in 2021. This indicates that reservoir operation can have an impact when the SBT is in operation during high *WL*. Due to the large bed slope of the reservoir in this zone 3, deposition of particles in this region caused movements of the deposited particles towards the dam not only because of the shear velocity but also because of the gravity force. Increasing sediment deposition in this region might endanger the life of the dam and might increase turbine abrasion in the future if sediment particles are resuspended.

The distribution of d_{50} along the reservoir each year matches with bathymetry changes (Figure 29 and Figure 31) and with the hydrograph of inflowing discharge and sediments to the reservoir (Figure 14 and Figure 27). In 2018, coarse particles exist in zones 1 and 2 in the upstream and middle parts of the reservoir. Figure 31 shows that in June 2019 the sediments were eroded by the incoming flood water and SBT operation with low reservoir *WL*. From June 2019 to the next measurement campaign in August 2019, the discharge to the reservoir was not large enough to transport bedload into the reservoir, but it was still large enough to transport fine sediments. Due to the increase of *WL* in the reservoir, fine particles were deposited upstream of the guiding wall (Figure 31). For that reason, the d_{50} distribution in 2019 is finer than 2018.

The bathymetry measurements of 2020 show erosion mainly from zone 1, to a lesser extent also from zone 2 (Figure 29). This erosion was caused by the SBT operation a few days before field measurements. In this operation, the reservoir *WL* was lowered down to around 814 m asl (Figure 14). This caused erosion of fine particles that were transported towards the SBT inlet, while larger particles remained at their position. As a result, d_{50} increased in 2020 compared to 2019.

From 2020 to 2021, the SBT was not in operation for a long time. Therefore, large particles transported by the approach flow were deposited in zone 1, and fine particles deposited in zone 2.

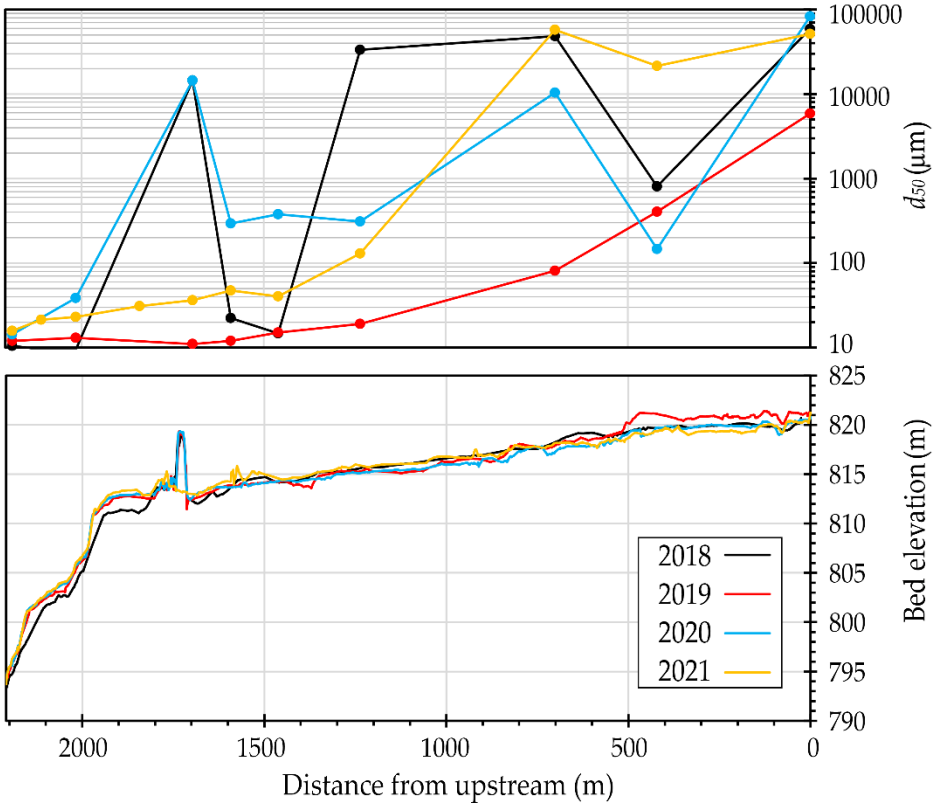

Figure 34: Fluctuations of d_{50} (upper) and bed elevation changes in the center line (lower) along the Solis reservoir from 2018 to 2021.

4.4.2 Suspended materials

The water flow into the reservoir is carrying suspended sediments. To obtain *SSC*, bottle samples were collected along the reservoir at different water depths. Due to the small inflow into the reservoir and the dilution of particles, the measured *SSC*s were very low during the measurement campaigns.

Figure 35 shows the contour maps of the measured *SCC* along the reservoir from 2018 to 2021. As the discharge in 2018 was low, the *SSC* values were very low and approximately uniform along the reservoir. Therefore, SSL_{fine} during low discharges are expected to be deposited in zone 3 between the guiding wall and the dam.

The reservoir discharge in 2019 was 53 m³/s and the velocities were higher than in other years. Figure 35 also shows that the *SSC* were approximately 10 times higher than those in 2018. The *SSC* were approximately constant from the inlet of the reservoir to the guiding wall, around 26 mg/l, showing no deposition and dilution of suspended sediments in this region, i.e., zones 1 and 2. After the guiding wall, the *SSC* decreased down to 14 mg/l close to the bed showing the desilting effect of the reservoir (Figure 35). Furthermore, after the guiding wall (zone 3), the *SSC* close to the bed was higher than the *SSC* close to the water surface, resembling the classical Rouse profiles. The incoming discharge of the Albula was around 25 m³/s on the measurement day in 2019, carrying suspended sediments with concentration and transport rates of around 101 mg/l and 0.96 l/s upstream of the Solis reservoir, respectively. The suspended transport rate at the inlet of the reservoir was 0.52 l/s. Therefore, at high discharges, around 46% of the incoming suspended sediments were deposited upstream of the reservoir inlet, in the gravel excavation area. The reason for this is that for higher discharges, larger particles were transported by the flow. By getting closer to the reservoir, the increasing water depth and decreasing flow velocity caused deposition of larger particles, so that the transport rate decreased

at the inlet of the reservoir. However, at lower discharges, very small particles were transported by the flow. The settling velocity of these small particles is so low that they do not settle to the bed even within the reservoir. Therefore, the transport rate remained uniform along the reservoir (as in 2018).

The inflow discharge to the reservoir in 2020 was 32 m^3/s, which is higher than the discharge in 2018, and the *SSC* was therefore slightly higher than in 2018. Figure 35 shows that the *SSC* decreased in zone 2, around 700 m upstream of the guiding wall, showing the desilting effect of the reservoir in zone 2. The suspended load transport rate at the inlet of the reservoir was 0.17 l/s. The discharge in the Albula river was around 25 m^3/s, like in 2019. Therefore, the SSL_{fine} in the Albula was 0.96 l/s. This shows that around 82% of fine suspended sediments were deposited upstream of the reservoir inlet.

The *SSC* in 2021 was measured by both bottle sampling and LISST (Figure 35). Using LISST dense *SSC* profiles in the water column were measured. Figure 35 shows that the values measured by LISST are around three times higher than the bottle samples. These deviations may be caused by the low suspended sediment concentrations and the application of the devices. Bottle sampling represents is a point measurement device, so that the *SSC* is affected by the instrument during sampling. The inflowing discharge to the reservoir was 15 m^3/s in 2021, i.e. the lowest discharge of all campaigns. Consequently, the *SSC* was very low, around 6 mg/l, from the inlet of the reservoir over around 1'500 m in downstream direction. The *SSC* increased to around 14 mg/l close to the previous location of the guiding wall and then decreased to 8 mg/l by getting closer to the dam. This increase of the concentration to a peak close to the guiding wall may be due to the construction operations of guiding wall removal, because the armoring of the bed was reduced and the small particles in this area were suspended more easily. On the other hand, the velocity distribution (Figure 21) shows that at low discharges, the flow featured higher velocities near the bed, causing resuspension of fine particles at this location. Figure 35 also shows that the concentration near the bed was relatively high in the location of the removed guiding wall.

Overall, measurements of SSC_{fine} show that most of the suspended particles were deposited upstream of the reservoir inlet, around the excavation area. The remaining suspended sediments were carried to the reservoir and deposited after the guiding wall in zone 3, based on the density of the particles and large flow depths with low flow velocities.

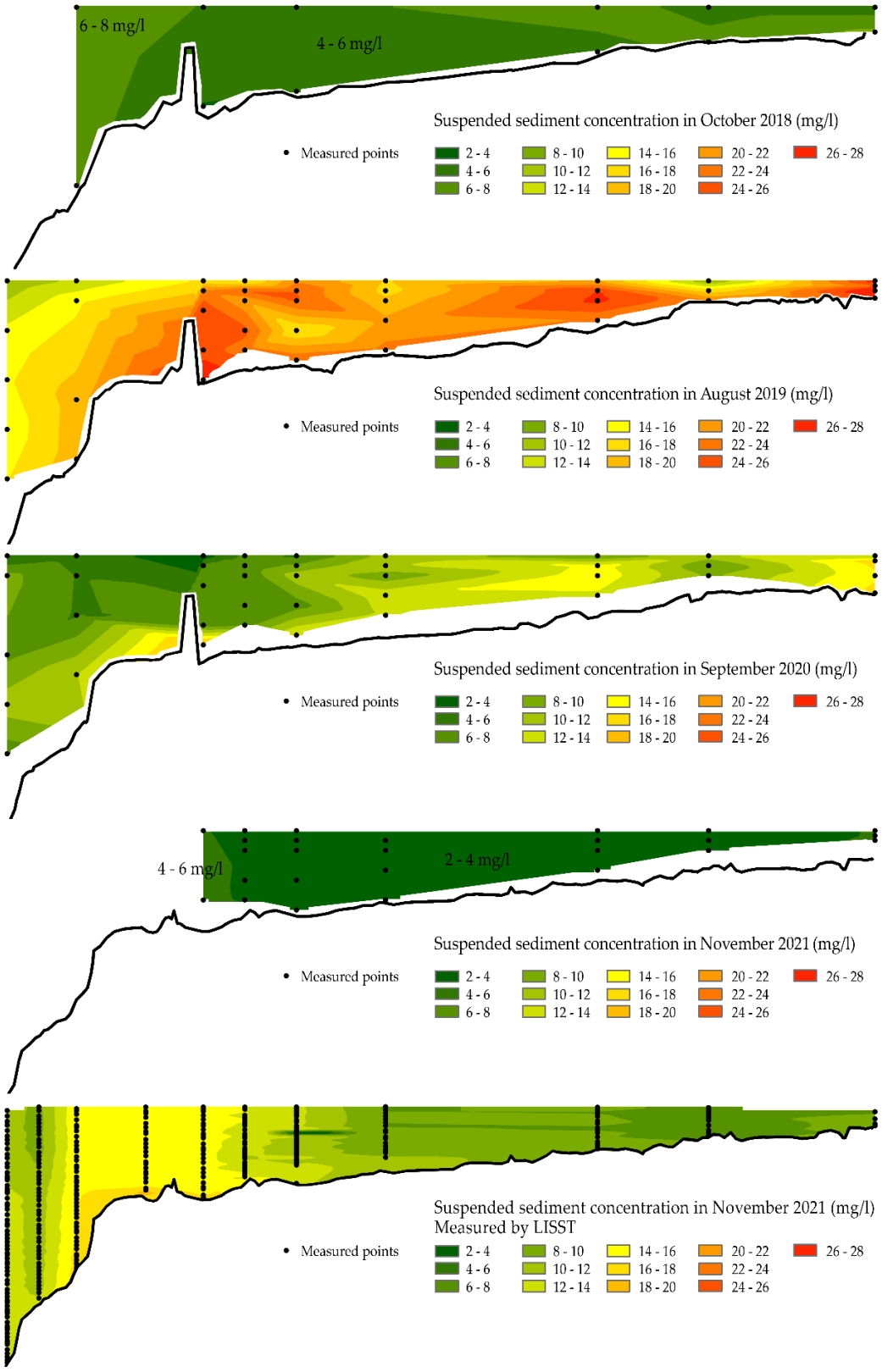

Figure 35: *SSC* distribution from bottle samples along the reservoir at different flow depths during each measurement campaign, and from LISST measurements for the November 2021 campaign (lowest figure).

To calculate the critical particle diameters which can settle along the reservoir, the settling velocities were calculated using the shear velocities for each measurement day. Figure 36 shows the dimensions of the suspended particles which can settled at each location. For a very low discharge into the reservoir (15 m^3/s in 2021), particles below 20 µm were deposited at 2'190 m downstream of the reservoir inlet (close to the dam). For relatively high discharge into the reservoir (53 m^3/s in 2019), particles below 44 µm were deposited in the same location. The *PSD* in the bed, in this location close to the dam, also shows that the d_{50} was 10 µm in 2018 and increased to 16 µm in 2021 (see Figure 33 and Figure 34). At the inlet of the reservoir, the d_{50} values of the settled suspended particles were from 150 µm to 640 µm in 2021 and 2020, respectively.

Overall, at the inlet of the reservoir, the bed shear velocity and bedload have more effects on d_{50} mainly in zone 1 and to a reduced extent in zone 2. No bedload is found in zone 3 due to the guiding wall effect keeping bedload upstream. However, the suspended sediment particles settle in zone 3 and their d_{50} in this zone is governed by the settling velocity. Therefore, further measurements are required to assess the effects of the guiding wall removal on the *PSD* of the bed material in zone 3.

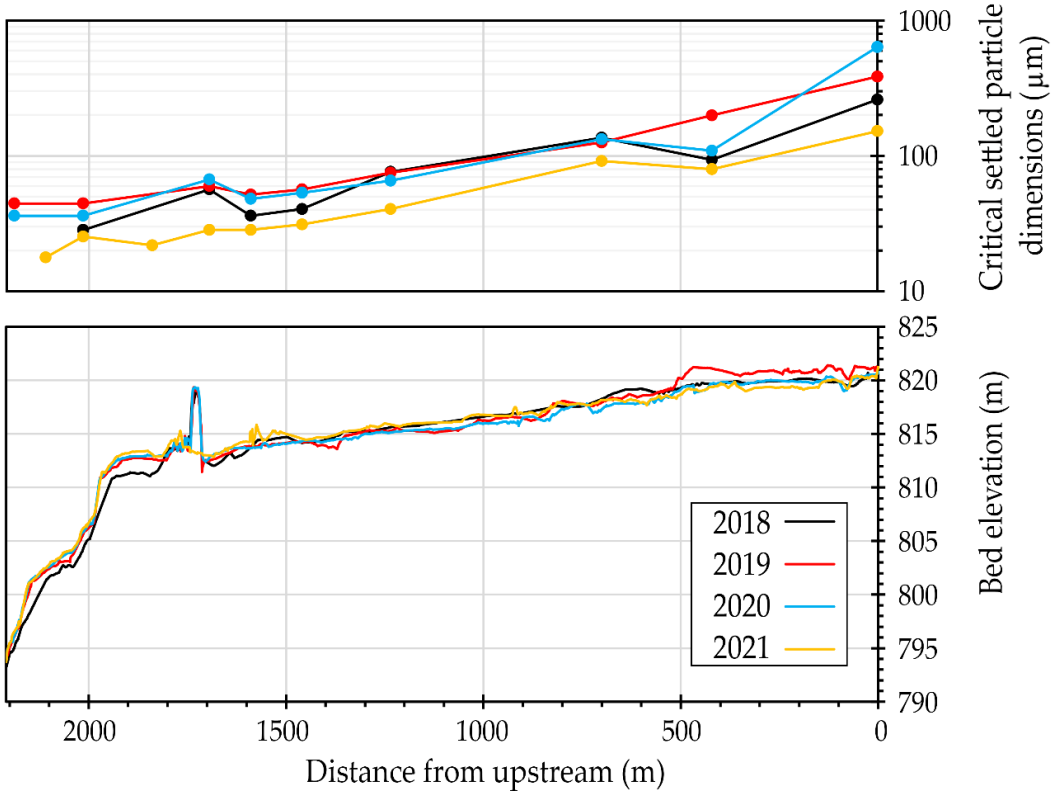

Figure 36: Critical settled paricle diameters along the reservoir for the different measurement campaigns (upper) and corresponding bed elevations (lower).

4.5 Sediment balance and bypass efficiency

4.5.1 Sediment balance

The main goal of this study is to evaluate the bypass efficiency of the reservoir (BE_r) under different reservoir and SBT operational conditions. BE_r is the ratio of outflow sediment volume to inflow sediment volume. For this purpose, the assumptions and developed equations are evaluated in this section. To validate our assumptions, the net volume between the incoming sediments and outgoing

sediments is compared to the net volume between erosion and deposition obtained from the bathymetry measurements. The main source of sediment input into the reservoir is the Albula River (supplying BL_{22}, SSL_{coarse}, and SSL_{fine}) plus 4'800 m^3/year of SSL_{fine} coming from HPP Tiefencastel. The main source of outflow sediments is the SBT (BL_{22}, SSL_{coarse}, and SSL_{fine}) plus 31'400 m^3/year from excavation (assuming that 50% is BL_{22} and 50% is SSL_{coarse}) and 16'300 m^3/year of SSL_{fine} being vented via the power waterways of HPPs Sils and Rothenbrunnen as well as through dam outlet structures like e-flow dotation, bottom outlet and spillway.

Table 9 shows that the net balance of sediments in the periods of 2018 – 2019 and 2020 – 2021 matches well with the results obtained from bathymetry calculations (with less than approximately 15% difference). For the period of 2019 – 2020, the difference between the bathymetry measurements and in- and outflow sediment balance is around 28%, which is still good for sediment studies. One reason for this high difference is that the period of 2019 – 2020 was a dry year with very low discharges into the reservoir. Therefore, the outflow SSC_{fine} from HPPs and dam structures was likely below the yearly average of 16'300 m^3. Considering this effect, the net sediment difference is expected to be similar to the net bathymetry difference. However, because no sediment measurement device is installed at HPP Rothenbrunnen and the dam outlet structures, the exact volume of outgoing sediments could not be measured. To improve this, the installation of continuous suspended sediment monitoring devices in real-time at the inlet and outlet of the reservoirs is required. Overall, the differences show that the equations and assumptions made to calculate inflow and outflow sediment volumes work well for the Solis Reservoir during normal hydrological years, and are still in a reasonable range in dry years.

Besides the periods mentioned in Table 9, the bathymetry changes from October 2018 to June 2019 and from June 2019 to August 2019 were calculated using the data provided by the operator. The bathymetry measurements on 25 June 2019 were conducted after SBT operation at a reduced *WL*. This SBT operation lasted from 10th until 17th of June 2019. The geophones also measured BL_{22} during this period. After this period, from 17th to 25th June 2019, although the SBT was still in operation, the *WL* was increased to 822 m. Therefore, it is assumed that only a small volume of sediments was transported to zones 2 and 3 from 17th to 25th June and this volume can be neglected in the calculation underlying Table 10, which shows the inflow and outflow sediment volumes between October 2018 and June 2019, and from June 2019 to August 2019, respectively. A total volume of 122'707 m^3 of sediments was transported by the Albula into the reservoir from beginning of October 2018 to end of June 2019. Within the same period of 9 months, 3'600 m^3 of SSL_{fine} were transported through HPP Tiefencastel into the Solis reservoir. The SBT bypassed 156'014 m^3 of sediments out of the reservoir. Assuming a constant rate of excavation and reservoir operations during a year, the volumes of 23'550 m^3 and 12'225 m^3 were excavated and released through HPPs and dam outlet structures, respectively. Therefore, a net volume of 65'482 m^3 was removed from the reservoir, which matches well with the bathymetry changes in this period (around 6% difference).

From June 2019 to August 2019, 106'834 m^3 of sediments were transported into the reservoir by the Albula River. At the same time, 800 m^3 of SSL_{fine} were supplied by the HPP Tiefencastel. The SBT bypassed 7'718 m^3 of sediments, including BL_{22}, SSL_{coarse} and SSL_{fine}, and in addition 5'232 m^3 of sediments were excavated and 2'716 m^3 of sediments were bypassed through the HPPs and dam outlets. Therefore, a net volume of 91'968 m^3 was deposited in the reservoir during this period of only two months. The bathymetry changes (Figure 31) in this period show a large volume of sediment deposition in zones 2 and 3, with a net deposition volume of 59'769 m^3. It must be noted that the operator only measured in zones 2 and 3; consequently, there is no information of sediment changes in zone 1 for these two periods. Therefore, the majority of the net difference of 91'968 – 59'769 = 32'199 m^3 of sediments is assumed to be deposited in zone 1 and upstream of the reservoir, because sediments were not transported to zone 2 and deposited in the upstream due to low flow velocities in this later period from June to August 2019.

Table 9: Incoming and outgoing sediment volumes between each measurement campaign.

Periods	Inflow sediment volumes by Albula River		Inflow sediment volumes by HPP Tiefencastel	**Total sediment inflow (m^3) (+)**	Outflow sediment volumes by SBT			Outflow sediment volumes by excavation		Outflow sediment volumes by HPPs and dam outlets	**Total sediment outflow (m^3) (-)**	Net sedimentation difference (m^3)	Net bathymetry difference (m^3)
	BL_{22} (m^3)	SSL_{coarse} (m^3)	SSL_{fine} (m^3)	SSL_{fine} (m^3)		BL_{22} (m^3)	SSL_{coarse} (m^3)	SSL_{fine} (m^3)	BL_{22} (m^3)	SSL_{coarse} (m^3)	SSL_{fine} (m^3)			
01.10.2018 – 22.08.2019	53’371	69’696	106’474	4’400	**233’941**	22’509	26’375	114’848	14’392	14’392	14’942	**207’458**	+ 26’483	+ 23’412
22.08.2019 – 03.09.2020	4’688	9’742	13’481	4’800	**32’711**	2’801	9’986	8’766	15’700	15’700	16’300	**69’253**	− 36’542	− 28’530
03.09.2020 – 02.11.2021	25’923	51’821	34’466	5’600	**117’810**	1’677	7’910	7’140	18’316	18’316	19’016	**72’375**	+ 45’435	+ 54’119

Table 10: Incoming and outgoing sediment volumes from October 2018 to June 2019, and from June 2019 to August 2019.

Periods	Inflow sediment volumes by Albula River		Inflow sediment volumes by HPP Tiefencastel	**Total sediment inflow (m^3) (+)**	Outflow sediment volumes by SBT			Outflow sediment volumes by excavation		Outflow sediment volumes by HPPs and dam outlets	**Total sediment outflow (m^3) (-)**	Net sedimentation difference (m^3)	Net bathymetry difference (m^3)
	BL_{22} (m^3)	SSL_{coarse} (m^3)	SSL_{fine} (m^3)	SSL_{fine} (m^3)		BL_{22} (m^3)	SSL_{coarse} (m^3)	SSL_{fine} (m^3)	BL_{22} (m^3)	SSL_{coarse} (m^3)	SSL_{fine} (m^3)			
01.10.2018 – 25.06.2019	27’401	26’949	68’357	3’600	**126’307**	22’504	23’621	109’889	11’775	11’775	12’225	**191’789**	−65’482	− 61’938
25.06.2019 – 22.08.2019	25’970	42’747	38’117	800	**107’634**	5	2’754	4’959	2’616	2’616	2’716	**15’666**	+ 91’968	+ 59’769

4.5.2 Bypass efficiency of the reservoir

Table 9 and Table 10 show that the sediment balances of Solis Reservoir based on the assumptions and calculations match well with the direct measurements of bathymetry changes. Here, using these latter data, the reservoir bypass efficiency BE_r were calculated. BE_r is the ratio of outflow sediment volume to inflow sediment volume. Table 11 shows the BE_r values for the three field campaign years and their average values. The average bypass efficiency of the Solis Reservoir with no SBT in operation would have amounted to 17% (hypothetical or theoretical value), which matches with 15% reported by Muller-Hagmann (2017) for the years from 1987 to 2016. BE_r has dramatically increased from 17% to 88% with the SBT in operation. This value is significantly higher than the value of 31% from previous years reported by Albayrak et al. (2019). The low BE_r values are related to the duration of SBT operation and corresponding *WL* of the reservoir. During a previous study (Muller-Hagmann, 2017), on the one hand, the mean annual operation duration of the Solis SBT was only 21.3 hours, whereas from October 2018 to November 2021, it was around 520 hours/year on average. On the other hand, in most of the SBT operations from 2018 to 2021, the *WL* was reduced to around 813 m asl, which had a significant impact on improving the BE_r. Overall, BE_r is in the range of other reservoirs with an SBT in operation (BE_r = 60% - 95% (Auel et al., 2016)), although there are also different types of SBTs (type A vs. type B like Solis). It must be noted that an SBT of type B can also have efficiencies higher than 100%, like for the 2019 to 2020 operations (Table 11), because SBT with submerged intakes in the reservoir may not only divert the incoming sediments, but also have the possibility to erode previously deposited sediments from the reservoir if the *WL* is sufficiently lowered to have free-flow conditions in the upstream part of the reservoir. If the reservoir *WL* is not sufficiently lowered, the location of the SBT intake within the reservoir causes intermediate deposition of sediments between the reservoir head and the SBT intake, which can negatively affect the bypass efficiency.

Table 11 shows that the BE_r reduced from 2020 to 2021, when the guiding wall was removed. At this period, the sediment inflow was around 117’810 m^3, but the SBT was in operation for a few times bypassing 16’727 m^3 of sediments. Considering the volumes of outflowing sediments through HPPs and dam outlet structures, a net volume of 45’435 m^3 of sediments was deposited in the reservoir. Results of bathymetry measurements (Figure 29) show that most of these sediments were deposited in zone 2. These sediments can be bypassed through the SBT or transported to zone 3 based on the hydrological situation and operation of the SBT and reservoir in the next years. Further measurements can determine how much the removal of the guiding wall affects the relocation of these sediments.

Table 11 shows that the SBT transported total volume of 202’012 m^3 (535’332 ton) sediments out of the reservoir between 2018 and 2021, while the excavation, HPPs and dam structures only released 96’814 m^3 and 50’257 m^3, respectively. Assuming the uniform deposition along the reservoir, these volumes of sediments could cause 202’012 / 190’410 ≈ 1 m increase in bed level of the reservoir. This shows the importance of SBT for lifetime of the reservoir.

Table 11: Sediment inflows and outflows of the Solis Reservoir and corresponding bypass efficiencies during measurement campaigns.

		Sediment inflow – excavation volume (m^3)	Without SBT		With SBT	
			Outflow (m^3)	BE_r (%)	Outflow (m^3)	BE_r (%)
01.10.2018 – 22.08.2019	BL_{22}	53’371 – 14’391 = 38’980	0	0	22’509	58
	SSL_{coarse}	69’696 – 14’391 = 55’305	0	0	26’375	48
	SSL_{fine}	106’474 + 4’400 – 0 = 110’874	14’941	13	114’848 + 14’941 = 129’789	117
	TL	233’941 – 28’782 = 205’159	14’941	7	178’673	87
22.08.2019 – 03.09.2020	BL_{22}	4’688 – 15’700 = –11’012	0	0	2’801	∞
	SSL_{coarse}	9’742 – 15’700 = –5’958	0	0	9’986	∞
	SSL_{fine}	13’481 + 4’800 – 0 = 18’281	16’300	89	8’766 + 16’300 = 25’066	137
	TL	32’711 – 31’400 = 1’311	16’300	1243	37’853	2887
03.09.2020 – 02.11.2021	BL_{22}	25’923 – 18’316 = 7’607	0	0	1’677	22
	SSL_{coarse}	51’821 – 18’316 = 33’505	0	0	7’910	23
	SSL_{fine}	34’466 + 5’600 – 0 = 40’066	19’016	47	7’140 + 19’016 = 26’156	65
	TL	117’810 – 36’632 = 81’178	19’016	23	35’743	44
TOTAL	**BL_{22}**	**83’982 – 48’407 = 35’575**	**0**	**0**	**26’987**	**76**
	SSL_{coarse}	**131’259 – 48’407 = 82’852**	**0**	**0**	**44’271**	**53**
	SSL_{fine}	**154’421 + 14’800 – 0 = 169’221**	**50’257**	**29**	**130’754 + 50’257 = 181’011**	**107**
	TL	**287’648**	**50’257**	**17**	**252’269**	**88**

4.5.3 Effects of reservoir operation on bypass efficiency of SBT

Table 11 shows that the average bypass efficiency of the reservoir from 2018 to 2021 (3 years) is around 88%. The SBT was the main reason of increasing the reservoir bypass efficiency. Therefore, the efficiency is controlled by the operation of the reservoir. To evaluate the effects of the reservoir operation on sediment outflow from the SBT, the efficiency of SBT (BE_{SBT}) is determined as the ratio of bypassing sediments from the SBT to the inflowing sediments transported by the Albula River. It is assumed that during the SBT operation, no excavation occurs, which seems reasonable as gravel excavation is difficult during large discharges. This SBT bypassing efficiency is calculated in Table 12 for each event.

Table 12: Sediment inflows and outflows of the Solis Reservoir and corresponding bypass efficiencies during SBT operations between 2018 and 2021. The red numbers are the values between the field campaign days.

Event		Duration (hr)	Average *WL* (m asl)	Average Q_{Albula} (m^3/s)	Average $Q_{Reservoir}$ (m^3/s)	Average Q_{SBT} (m^3/s)	Sediment inflow from Albula (m^3)				Sediment outflow through SBT (m^3)				BE_{SBT} (%)
							BL_{22}	SSL_{coarse}	SSL_{fine}	***TL***	BL_{22}	SSL_{coarse}	SSL_{fine}	***TL***	
08.10.2018 05:00 – 08.10.2019 16:49	Event 1	11.81	813.135	9	24	23	0	0	2	**2**	105	58	10	**173**	8650
03.06.2019 20:30 – 04.06.2019 11:20		14.83	822.348	49	83	19	582	1'226	619	**2'427**	0	58	59	**117**	5
04.06.2019 18:00 – 06.06.2019 19:30		49.5	814.673	59	104	91	2'800	4'182	4'181	**11'201**	3'299	8'893	12'973	**25'165**	224
06.06.2019 19:30 – 10.06.2019 15:30	Event 2	98	822.67	59	92	20	5'272	7'887	7'929	**21'088**	0	331	665	**996**	5
10.06.2019 15:30 – 17.06.2019 13:30		165.5	813.931	83	142	124	16'813	9'521	51'601	**77'935**	19'100	14'281	96'182	**129'563**	166
17.06.2019 13:30 – 05.07.2019 15:00		433.5	822.097	56	100	33	22'456	35'465	31'906	**89'827**	0	2'595	4'669	**7'264**	8
12.08.2019 21:00 – 13.08.2019 18:40	Event 3	21.66	822.574	48	81	47	815	1'268	1'184	**3'267**	5	159	290	**454**	14
10/2018 – 08/2019		**794.8**	**819.889**	**61.13**	**106.04**	**53.93**	**48'738**	**59'549**	**97'422**	**205'747**	**22'509**	**26'375**	**114'848**	**163'732**	**79**
29.08.2020 06:00 – 31.08.2020 17:00	Event 4	59	814.242	47	92	88	2'086	3'927	2'342	**8'355**	2'801	9'969	8'746	**21'516**	257
31.08.2020 17:00 – 02.09.2020 14:15		45.25	821.484	31	49	7	276	621	370	**1'267**	0	17	20	**37**	3
08/2019 – 09/2020		**104.25**	**817.385**	**40.05**	**73.33**	**52.84**	**2'362**	**4'548**	**2'712**	**9'622**	**2'801**	**9'986**	**8'766**	**21'553**	**224**
08.06.2021 06:40 – 14.06.2021 10:30		147.83	822.867	43	66	24	3'693	7'612	6'908	**18'213**	0	292	530	**822**	4
14.06.2021 10:30 – 18.06.2021 14:30	Event 5	100	816.429	48	82	76	3'782	7'305	4'041	**15'128**	1'636	5'126	3'923	**10'685**	70
18.06.2021 14:30 – 25.06.2021 23:30		177	822.714	47	74	37	6'508	12'268	7'255	**26'031**	0	1'203	1423	**2626**	10
01.08.2021 09:20 – 11.08.2021 4:20	Event 6	235	822.807	40	81	36	5'700	11'414	5'781	**22'895**	41	1'289	1264	**2594**	11
09/2020 – 11/2021		**659.83**	**821.829**	**43.76**	**75.91**	**39.64**	**19'683**	**38'599**	**23'985**	**82'267**	**1'677**	**7'910**	**7'140**	**16'727**	**20**

From October 2018 to August 2019, the SBT was in operation three times. To understand the sediment transport processes during this period, as well as to evaluate the SBT efficiency, the sedimentation in each of these three events, as well as between the events is investigated hereafter.

The first bathymetry measurement was conducted on 1st October 2018. From 1st October 2018 until 8th October 2018, 5:00 AM (the starting date of SBT operation), the Albula discharge was around 10 m^3/s. Therefore, no BL_{22} and SSL_{coarse} are assumed to have been moved towards the reservoir, so that only a volume of 34 m^3 of SSL_{fine} was transported by the Albula. Figure 36 shows that for a reservoir discharge of 15 m^3/s (the measured discharge in 2021, orange colour), suspended particles larger

than around 0.15 mm were deposited at the inlet of the reservoir. Therefore, most of SSL_{fine} were deposited at the inlet of the reservoir.

Event 1 (08.10.2018)

The first SBT operation was on 8th of October 2018, from 5:00 AM until 4:49 PM. Although, the discharge in the Albula was around 9 m^3/s with no bedload transport to the reservoir, the geophones in the SBT detected bedload transport due to the reduction of *WL* to 811.236 m asl, which increased bed shear stresses and hence initiated bedload transport. The *PSD* of the reservoir bed in 2018 shows that d_{50} of the bed material close to the SBT inlet and upstream of the guiding wall was around 14.5 mm (Figure 33, location 1'695 m and Figure 34). Therefore, such large sediment particles were eroded from zone 2 and bypassed out of the reservoir through the SBT, which was detected by the geophones in terms of BL_{22} transport. On the other hand, as the discharge of the SBT equals quasi the incoming discharge of the reservoir, all fine sediments transported by the Albula as well as previously deposited fine sediments in zones 1 and 2 were resuspended and transported towards the SBT and bypassed out of the reservoir. When the *WL* reduced, the SSC_{fine} in the SBT was two times higher than the incoming SSC_{fine} in the Albula. Therefore, the volume of SSL_{fine} passing the SBT was around 10 m^3. As the incoming BL_{22} was zero in the Albula, the volume of SSL_{coarse} in the SBT was the average of BL_{22} and SSL_{fine}.

After closing the SBT gates until June 2019, the average discharge in the Albula and at the reservoir inlet were 10 m^3/s and 19 m^3/s, respectively. Therefore, volumes of BL_{22} = 1'695 m^3, SSL_{coarse} = 3'655 m^3 and SSL_{fine} = 3'714 m^3 were transported towards the reservoir. The shear velocity at the inlet of the reservoir calculated for *WL* between 822 and 823.6 m asl and discharge of 53 m^3/s, indicates that the critical diameter of the sediments which can be transported as bedload were below 4 mm. Because of the low discharges, BL_{22} and SSL_{coarse} did not reach the reservoir and were excavated from the river. Only some portions of SSL_{fine} reached the reservoir and settled there.

Event 2 (03.06.2019 – 05.07.2019)

The next SBT operation was in June 2019, during a 5-year flood (Q = 170 m^3/s). During this flood, the SBT was in operation from 3rd of June 2019, 8:30 PM until 5th of July, 3:00 PM (around 32 days). In this period, the SBT discharge as well as *WL* were fluctuating between 20 and 140 m^3/s and 812 and 823 m asl, respectively, although the Albula and reservoir discharges were always higher than 40 m^3/s and 80 m^3/s, respectively. This period is investigated in detail hereafter:

(i) From 3rd June, 8:30 PM until 4th June, 11:20 AM, 582 m^3, 619 m^3 and 1'127 m^3 of BL_{22}, SSL_{fine} and SSL_{coarse}, respectively, were transported by the Albula. Because of no reduction in *WL* during this period, SSC_{fine} at the inlet of the SBT equalled to only 25% of the incoming SSC_{fine} transported by the Albula.

(ii) From 4th June, 11:20 AM until 06:00 PM, the SBT gate was closed for 6 hours and 40 minutes. All sediments transported in this period were assumed to have deposited in the reservoir.

(iii) On 4th June 2019, 06:00 PM, the SBT was put in operation again. Fully opening the SBT gate, a fast decrease of *WL* to a minimum of 812.053 m asl and high reservoir and Albula discharges caused BL_{22} transport through the SBT. This operation lasted until 6th June 2019, 07:30 PM. From then on, although the SBT was still in operation, the discharge was below 30 m^3/s, and *WL* was above 822.5 m asl. Therefore, sediment transport from 4th June, 06:00 PM to 6th June, 07:30 PM was investigated separately to analyse the effect of reservoir and SBT operation on the SBT bypassing efficiency. By reducing *WL* to 812.053 m asl, the transported volume of BL_{22} through the SBT was higher than that in the Albula, resulting in bed erosion and transport of BL_{22} from zones 1 and 2 which had been deposited in these areas in previous years. The outflow SSC_{fine} in the SBT was also two times higher than the inflow SSC_{fine} in the Albula. Therefore, the efficiency of SBT in this operation was even higher than 100%.

(iv) From 6th June, 07:30 PM to 10th June, 03:30 PM, the *WL* increased to its maximum value of 823.19 m asl. In this period, BL_{22} = 5'272 m³ and SSL_{coarse} = 7'887 m³ coming from the Albula were deposited in the reservoir. When the *WL* was not lowered, the SSC_{fine} in the SBT was 25% of the SSC_{fine} value in the Albula. Therefore, only a volume of 665 m³ was transported through the SBT and the rest deposited in the reservoir.

(v) From 10th June, 03:30 PM to 17th June, 01:30 PM, the *WL* in the reservoir decreased from around 823 m asl to 811.748 m asl. This reduction was in line with the increasing in discharge in both the Albula and SBT. The Albula discharge in this period increased from around 75 m³/s to around 90 m³/s and the discharge in the SBT increased from around 50 m³/s to around 130 m³/s. It took 23.5 hr to fully open the SBT gate and lower the *WL*; the SBT was in operation for 5 days and 17 hours at low *WL*, before the SBT was closed and *WL* increased again over 5 hours. This was a very long operation, with *WL* varying between high and low values. Therefore, the SSC_{fine} in the SBT was assumed to be 1.25 SSC_{fine} of the Albula.

(vi) From 17th June, 01:30 PM to 5th July, 03:00 PM, the SBT was still in operation. However, no BL_{22} was detected by the geophones installed in the SBT. The reason for this is the fact that the incoming discharges from both the Albula and in the reservoir were low, and *WL* increased to 822 m asl. Consequently, the SBT discharge decreased. Although on 28th June the SBT and reservoir discharges increased, no BL_{22} was detected in the SBT because of a low discharge in the Albula (60 m³/s) and high *WL* (822 m asl). As the *WL* in the reservoir was high, 0.25 of the Albula SSC_{fine} was assumed to be transported through the SBT.

Between SBT operation events 2 and 3, i.e. from 5th July, 03:00 PM until 12th August, 09:00 PM, the inflow volumes of BL_{22}, SSL_{coarse} and SSL_{fine} were 2'336 m³, 5'194 m³ and 4'090 m³, respectively. The average discharge in this period was 25 m³/s in the Albula, while it was 40 m³/s in the reservoir. Therefore, based on the *WL*, the discharge and measured u_* by ADCP in the different campaigns, all BL_{22} and SSL_{coarse} were expected to be deposited in zone 1 and upstream of the reservoir inlet, while the SSL_{fine} was deposited in zone 2.

Event 3 (12 – 13.08.2019)

From 12th August, 09:00 PM until 13th August, 06:40 PM, the SBT was in operation, with no reduction of *WL* (around 822.5 m asl). Only 5 m³ of BL_{22} were transported through the SBT, and the rest of inflowing sediments was deposited mainly in the reservoir. This volume of bypassed BL_{22} was deposited behind the guiding wall from previous floods when the discharge in the reservoir was high and the SBT was not in operation. The outflow SSC_{fine} in the SBT was 25% of the inflow SSC_{fine} in the Albula, because of high *WL*.

After this period, until the next measurement campaign, 363 m³, 820 m³ and 937 m³ of BL_{22}, SSL_{coarse} and SSL_{fine} were transported by the Albula and hence deposited in the reservoir.

Despite all abovementioned SBT operations, the SBT was in operation in some other times (detected by gate opening of the SBT), including the period from 20th August 2019 to 22nd August 2019, with an average SBT discharge of 19 m³/s, average and maximum Albula discharges of 28 m³/s and 39 m³/s, respectively, and minimum *WL* of 822.45 m asl. At these discharges, no BL_{22} was detected in the SBT and it is assumed that these operations had only a small impact on the sediment balances calculated above due to the low discharges with little sediment transport.

Overall, a volume of 163'732 m³ was bypassed by the SBT from 01.10.2018 to 22.08.2019. The total volume of sediment inflow by the Albula during the SBT operations was 205'747 m³, which resulted in a SBT efficiency of around 79%. It must be noted that this value was obtained based on the sediment outflow and inflow during SBT operations, not over the whole year.

The second surveying campaign was conducted in 22.08.2019. Therefore, sedimentation in the reservoir is investigated between 22.08.2019 until the third measurement on 03.09.2020. In this period, the SBT was in operation on 21st October 2019, 29th October 2019, and 29th August 2020. No BL_{22} was detected in the first two operations. *WL* as well as discharges in the first two periods were as follows:

On 21st October 2019, the minimum *WL* was 818.02 m asl, the average discharges in the Albula and SBT were 19 m^3/s and 14 m^3/s, respectively.

On 29th October 2019, the minimum *WLE* was 821.23 m asl and the Albula had a maximum discharge of 26 m^3/s.

Due to the low discharges in the Albula and SBT, the effects of these two operations were neglected. The next operation was on 29th August 2020. In this period, BL_{22} was measured by the SBT geophones. Therefore, only this event is investigated in detail as event 4.

Event 4 (29.08.2020 – 02.09.2020)

The SBT was in operation from 29th of August 2020, 06:00 AM to 2nd of September 2020, 2:15 PM. This period is investigated in the following:

(i) From 29th August, 6:00 AM until 31st August, 5:00 PM, the SBT was in operation with high discharge. The *WL* in the reservoir was reduced to 812.645 m asl. At this period, BL_{22} was measured by the SBT geophones. The average discharge of the Albula in this period was 47 m^3/s. Due to this relatively low discharge in the Albula, the inflowing coarse sediments were deposited upstream of the reservoir and the volumes of 2'801 m^3 of BL_{22}, and 9'969 m^3 of SSL_{coarse} were eroded from zones 1 and 2 of the reservoir and bypassed through the SBT. The SSC_{fine} in the SBT was also two times higher than the Albula SSC_{fine}.

(ii) From 31st August, 05:00 PM until the last day of SBT operation on 02nd September 2020, 02:15 PM, the SBT discharge was reduced to around 10 m^3/s. Meanwhile, *WL* was increased to around 822 m asl. The average Albula discharge was 31 m^3/s. Therefore, the geophones in the SBT detected no BL_{22} and due to the low discharge, high *WL* and corresponding low shear velocities, only a small volume of SSL_{coarse} was transported through the SBT in this period. Only SSL_{fine} with concentration of 0.25 times SSC_{fine} of the Albula was transported through the SBT in this period.

The *PSD* along the reservoir in 2020 shows an increase of d_{50} along the reservoir. It confirms that the smaller particles (which were deposited by the floods of previous years), were eroded during this operation and as a result, coarser particles remained in their position and increased the d_{50} of bed materials. The inflowing discharge to the reservoir was very low from 22.08.2019 to 03.09.2020. Therefore, the SBT was in operation only a few times and for a few hours. During the SBT operation, 21'553 m^3 of sediments were bypassed. These sediments were mainly eroded from zones 1 and 2 (where they had deposited in previous floods). As a result, the ratio of sediment outflow through the SBT to sediment inflow by the Albula during the SBT operation was 224%.

The 4th field campaign was conducted on 02 November 2021, 14 months after the third campaign. In this period, the guiding wall in the reservoir was removed. The recorded data of the reservoir show only one SBT operation in May 2021. While the SBT measurements show that the SBT was in operation twice, namely in June and August 2021. The operator said that the SBT was in operation only in June 2021. To better analysis all data, the sediment volumes are investigated in different parts, assuming that the SBT was in operation in June 2021 and August 2021 (based on SBT recording data).

Event 5 (08.06. – 25.06.2021)

The first SBT operation was from 08th June 2021, 06:40 AM until 25th June 2021, 11:30 PM. In this period, the average discharges in the Albula and SBT were 46 m^3/s and 42 m^3/s, respectively. The *WL* was only reduced for around 5 days in this period. During this 5-day *WL* drawdown, the SBT discharge was high, about 100 m^3/s, and there was bedload transport through the SBT. The total period of 17 days is investigated in three subperiods.

(i) From 08th June 2021, 06:40 AM until 14th June 2021, 10:30 AM, the *WL* was high at 822.87 m asl on average. The average discharges in the Albula, SBT and reservoir were 43 m^3/s, 24 m^3/s and 66 m^3/s, respectively. Only 0.5 m^3 of BL_{22} were detected in the SBT which can be neglected. Therefore, all BL_{22} coming from the Albula was deposited upstream of the SBT inlet.

(ii) From 14th June 2021, 10:30 AM until 18th June 2021, 02:30 PM, the *WL* was lowered down to a minimum value of 812.55 m asl. As a result, the BL_{22} measured in the SBT was 1'636 m^3. It must be noted that due to the long period of operation in this time, the SSC_{fine} in the SBT was assumed to be 1.25 SSC_{fine} of the Albula.

(iii) From 18th June 2021, 02:30 PM until 25th June 2021, 11:30 PM the SBT was still in operation but no BL_{22} was measured in the SBT. The average *WL* in reservoir was at 822.71 m asl.

After this period, from 25th June 2021, 11:30 PM until 1st August 2021, 09:20 AM, 1'818 m^3 of BL_{22} were transported by the Albula as well as 676 m^3 and 4'778 m^3 of SSL_{coarse} and SSL_{fine}, respectively. The average discharge in the Albula amounted to 27 m^3/s.

Event 6 (01.08 – 11.08.2021)

The next SBT operation was from 1st August, 09:20 AM until 11 August 2021, 04:20 AM. The minimum *WL* in this period was at 821.4 m asl, while the maximum *WL* was 823 m asl. Therefore, no BL_{22} was transported. Although, due to large depositions in front of the SBT inlet from previous events, a small amount of 41 m^3 of BL_{22} was measured by the geophones in the SBT. BL_{22} transported by the Albula was 5'700 m^3 in this period. The SBT SSC_{fine} was 0.25 of inflow SSC_{fine} by the Albula, due to high *WL*.

Overall, a volume of 16'727 m^3 was bypassed through the SBT during the period from 03.09.2020 to 02.11.2021. During the SBT operations, the total volume of incoming sediments by the Albula was 82'267 m^3, which resulted in a SBT efficiency of around 20% in this period. There are several reasons for this low SBT efficiency in this period, in comparison with previous periods. One reason is that the reservoir *WL* was not as low as in some of the previous periods. A second reason is the low average discharge through the SBT during operation. A third reason might be the removal of the guiding wall from the reservoir. The effect of the guiding wall on the efficiency of the SBT, and on sedimentation patterns in the reservoir should be investigated in future studies.

For a better evaluation of operational effects on the SBT bypass efficiency (BE_{SBT}), the results from Table 12 are presented in Figure 37. Figure 37 shows that reservoir operation in terms of minimum *WL* has a significant effect on BE_{SBT}. BE_{SBT} is below 20% for *WL* above about 814 m asl. Decreasing *WL* from 814 to 813 to 812 m asl, the BE_{SBT} starts increasing from 70% to more than 250%. This is because by decreasing the *WL*, the bed shear stresses increase and more sediments are transported towards the SBT. The ratio of the discharge through the SBT to the discharge in the reservoir also shows an SBT efficiency above 70% that when this ratio is higher than 85%. A higher ratio means that the SBT outflow discharge is approximately similar to the inflow discharge. Given that further dam outlets are in operation, the *WL* then also decreases, since the total outflow exceeds the total inflow. Figure 37 also shows fits between BE_{SBT} and minimum *WL*, and BE_{SBT} and $Q_{SBT}/Q_{Reservoir}$.

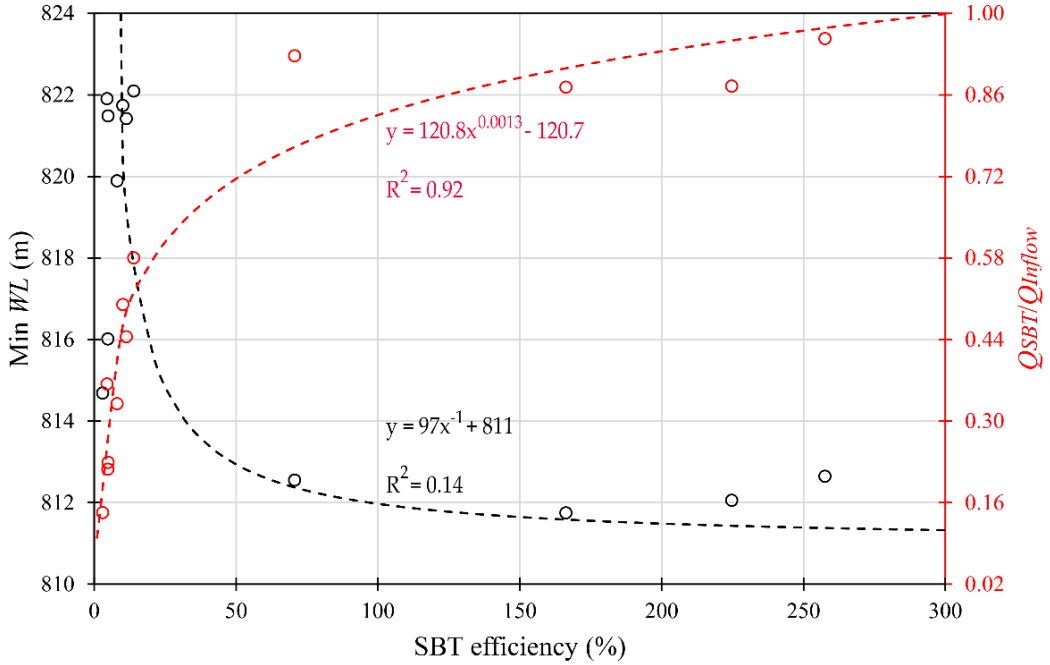

Figure 37: Effects of reservoir operation (minimum *WL* and ratio of discharge through SBT to discharge in the reservoir) on SBT efficiency of Solis Reservoir.

4.6 Economical calculations

A rough economical assessment based on the bypass efficiencies with/without a SBT is presented in this section. The maximum *WL* of the reservoir is 823.75 m asl while the minimum *WL* is at 816 m asl for the operation of the HPPs fed by the Solis reservoir. Figure 37 shows that high bypass efficiencies are reached for *WL* ≤ 813 m asl. Figure 38 shows the water depths at different reservoir *WL*. This figure is based on the latest bathymetry measurements conducted in November 2021. The blue boundary shows the full supply level of 823.75 m asl. When lowering the water level to 816 m asl (minimum HPP operation level), the reservoir extends to upstream of the SBT inlet, meaning that the incoming sediments, especially bedload, can deposit upstream of the SBT inlet. Further reducing the water level to 813 m asl, the reservoir inlet matches with the SBT inlet. This means that all incoming sediments from the Albula river, including bedload, are transported to the inlet of the SBT. From there, the sediments are conveyed through the SBT or enter zone 3 (because the guiding wall was removed). If the water level reduces to 812 m, the reservoir impoundment starts downstream of the SBT inlet within zone 3, about halfway between the SBT inlet and the dam. Figure 38 shows that the optimum *WL* is 813 m asl to have the best performance of the SBT to bypass sediments. Reducing *WL* to less than 813 m asl is not recommended and has no positive effect on the bypass efficiency. The optimum *WL* of 813 m asl matches well with the results of Figure 37. In all 4 events with bypass efficiencies higher than 70%, the minimum *WL* reached to below 813 m asl.

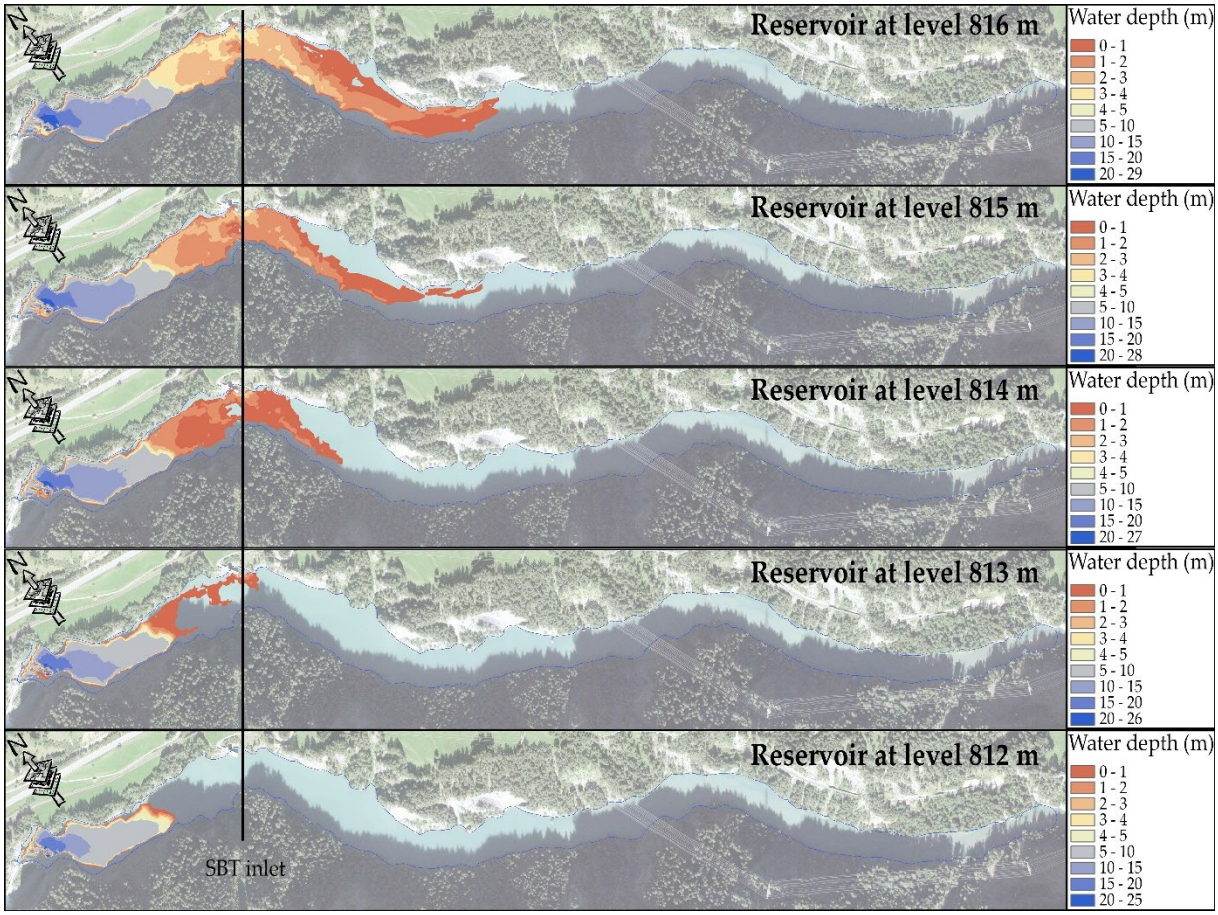

Figure 38: Reservoir water surface extension at different water levels. The blue boundary is the reservoir at full supply level of 823.75 m asl.

Figure 39 shows the relation between *WL* and reservoir volume, also termed stage-volume curve, based on the latest bathymetry measurements in November 2021. The reservoir capacity at full supply level (823.75 m asl) is 1'413'450 m^3. The minimum water level for HPP operation is 816 m asl, therefore, reducing the water level from 823.75 m to 816 m asl can be conducted by HPP operation and is assumed to cause no power production loss for the operator. For the water levels below 816 m asl, the water level drawdown can be conducted through dam bottom outlet or SBT operation. Therefore, these volumes of released water cannot be used for electricity production. Thanks to the Solis reservoir, in contrast to run of river HPPs, the Solis fed HPPs do not have to continuously produce energy. For storage HPPs like the Solis, the water loss should therefore be minimized. We assessed the total water lost due to bypassing for the periods when *WL*<816 m asl. In other periods, we assume that during inflows well above the combined design discharges of 47 m^3/s (design discharge of Sils and Rothenbrunnen HPPs are 22 m^3/s and 25 m^3/s, respectively) the water bypassed through the SBT would otherwise be spilled via the spillway, as the small reservoir would be filled fast anyway. So, these bypassing losses are not critical. The energy conversion coefficient *a* [kWh/m^3] of Sils and Rothenbrunnen HPPs are 0.35 and 0.447, respectively. Therefore, the design discharge-weighted average energy conversion coefficient when both HPPs are in operation is 0.402 kWh/m^3. By multiply this value with the total volume of water lost for power production at low *WL*< 816 m asl, we obtain an energy value [GWh]. Then, assuming minimum and maximum unit prices of 50'000 €/GWh

and 300’000 €/GWh to cover typical ranges of market prices in recent years, we obtain a monetary price value range.

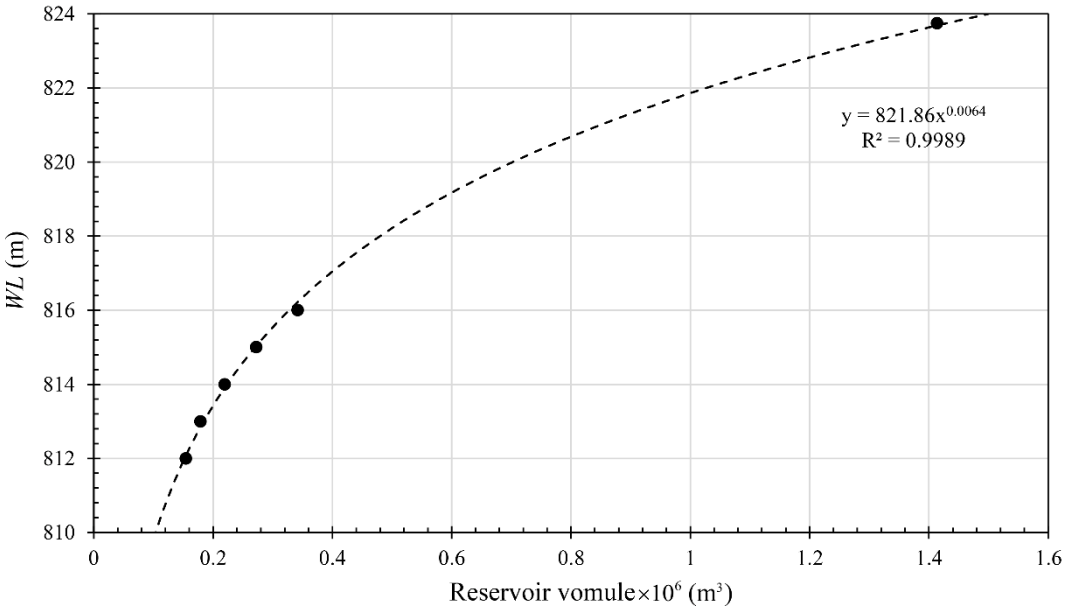

Figure 39: *WL* versus reservoir volume based on the latest bathymetry measurements from November 2021.

Table 13 shows the results of the economical calculations. The total water volume bypassing through the SBT and bottom outlets when *WL*<816 m asl is also presented in this table. This volume of water might be stored if the reservoir has enough capacity. The volume of water exceeding the reservoir capacity will overflow via spillways and is thus lost for power production. Therefore, the economical calculations are based on the usable volume of water (column 12 in Table 13). To calculate the usable water volume, based on Figure 39, the reservoir capacity between the average *WL* at each SBT operation with *WL*<816 m asl and the maximum *WL* of the reservoir 823.75 m asl is considered on the one hand. On the other hand, the total volume of water which could be conveyed through both HPPs is calculated. If the sum of these two values is less than the total volume of water passing through SBT and bottom outlets, the difference would overflow the dam spillway and cannot be used for energy production. Then the approximate costs are calculated based on the usable water and the two unit prices of 50’000 €/GWh and 300’000 €/GWh (columns 14 and 15 in Table 13). Overall, these calculations show the total cost between 1’128’650 and 6’771’900 € (≈375’000 – 2’250’000 €/year) for SBT operations with efficiencies higher than 70%, from October 2018 to November 2021. These five operations released 187’102 m^3 of sediments out of the reservoir, which is around 13% of the reservoir capacity at full supply level of 823.75 m asl according to the latest bathymetry measurements in 2021. Overall, an annual reservoir capacity loss of 4% would occur if the SBT was operated at reservoir levels above 816 m asl with almost 0% bypass efficiency, indicating that the reservoir would be filled with sediments within 25 years. Under such conditions, within 16 years the reservoir would be filled up to 816 m asl, seriously impacting HPP operation. Therefore, based on the present findings, it is recommended to operate the SBT at 813 m asl with more than 100% bypass efficiency at the cost of revenue loss but with the benefit of extending the reservoir life. It should be also noted that operation of the HPPs during flood events with high sediment concentration may cause turbine abrasion, resulting in a high maintenance cost or turbine replacement (Felix, 2017) and high risk of driftwood clogging at the turbine intakes. Therefore, such negative consequences should additionally be considered in the cost-benefit analysis.

Table 13: Duration of SBT operation when the *WL* was below 816 m asl (only operations with minimum *WL* below 816 m asl are presented in this table).

Event	Average *WL* when *WL*<816 (m asl)	Minimum *WL* (m asl)	Average $Q_{Reservoir}$ when *WL*<816 (m^3/s)	SBT efficiency (%)	Total duration (hr)	Duration with *WL* below 816 m asl (hr)	Water passing through left bottom outlet when *WL*<816 m (m^3)	Water passing through right bottom outlet when *WL*<816 m (m^3)	Water passing through SBT when *WL*<816 m (m^3)	Total water passing through SBT and both bottom outlets when *WL*<816 m (m^3)	Usable volume (m^3)	Energy (GWh)	Minimum costs (for 50' 000 €/GWh unit price)	Maximum costs (for 300' 000 €/GWh unit price)
08.10.2018–08.10.2018	813.45	811.236	24.64	8'650	11.81	11.81	215'786	0	992'512	1'208'298	1'208'298	0.486	24'300	145'800
04.06.2019–06.06.2019	812.958	812.053	109.135	224	49.5	36	0	649'623	13'482'521	14'132'144	7'382'887	2.968	148'400	890'400
10.06.2019–17.06.2019	813.07	811.748	142.215	166	165.5	142	0	11'521'651	66'003'074	77'524'726	25'356'418	10.193	509'650	3'057'900
29.08.2020–31.08.2020	813.691	812.645	92.956	257	59	52.5	888'444	0	17'181'793	18'070'237	10'147'107	4.079	203'950	1'223'700
14.06.2021–18.06.2021	814.479	812.55	86.582	70	100	40	0	712'530	21'023'187	21'735'717	12'058'625	4.847	242'350	1'454'100
Total	**813.527***	**812.046***	**112.419***	**422***	**385.81**	**282.31**	**1'104'230**	**12'883'804**	**118'683'087**	**132'671'122**	**56'153'335**	**22.573**	**1'128'650**	**6'771'900**

* These values are weighted average

5 Conclusions

We successfully conducted four two-day field campaigns in the Solis Reservoir in 2018, 2019, 2020 and 2021. Based on the experiences from the first campaign in 2018, we upgraded our DGPS with an RTK-GPS system for accurate bathymetry measurements. Furthermore, we implemented a new bathymetry measurement technique, which resulted in higher resolution bathymetry maps compared to the 2018 map. In 2021, in addition to the bottle samples, we measured suspended sediment concentrations (*SSC*) using LISST-100X, which gives valuable information on *SSC* distributions in the water column at 11 measurement locations along the reservoirs.

High resolution velocity and bathymetry data were obtained during the four different field measurement campaigns. The reservoir bathymetry was mapped with high accuracy. We captured the effects of floods with one-year and five-year return periods in 2019 and one-year return period in 2020 on the reservoir sedimentation and evaluated the different SBT and reservoir operation modes on the reservoir and SBT bypass efficiencies (in terms of reservoir water level). Bathymetry changes show that from October 2018 to August 2019, a net volume of approx. 23'412 m^3 of sediments were deposited along the reservoir. From August 2019 to September 2020 a net volume of around 28'530 m^3 of sediments were eroded from the reservoir. From September 2020 to November 2021 a net volume of around 54'119 m^3 of sediments were deposited along the reservoir.

Sediment balances and annual reservoir bypass efficiencies were calculated during the three periods, from October 2018 to November 2021. To calculate sediment balances, in- and outflow sediment concentrations and transport rates were measured with installed turbidimeters and geophones, respectively, and sediment volumes were then estimated using well-known sediment transport equations and applying assumptions to cover a range of particle sizes. The results show that the assumptions made for Solis Reservoir are in a good agreement with the bathymetry changes, with differences of less than 15% for the periods from 2018 to 2019 and 2020 to 2021. The bathymetry data show that the assumptions lead to a 28% difference for the dry period from 2019 to 2020, which is still good for sediment research studies.

The continuous data from the turbidimeters installed at the SBT outlet and in the Albula River were used to calculate fine suspended sediment loads. Turbidimeters may not provide accurate data because of their sensitivity to sediment size, shape and concentration (Felix et al., 2018). They provide suspended sediment concentrations with particle sizes less than 0.5 mm if calibrated. Because of this, suspended sediment concentrations of coarse particles with sizes larger than 0.5 mm were estimated based on assumptions. Two Swiss Plate Geophone Systems were used to measure bedload transports in the Albula River and through the SBT. The geophones installed at the SBT outlet were calibrated both in the laboratory and the field, under different flow conditions. Therefore, the measured bedload transport rates are judged reliable. However, the geophones installed in the Albula River were calibrated during low flow discharges, which likely results in an underestimation of bedload transport rates. To overcome this, bedload transport rates were estimated with well-known literature equations, which matched well with the bathymetry changes results.

The reservoir bypass efficiency was evaluated based on sediment in- and outflow volumes. The results show that the average bypass efficiency increased from 17% without the operation of the SBT (hypothetical consideration) to 88% with the SBT in operation. This shows the importance of an SBT in increasing the lifetime of the reservoir.

The results highlight that the SBT bypass efficiency is highly dependent on the water level of the reservoir. For high efficiencies in excess of 70%, an optimal value of the minimum *WL* is around 813 m asl. Further lowering *WL* to less than 813 m asl is expected to have no significant effect on increasing

the efficiency. These results with bypass efficiencies up to 250% indicate that type B SBTs such as the Solis SBT do not only stop sedimentation, but can also increase the active reservoir volume if they are operated under optimal conditions in terms of reservoir *WL*.

A total sediment volume of 202'012 m^3 was bypassed through the SBT between October 2018 and November 2021 (around 3 years) when operating at low water levels. Without SBT operation, these volumes of sediments would increase the reservoir bed level by 1 m on average. Bathymetry information shows that within three years, 155'000 m^3 and 106'000 m^3 of sediment were deposited and eroded, respectively, resulting in a net deposition volume of around 49'000 m^3. Around 34'000 m^3 of sediment were deposited in zone 3, i.e. downstream of the guiding wall, which can endanger the operation of the dam in future.

The findings of this project contribute to improved SBT and reservoir operation regimes with regard to decreasing the sedimentation rates and extending the reservoir lifetime. Furthermore, they are expected to contribute to a sustainable use of hydropower, to provide a basis for improving sediment management in reservoirs, and to the realization of the Swiss Energy Strategy 2050.

6 Outlook and next steps

The operator has removed the guiding wall at the beginning of 2021. The removal of the guiding wall may increase sedimentation in zone 3 and decrease the SBT efficiency. Therefore, more studies are required to evaluate the effects of the guiding wall on the sedimentation of the Solis Reservoir.

To mitigate less accurate quantification of suspended and bedload transports, continuous suspended sediment monitoring devices in real-time at the inlet and outlets of the reservoir are recommended. For bedload measurements, more studies are required to calibrate the SPGS installed in the Albula River. A combination of this system with other devices like the Japanese pipe microphone (Koshiba et al. 2022) would also improve the detectable size range of bedload particles and thus the measurement results.

The net sediment volume of 34'000 m^3 deposited in zone 3 cannot be removed through the SBT and needs to be relocated by means of flushing through dam bottom outlets, hydro-suction technique, or excavation. Further studies are required to check the efficiency of each method to transport these sediments out of this zone.

7 National and international cooperation

In this project, VAW conducted field investigations on reservoir sedimentation together with its partner ewz, operator of the Solis reservoir and hydropower plants in the Mittelbünden region, between 2018 and 2021. ewz supported the project with their staff during the field campaigns and provided the operation data to VAW.

VAW is in contact with other operators in Switzerland and Austria on the topic of reservoir sedimentation management techniques and is part of HydroSediNET initiated by the World Bank and funded by Austrian Federal Ministry of Finance. It is an international network fostering collaboration between those involved in sediment management including hydropower companies, utilities, manufacturers, consulting firms, universities and research institutions, governmental agencies, NGOs and financial institutions.

Dr. Ismail Albayrak is a member of the IAHR working group on Reservoir Sedimentation, and Prof. Robert Boes is a co-opted member of the ICOLD Technical Committee on reservoir sedimentation. This latter committee is about to publish a bulletin on sediment bypassing and transfer in 2023.

8 Publications

Maddahi, M.R., Rahimpour, M., Boes, R.M., Albayrak, I. (2021). Determining minimum number of transects for accurate flow measurements using moving vessel ADCPs. In Proc. 13th Symposium on Ultrasonic Doppler Methods for Fluid Mechanics and Fluid Engineering, Zurich, Switzerland, 48-51, https://www.isud-conference.org/proc/split/ISUD-13/ext_abstract_ISUD13_28.pdf.

9 References

Abbott, J.E., Francis, J.R.D. (1977). Saltation and suspension trajectories of solid grains in a water stream. *Philosophical Transactions of the Royal Society of London. Series A, Mathematical and Physical Sciences, 284*(1321), 225–254. https://doi.org/10.1098/rsta.1977.0009.

Agrawal, Y.C., Pottsmith, H.C. (2000). Instruments for particle size and settling velocity observations in sediment transport. *Marine Geology* 168: 89-114.

Albayrak, I., Müller-Hagmann, M., Boes, R.M. (2019). Efficiency evaluation of Swiss Sediment Bypass Tunnels. In *Proc. 3nd Intl. Workshop on Sediment Bypass Tunnels*, Taipei, Taiwan, 239-245.

Albayrak, I., Arnold, R., Yüzügüllü-Demiral, D., Müller-Hagmann, M., Boes, R. (2022). Field monitoring of sediment transport, hydraulics and hydroabrasion at Swiss Sediment Bypass Tunnels. Final report of the research project funded by Swiss Federal Office for Energy (SFOE). https://www.aramis.admin.ch/Dokument.aspx?DocumentID=69420.

Antoniazza, G., Nicollier, T., Boss, S., Mettra, F., Badoux, A., Schaefli, B., Rickenmann, D., Lane, S.N. (2022). Hydrological drivers of bedload transport in an Alpine watershed. Water Resources Research 58(3): e2021WR030663.

Auel, C. (2014). Flow characteristics, particle motion and invert abrasion in sediment bypass tunnels. *VAW-Mitteilungen* 229 (R. Boes, ed.), ETH Zurich, Switzerland.

Auel, C., Boes, R.M., Ziegler, T., Oertli, C. (2011). Design and construction of the sediment bypass tunnel at Solis. *Hydropower and Dams* (3): 62-66.

Auel C., Kantoush S., Sumi T. (2016). Positive effects of reservoir sedimentation management on reservoir life - Examples from Japan. In Proc. 84th ICOLD Annual Meeting, Johannesburg, South Africa: 4.11-14.20.

Black, K., Rosenberg, M. (1994). Suspended sand measurements in a turbulent environment: field comparison of optical and pump sampling techniques. *Coastal Engineering*, 24 (1): 137-150.

Boes, R.M. (2011). Nachhaltigkeit von Talsperren angesichts der Stauaumverlandung ('Sustainability of dams considering reservoir sedimentation'). *Proc. Internationals Wasserbau-Symposium,* 164 (H. Schüttrumpf, ed.), Aachen, Germany: 161-174 (in German).

Boes, R.M., Baumer, A., Pfeifer, S., Albayrak, I., Felix, D. (2021). Techniques to redcue sedimentation in bed load and suspended load dominated reservoirs. In *Proc. 27th Congress of the international commission on large dams (ICOLD)*, June 2021, Marseille, France (accepted).

Bose, S.K., Dey, S. (2013). Sediment entrainment probability and threshold of sediment suspension: Exponential-based approach. *Journal of Hydraulic Engineering,* 139(10): 1099-1106. https://doi.org/10.1061/(ASCE)HY.1943-7900.0000763.

Campbell, D.E., Spinrad, R.W. (1987). The relationship between light attenuation and particle characteristics in a turbid estuary. *Estuarine, Coastal and Shelf Science*, 25 (1): 53-65.

Demiral Yüzügüllü, D. (2021). Hydro-abrasion processes and modelling at hydraulic structures and steep bedrock rivers. *VAW-Mitteilungen* 261 (R. Boes, ed.), ETH Zurich. Switzerland.

Dhont, B.E.M., Rousseau, G., Ancey, C. (2017). Continuous monitoring of bedload transport in a laboratory flume using an impact sensor. *Journal of Hydraulic Engineering,* 143 (6).

Facchini, M. (2017). Downstream morphological effects of sediment bypass tunnels. *VAW-Mitteilungen* 243 (R. Boes, ed.), ETH Zurich, Switzerland.

Felix, D. (2017). Experimental investigation on suspended sediment, hydro-abrasive erosion and efficiency reductions of coated pelton turbines. *VAW-Mitteilungen* 238 (R. Boes, ed.), PhD Thesis, ETH Zurich, Switzerland.

Felix, D., Albayrak, I., Boes, R.M. (2018). In-situ investigation on real-time suspended sediment measuring techniques: turbidimetry, acoustic attenuation, laser diffraction (LISST) and vibrating tube densimetry. *International Journal of Sediment Research,* 33(1): 3–17, https://doi.org/10.1016/j.ijsrc.2017.11.003.

Ferguson, R.I., Church, M. (2004). A simple universal equation for grain settling velocity. *Journal of Sedimentary Research* 74(6): 933-937.

Francis, J.R.D., Bagnold, R.A. (1973). Experiments on the motion of solitary grains along the bed of a water-stream. *Proc. Royal Society of London. A. Mathematical and Physical Sciences, 332*(1591), 443–471. https://doi.org/10.1098/rspa.1973.0037.

Gippel, C.J. (1995). Potential of turbidity monitoring for measuring the transport of suspended solids in streams. *Hydrological Processes*, 9: 83-97.

Koshiba, T., Auel, C., Tsutsumi, D., Kantoush, S.A., Sumi, T. (2018). Application of an impact plate - bedload transport measuring system for high-speed flows. *International Journal of Sediment Research* 33(1): 35-46.

Koshiba, T., Miura, S., Sumi, T. (2022). Study on the Koshibu Dam sediment bypass tunnel operation based on sediment transport monitoring in upstream reaches. E3S Web of Conferences 346(4):03013.

Lenzi, M.A., Marchi, L. (2000). Suspended sediment load during floods in a small stream of the Dolomites (northeastern Italy). *Catena* 39(4): 267-282.

Maddahi, M.R, Rahimpour, M., Boes, R.M., Albayrak, I. (2021). Determining minimum number of transects for accurate flow measurements using moving vessel ADCPs. In Proc. *13th Symposium on Ultrasonic Doppler Methods for Fluid Mechanics and Fluid Engineering*, Zurich, Switzerland, 48-51.

Maniak, U. (2010). Hydrologie und Wasserwirtschaft: Eine Einführung für Ingenieure ('Hydrology and water management: An introduction for engineers'). Springer-Verlag, 6. Auflage (in German).

Marti, C. (2006). Morphologie von verzweigten Gerinnen: Ansätze zur Abfluss-, Geschiebetransport- und Kolktiefenberechnung ('Morphology of branched streams: approaches for discharge, bedload and scour calculations '). *VAW-Mitteilungen* 199 (H.-E. Minor, ed.), VAW, ETH Zurich, Switzerland (in German).

Morach, S. (2011). Geschiebemessung mittels Geophonen bei hohen Fliessgeschwindigkeiten - Hydraulische Modellversuche ('Bedload transport measurement at high flow velocities - hydraulic model tests'). *Master Thesis, VAW*, ETH Zurich, Switzerland (in German, unpublished).

Moridi, A., Yazdi, J. (2017). Sediment flushing of reservoirs under environmental considerations. *Water Resources Management,* 31: 1899-1914. https://doi.org/10.1007/s11269-017-1620-y.

Müller-Hagmann, M. (2017). Hydroabrasion in high speed flow at sediment bypass tunnels. *VAW-Mitteilungen* 239 (R. Boes, ed.), ETH Zurich, Switzerland.

Müller, P., De Cesare, G. (2009). Sedimentation problems in the reservoirs of the Kraftwerke Sarganserland - Venting of turbidity currents as the essential part of the solution. *Proc. 23rd ICOLD Congress*, Brasilia, Brazil.

Nezu, I., Nakagawa, H. (1993). *Turbulence in open channel flows*. IAHR Monograph Series. A.A. Balkema, Rotterdam, Netherlands.

Nicollier, T., Rickenmann, D., Hartlieb, A. (2019). Field calibration of the Swiss plate geophone system at the Albula stream and comparison with controlled flume experiments. *SedHyd2019, Federal Interagency Sedimentation and Hydrologic Modeling Conference*. June 2019, Reno NV.

Nikuradse, J. (1933). Strömungsgesetze in rauhen Rohren ('Flow field law in rough pipes'). *Forschungsheft* 4, VDI-Verlag, Berlin, Germany (in German).

Oertli, C., Auel, C. (2015). Solis sediment bypass tunnel: First operation experiences. *Proc. First International Workshop on Sediment Bypass Tunnels*, VAW-Mitteilungen 232 (R. Boes, ed.), VAW, ETH Zurich, Switzerland: 223-234.

Panthi, M., Lee, A.A., Dahal, S., Omer, A., Franca, M.J., Crosato, A. (2022). Effects of sediment flushing operations versus natural floods on Chinook salmon survivals. *Scientific Reports,* 12, 15354. https://doi.org/10.1038/s41598-022-19294-2.

Prosser, I.P., Rustomji, P. (2000). Sediment transport capacity relations for overland flow. *Progress in Physical Geography: Earth and Environment*, 24(2): 179-193. https://doi.org/10.1177/030913330002400202.

Rickenmann, D. (2005). Geschiebetransport bei steilen Gefällen ('Bedload transport in steep slopes'). *Proc. 75 Jahre VAW, VAW-Miitteilung* 190 (H.-E. Minor, ed.), ETH Zurich, Switzerland: 107-119 (in German).

Rickenmann, D. (2001). Comparison of bed load transport in torrents and gravel bed streams. *Water Resources Research* 37(12): 3295-3305.

Rickenmann, D., Antoniazza, G., Wyss, C.R., Fritschi, B., Boss, S. (2017). Bedload transport monitoring with acoustic sensors in the Swiss Albula mountain river. *Proc. International Association of Hydrological Sciences (PIAHS)*, 375: 5-10.

Rickenmann, D., Nicollier, T., Boss, S., Badoux, A. (2020). Four years of bedload transport measurements in the Swiss mountain river Albula. In W. Uijttewaal, M. J. Franca, D. Valero, V.

Chavarrias, C. Ylla Arbós, R. Schielen, & A. Crosato (Eds.), River flow 2020. *Proceedings of the 10th conference on fluvial hydraulics* (pp. 1749-1755). https://doi.org/10.1201/b22619-245.

Rickenmann, D., Turowski, J.M., Fritschi, B., Klaiber, A., Ludwig, A. (2012). Bedload transport measurements at the Erlenbach stream with geophones and automated basket samplers. *Earth Surface Processes and Landforms* 37(9): 1000-1011.

Smart, G.M., Jaeggi, M.N.R. (1983). Sedimenttransport in steilen Gerinnen ('Sediment transport in steep channels'). *VAW-Mitteilung* 64 (D. Vischer, ed.), VAW, ETH Zürich, Switzerland (in German).

Sommer, N. (1980). Untersuchungen über die Geschiebe- und Schwebstofführung und Transport von gelösten Stoffen in Gebirgsbächen ('Investigation of bedload and suspended load transport and solution load in mountanous streams'). *International Symposium Interprevent*: 69-94 (in German).

Teixeira, L.C.d.P., João Batista Dias, da Silva Pereira, J.E., de Moura Lisbôa, R. (2016). Relationship between turbidity and suspended sediment concentration from a small hydrographic basin in Santa Maria (Rio Grande do Sul, Brazil). *International Journal of River Basin Management*, 14 (4): 393-399.

Turowski, J.M., Böckli, M., Rickenmann, D., Beer, A.R. (2013). Field measurements of the energy delivered to the channel bed by moving bed load and links to bedrock erosion. *Journal of Geophysical Research: Earth Surface* 118 (4): 2438-2450.

Turowski, J.M., Rickenmann, D., Dadson, S.J. (2010). The partitioning of the total sediment load of a river into suspended load and bedload: A review of empirical data. *Sedimentology* 57, 1126–1146.

VAW, (2008). Entlandung Stausee Solis - Hydraulische Modellversuche zum Variantenstudium der ewz ('De-sedimentation Slis Reservoir - Hydraulic modell investigation on the variant study of ewz'). *VAW-Bericht 4243,* ETH Zürich, Switzerland (in German, unpublished).

Wyss, C.R. (2016). Sediment transport measurements with geophone sensors. *VAW-Mitteilungen* 234 (R. Boes, ed.), Also published as a Doctoral Thesis. Nr. 23353, ETH Zurich. ETH Zurich, Switzerland.

Wyss, C.R., Rickenmann, D., Fritschi, B., Turowski, J.M., Weitbrecht, V., Boes, R.M. (2016a). Laboratory flume experiments with the Swiss plate geophone bed load monitoring system: 1. Impulse counts and particle size identification. *Water Resources Research,* 52(10): 7744-7759.

Wyss, C.R., Rickenmann, D., Fritschi, B., Turowski, J.M., Weitbrecht, V., Travaglini, E., Bardou, E., Boes, R.M. (2016b). Laboratory flume experiments with the Swiss plate geophone bed load monitoring system: 2. Application to field sites with direct bed load samples. *Water Resources Research,* 52(10): 7760-7778.

Wyss, C.R., Rickenmann, D., Fritschi, B., Turowski, J.M., Weitbrecht, V., Boes, R.M. (2016c). Measuring bedload transport rates by grain-size fraction using the swiss plate geophone signal at the Erlenbach. *Journal of Hydraulic Engineering*, 142 (5): 04016003.

Zarn, B. (2009). Geschiebeumleitstollen Solis: Auswirkungen auf den Geschiebehaushalt ('Solis sediment bypass tunnel: Effects on bed load transport') A-482, Hunziker, Zarn & Partner, Domat Ems, Switzerland (in German, unpublished).

Zarn, B. (2010). Kraftwerk Tiefencastel Plus: Beilage zum Umweltbericht – Teilbereich Feststofftransport und Hochwasserschutz ('Power plant Tiefencastel Plus: Supplement to the envirnomental report - Subdomain sediment transport and flood protection') A-525, Hunziker, Zarn & Partner, Domat Ems, Switzerland (in German, unpublished).

10 Appendix

10.1 Appendix A

Table 3 shows the naming of the measured cross sections and locations where the sediment samples were collected. Because of limitations in the field, the naming in the field slightly differs from values in Table 3. Therefore, the naming in the field is presented in Table 14.

Table 14: Velocity and sediment sampling locations in 2018, 2019, 2020, and 2021 with the naming in the measurement day. ST = Station.

Distance	2018			2019			2020			2021		
	Cross sectional meas.	Bedload samples	Bottle samples	Cross sectional meas.	Bedload samples	Bottle samples	Cross sectional meas.	Bedload samples	Bottle samples	Cross sectional meas.	Bedload samples	Bottle samples
0 m	A	ST 1	ST 1	A	ST 1	ST 1	A	ST 1	ST 1	A	ST 1	ST 1
420 m	B	ST 2	ST 2	B	ST 2	ST 2	B	ST 2	ST 2	B	ST 2	ST 2
700 m	C	ST 3	ST 3	C	ST 3	ST 3	C	ST 3	ST 3	C	ST 3	ST 3
1235 m	D	ST 4	ST 4	D	ST 4	ST 4	D	ST 4	ST 4	D	ST 4	ST 4
1460 m	E	ST 5	ST 5	E	ST 5	ST 5	E	ST 5	ST 5	E	ST 5	ST 5
1590 m	F	ST 6	ST 6	F	ST 6	ST 6	F	ST 6	ST 6	F	ST 6	ST 6
1695 m	G	ST 7	ST 7	G	ST 7	ST 7	G	ST 7	ST 7	G	ST 7	ST 7
1840 m	-	-	-	-	-	-	-	-	-	H	ST 8	ST 8
2015 m	H	ST 9	ST 9	H	ST 9	ST 9	H	ST 8	ST 8	I	ST 9	ST 9
2110 m	-	ST 10	-	-	-	-	-	-	-	J	ST10	ST 10
2190 m	-	ST 11	-	I	ST 11	ST 11	I	ST 9	ST9	-	ST 11	ST 11

10.2 Appendix B

HPPs are one of the sources which bring SSL_{fine} into and out of the reservoir. There is one turbidimeter at the outlet of HPP Sils which measures the SSC_{fine}. No monitoring of the *SSC* in the water released by the HPPs Tiefencastel and Rothenbrunnen exists. Therefore, the SSC_{fine} time series of these two HPPs was assumed to be equal to that of the HPP Sils (Müller-Hagmann, 2017). The annual average *SSC* at the HPP Sils is around 25.9 ± 13% mg/l. This average value was used to estimate the SSL_{fine} at the HPPs Tiefencastel and Rothenbrunnen.

The fine suspended sediment is released by different dam outlet structures, i.e., the bottom outlet, the spillway, and the environmental flow release. The sediment load of the environmental flow is insignificant and therefore was neglected (Müller-Hagmann, 2017). No *SSC* and turbidity data from the spillway and the bottom outlet were available. The *SSC* time series of the bottom outlet and the spillway were assumed to be similar to the *SSC* time series in the Albula with a reduced amplitude due to the desilting effect of the Solis Reservoir. A linear dilution profile over the water depth was assumed at the dam (Figure 40). The desilting factor *DF* at the HPP intakes (z = 35 m above bottom outlet) defined as the ratio between fine suspended sediment concentration in the Albula and the HPPs (*DF* =

SSC_{Albula} / $SSC_{HPPSils}$) was 9.3 based on turbidity measurements. A desilting factor of 6 was assumed at the bottom outlet (z = 1.2 m) based on the observations at the Mapragg Reservoir, located 30 km north of Solis in Canton St. Gallen and exhibiting a similar shape, size, depth and capacity of 5.3 × 10^6 m^3 (Müller and De Cesare, 2009). Using these two points, a linear fit resulted in $DF = 0.1z + 5.9$ (Müller-Hagmann, 2017; Figure 40). A desilting of DF = 10 was obtained for the spillway (z = 42 m) using this relationship. The SSC times series in the bottom outlet and the spillway were calculated by applying these desilting factors to the SSC time series in the Albula.

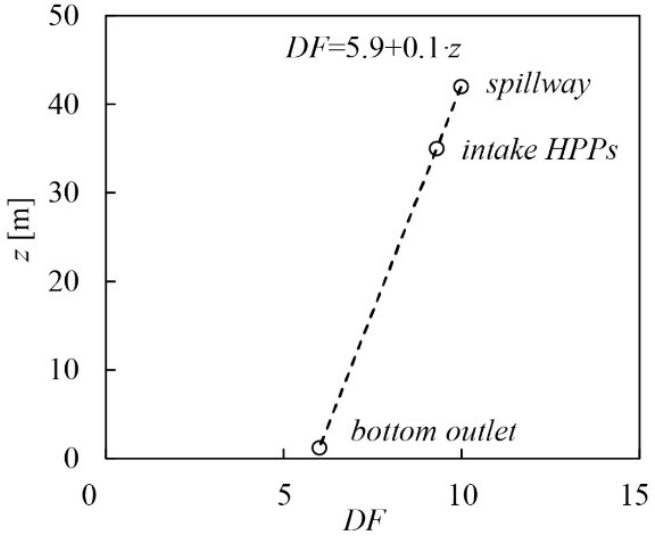

Figure 40: Desilting profile over depth at Solis dam (Müller-Hagmann, 2017).

10.3 Appendix C

Measured velocity fields in different cross sections are presented in Figure 41 to Figure 49, where the views are always in downstream direction.

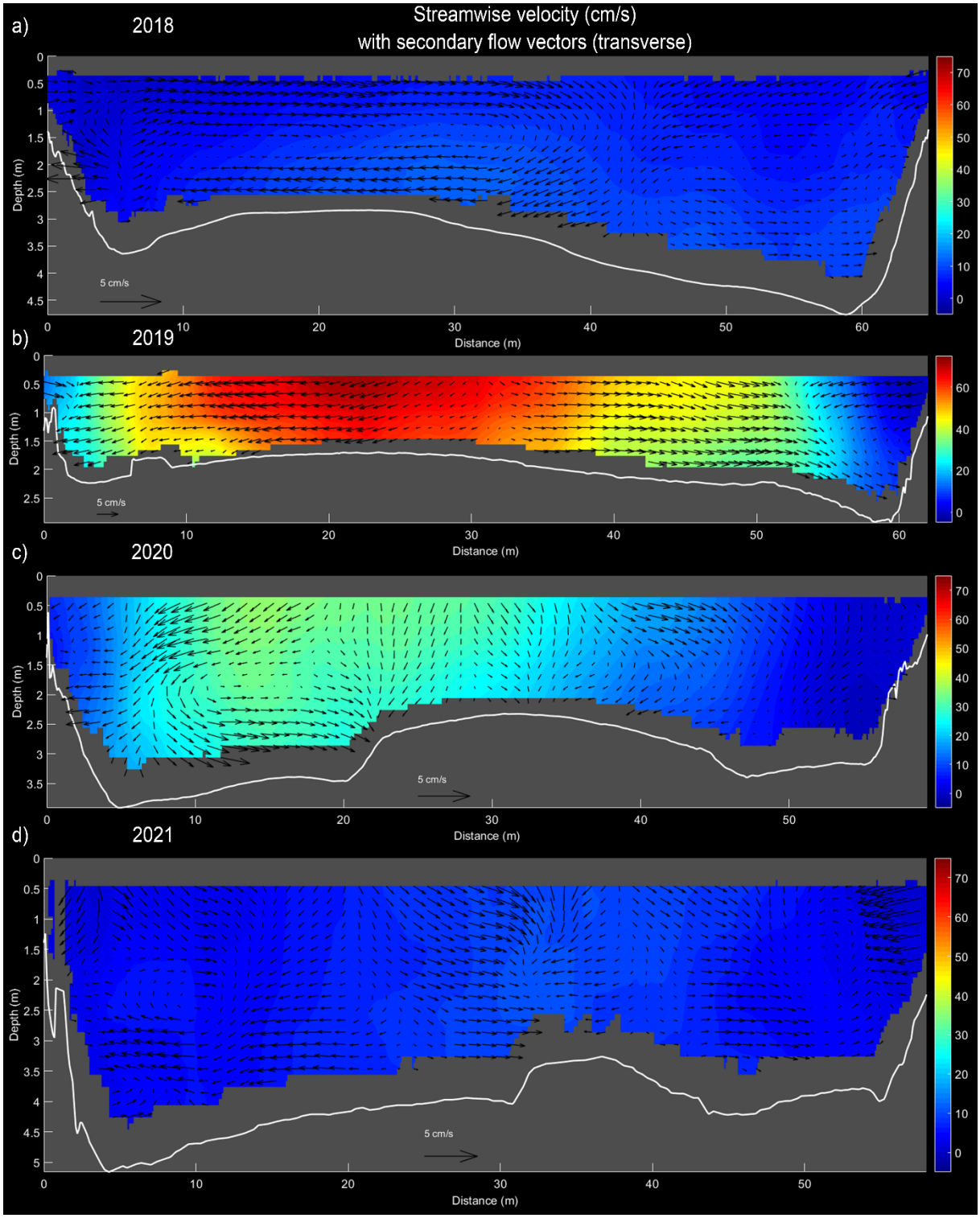

Figure 41: Velocity field in location B. The background is streamwise velocity and the vectors show transverse and vertical secondary currents.

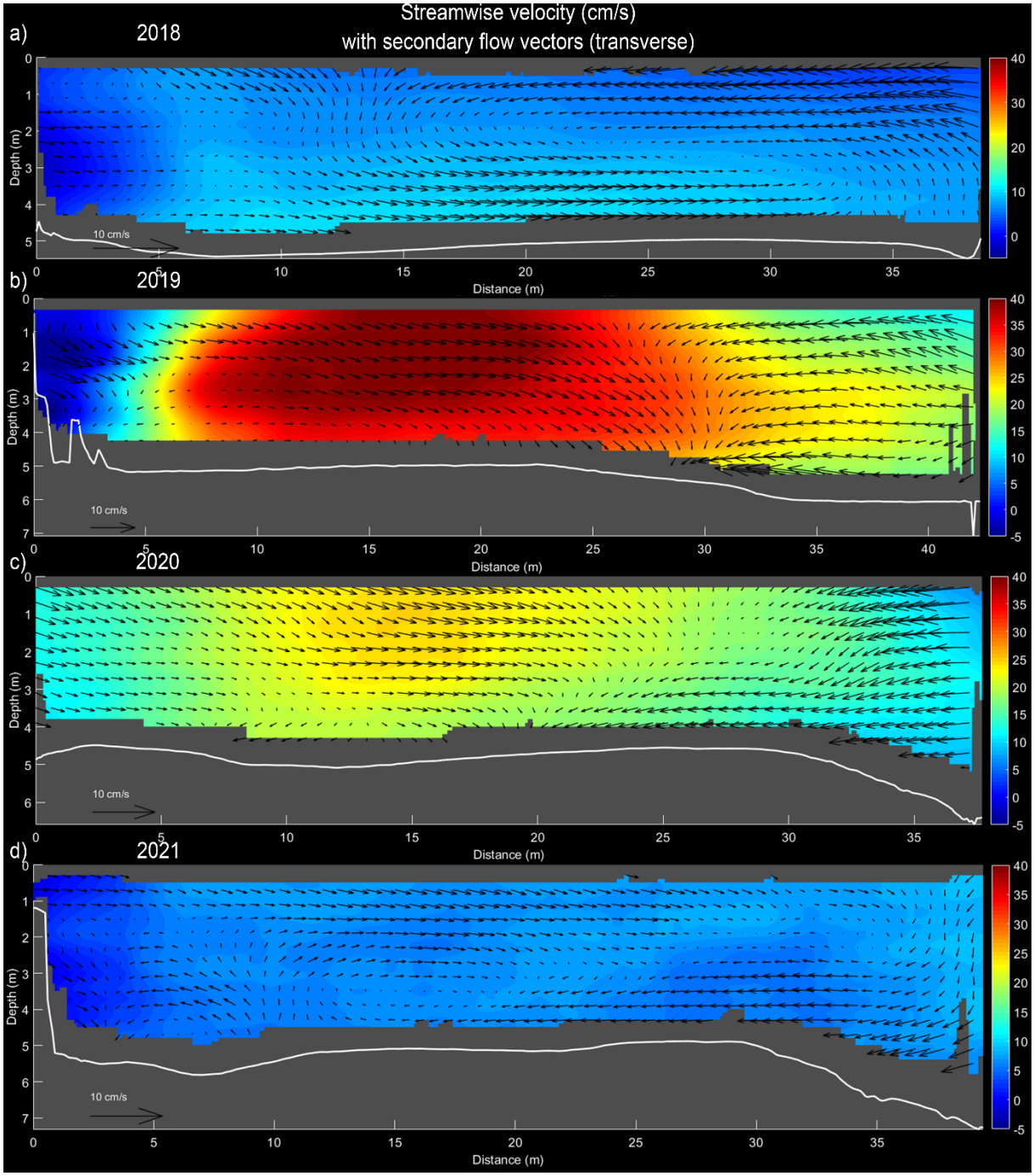

Figure 42: Velocity field in location C. The background is streamwise velocity and the vectors show transverse and vertical secondary currents.

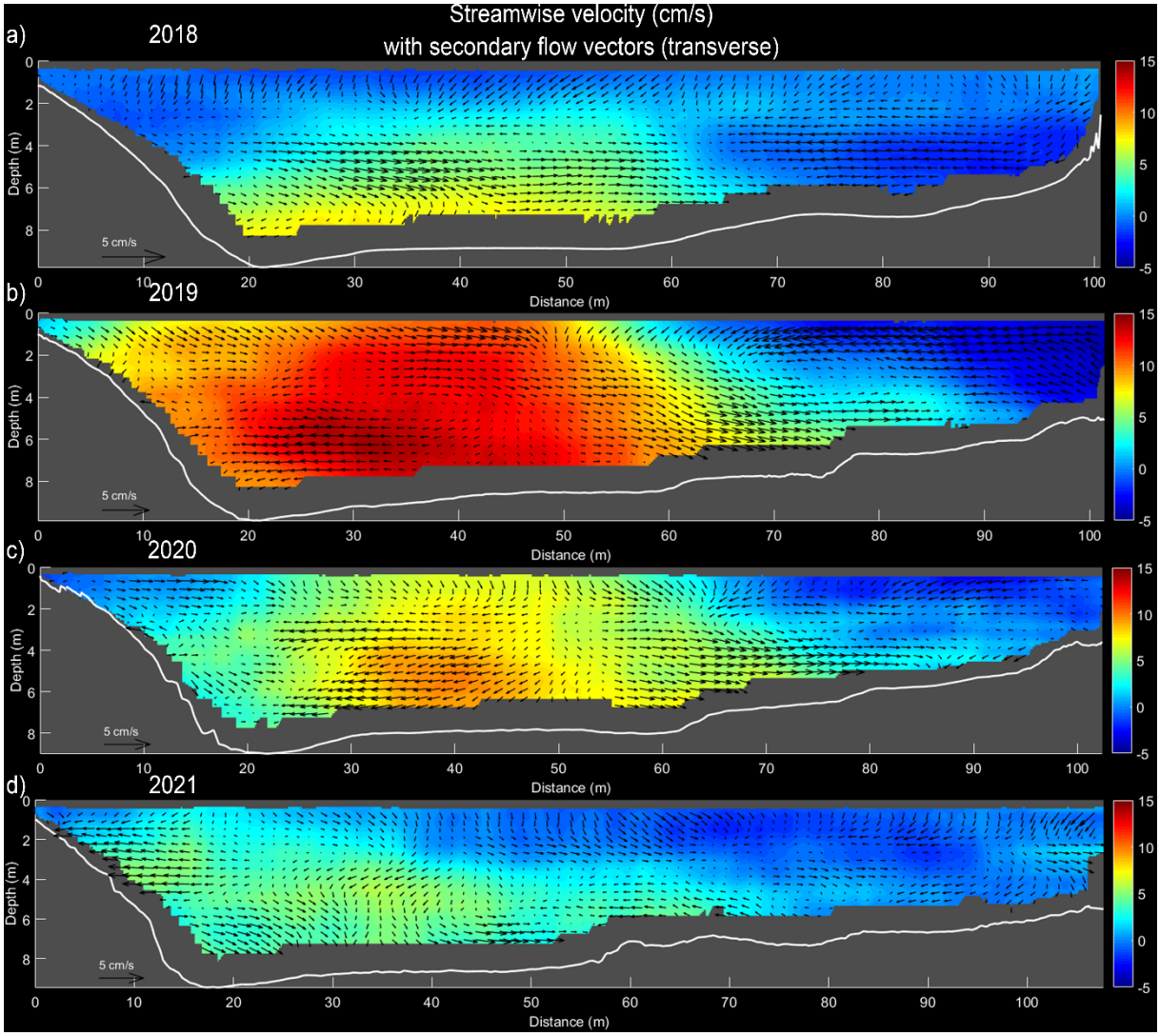

Figure 43: Velocity field in location E. The background is streamwise velocity and the vectors show transverse and vertical secondary currents.

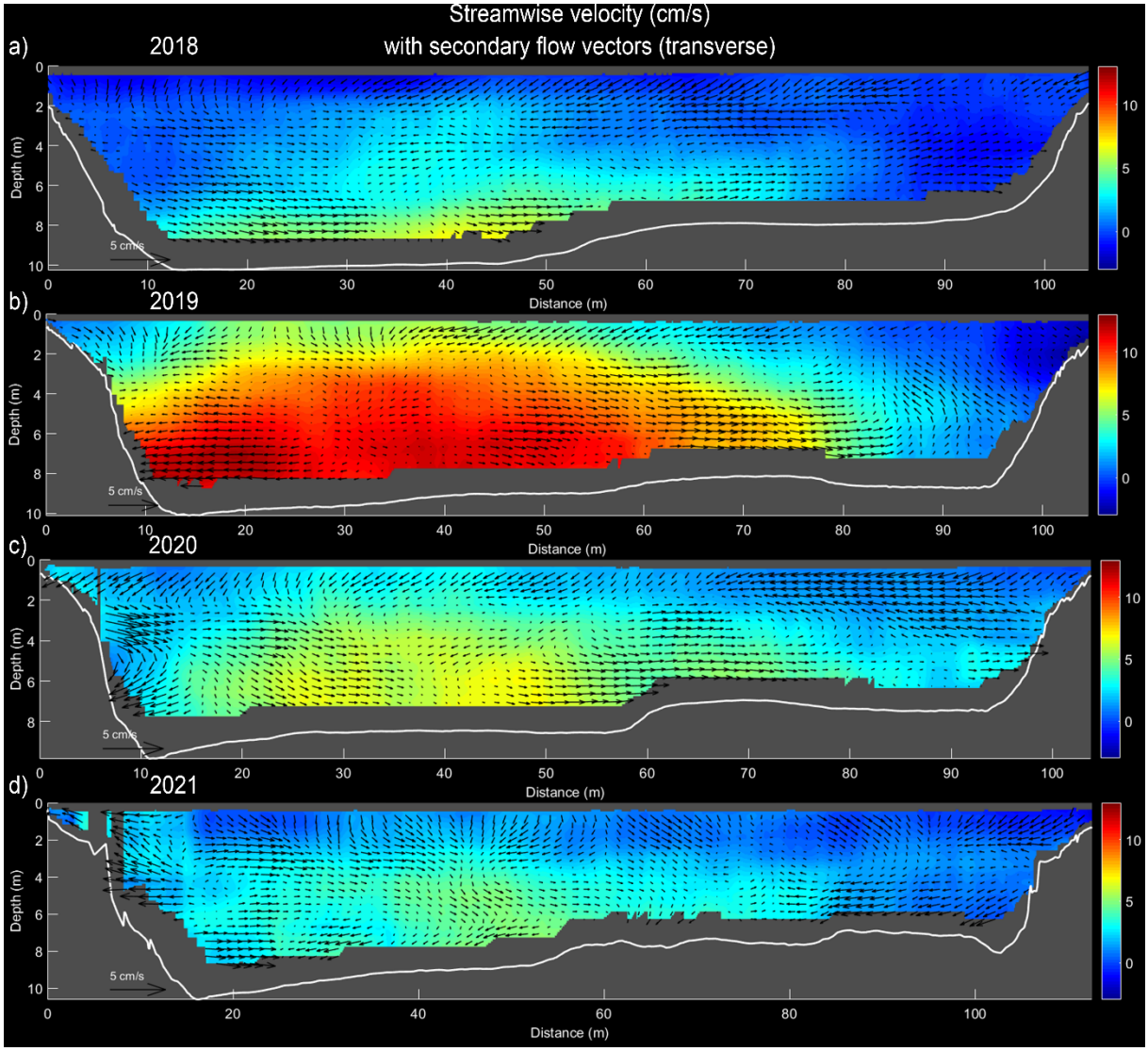

Figure 44: Velocity field in location F. The background is streamwise velocity and the vectors show transverse and vertical secondary currents.

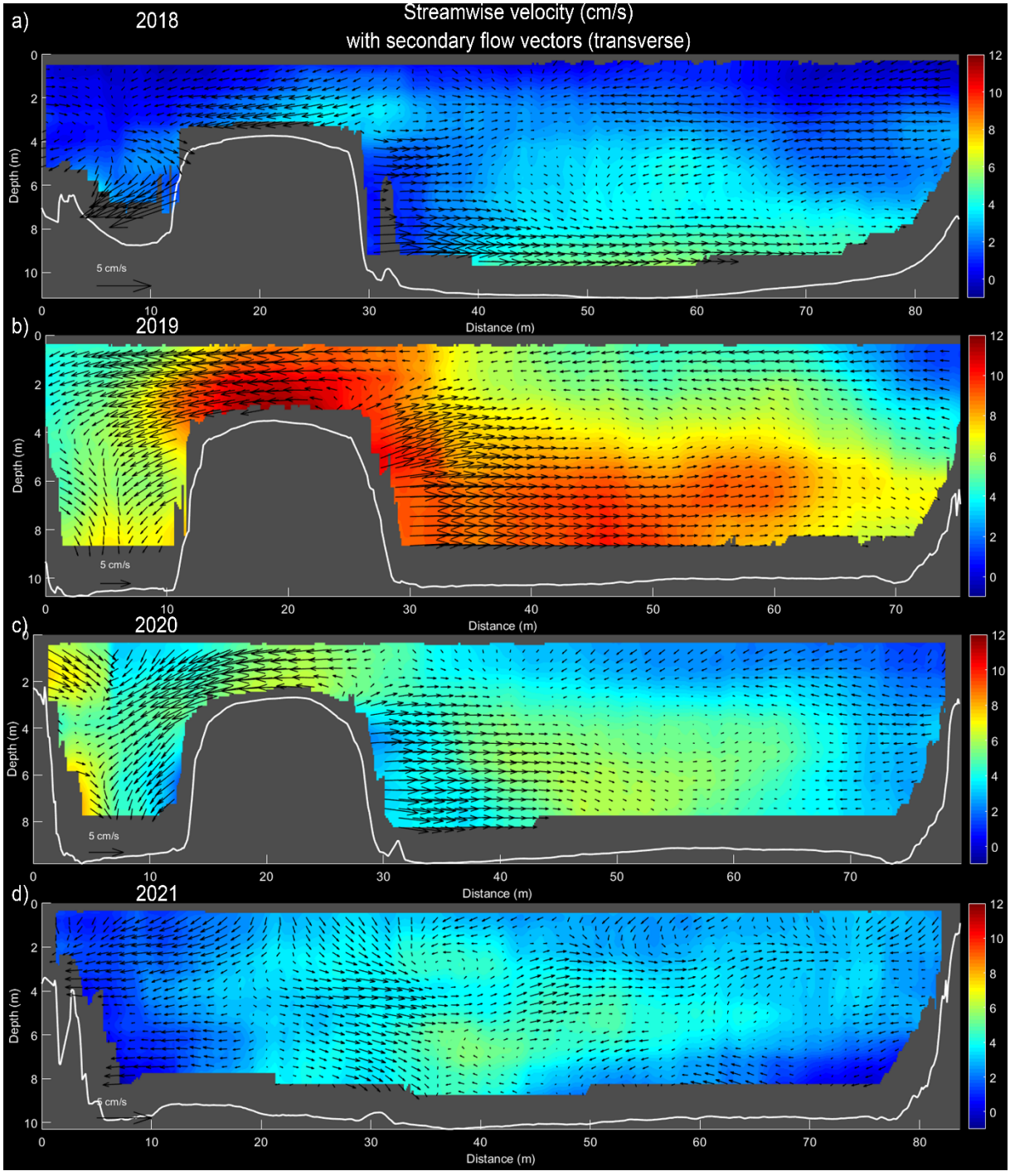

Figure 45: Velocity field in location G. The background is streamwise velocity and the vectors show transverse and vertical secondary currents.

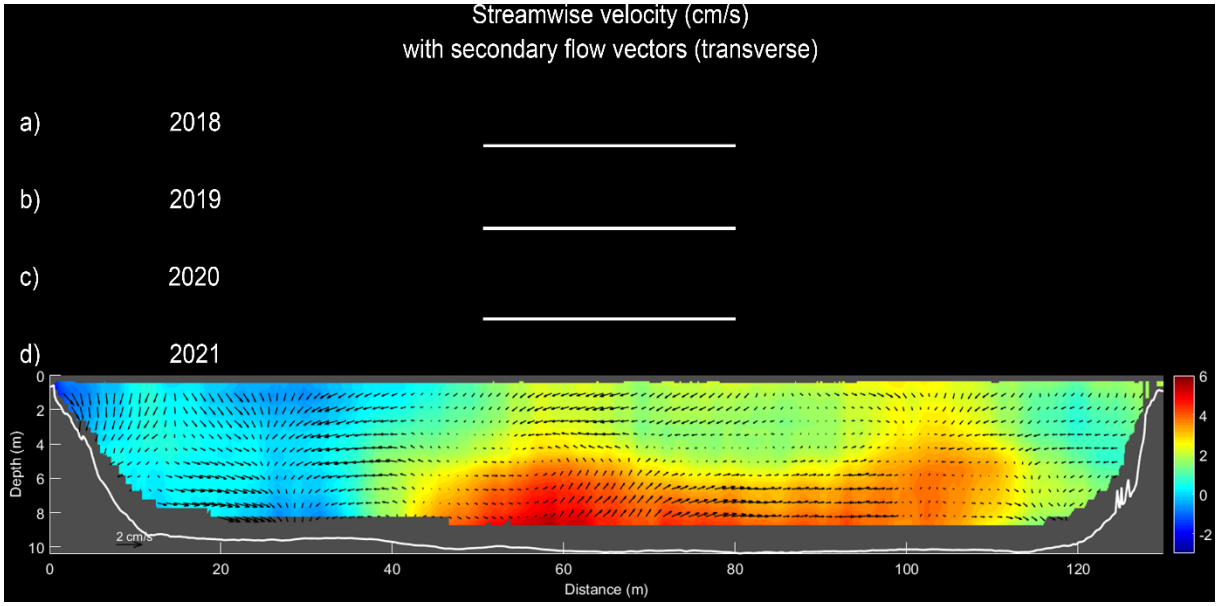

Figure 46: Velocity field in location H. The background is streamwise velocity and the vectors show transverse and vertical secondary currents. No cross section was measured in 2018, 2019, and 2020.

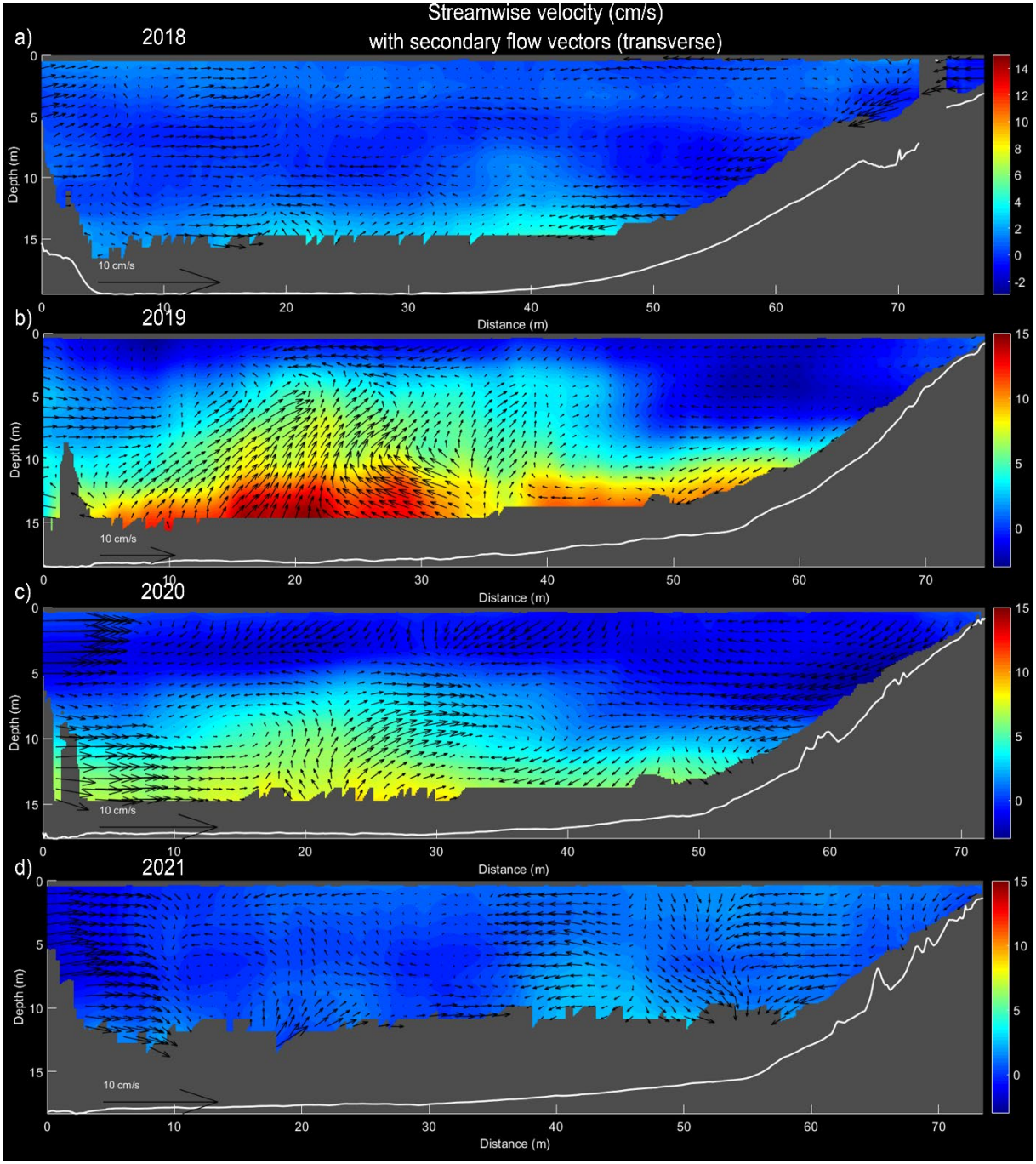

Figure 47: Velocity field in location I. The background is streamwise velocity and the vectors show transverse and vertical secondary currents.

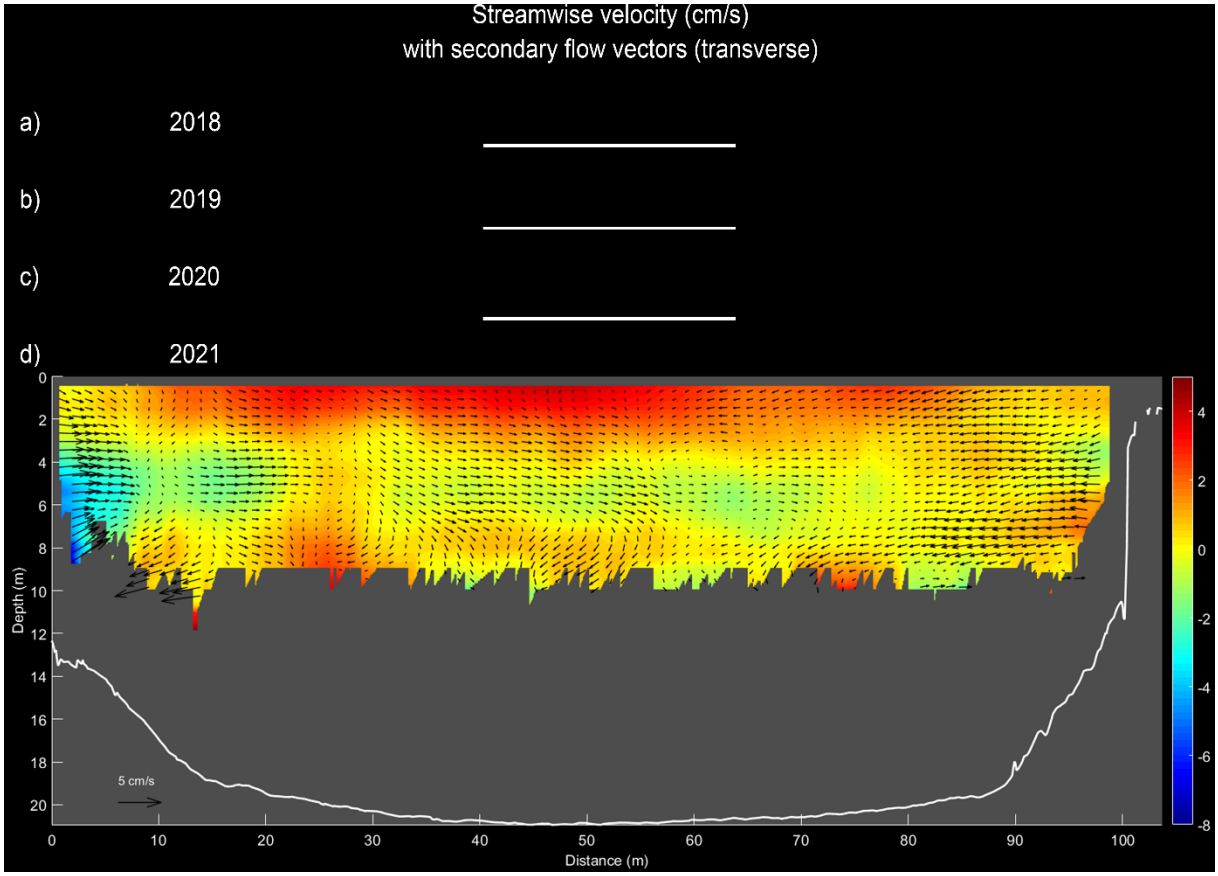

Figure 48: Velocity field in location J. The background is streamwise velocity and the vectors show transverse and vertical secondary currents. No cross section was measured in 2018, 2019, and 2020.

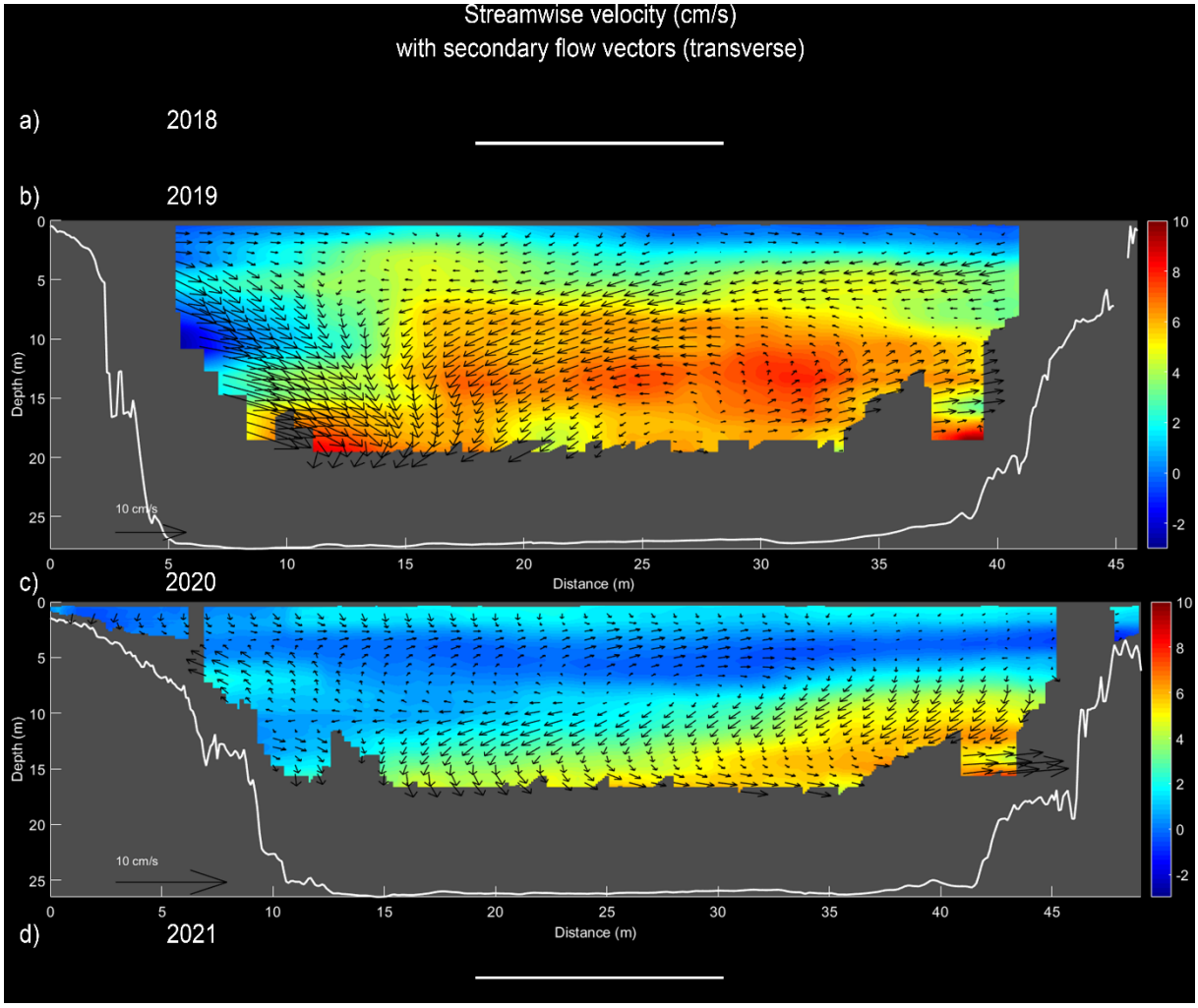

Figure 49: Velocity field in location K. The background is streamwise velocity and the vectors show transverse and vertical secondary currents. No cross section was measured in 2018 and 2021.

10.4 Appendix D

There were no measurements from the SPGS in the Albula River neither in June, August, and September 2019, nor in January, February, March, and April 2020. The missing data from the Albula SPGS are estimated based on the relationship between the river discharge and the bedload transport rate given by Rickenmann et al. (2020). Figure 50 shows the discharge fluctuations during the days when no SPGS data are available. The black line in this figure is the average discharge used to estimate the SPGS values. Using the discharge and Figure 51, the bedload transport in estimated. Table 15 shows the average discharge on missing dates and the corresponding bedload transport rate based on Figure 51.

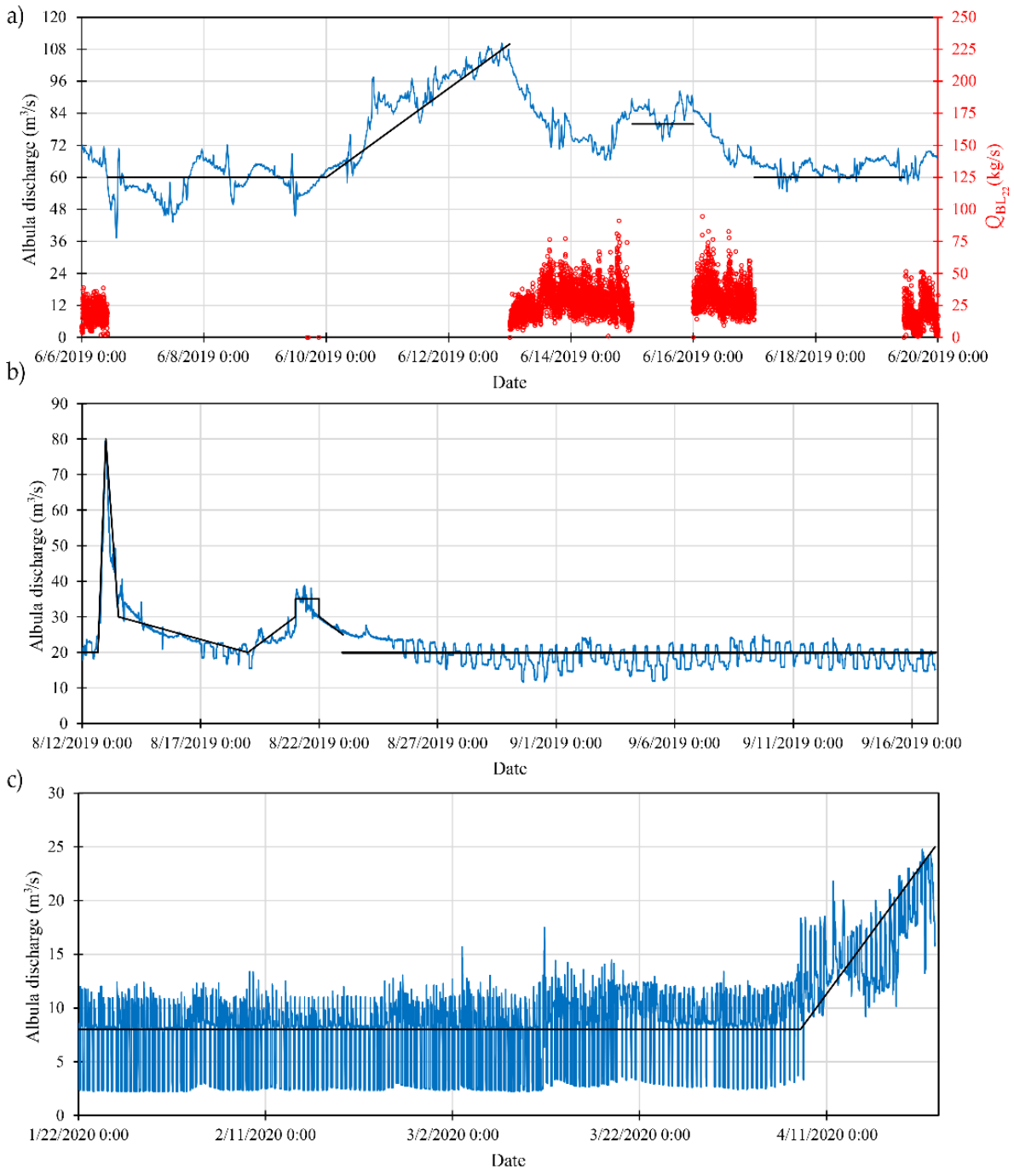

Figure 50: Albula discharge fluctuatuations during the time when the SPGS did not record data in a) June 2019, b) August and September 2019, and c) January, February, March, and April 2020. The red dots are SPGS measurements, the blue line is instantanous discharge at intervals of 15 minute, and the black line is average discharge.

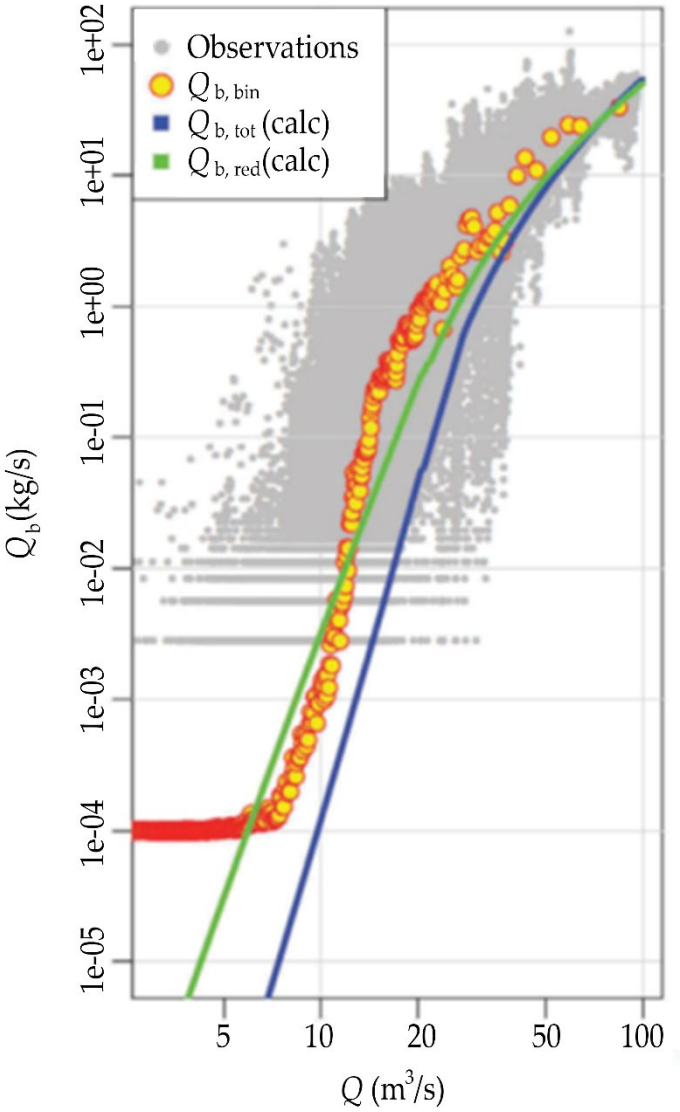

Figure 51: Comparison of observed bedload transport rates Q_b (small grey dots) from the Albula SPGS, as inferred from the geophone measurements, with bedload transport calculations, $Q_{b,\,tot}$, using total shear stress (blue line), and $Q_{b,\,red}$, using effective shear stress (green line), shown as a function of discharge Q. The $Q_{b,\,bin}$ values (yellow dots) are binned geometric mean values of the observations, where values of Q_b = 0 were replaced with Q_b = 1e-04 kg/s. (Rickenmann et al., 2020).

Table 15: Average discharge on missing dates and corresponding bedload transport rate.

Date	Duration of missing data (minutes)	Average discharge (m^3/s)	Corresponding bedload transport rate (kg/s)
06.06.2019 10:06 – 10.06.2019 0:00	5’154	60	20
10.06.2019 0:00 – 13.06.2019 0:00	4’320	60 - 110	20 - 100
15.06.2019 0:00 – 16.06.2019 0:00	1’440	80	25
12.08.2019 0:00 – 12.08.2019 16:00	960	20	0.05
12.08.2019 16:00 – 13.08.2019 0:00	480	20 - 80	0.05 – 25
13.08.2019 0:00 – 13.08.2019 13:00	780	80 - 30	25 – 3
13.08.2019 13:00 – 19.08.2019 0:00	7’860	30 - 20	3 – 0.05
19.08.2019 0:00 – 21.08.2019 0:00	2’880	20 - 30	0.05 – 3
21.08.2019 0:00 – 22.08.2019 0:00	1’440	35	5
22.08.2019 0:00 – 23.08.2019 0:00	1’440	25	0.06
23.08.2019 0:00 – 17.09.2019 0:00	36’000	20	0.05
22.01.2020 0:00 – 08.04.2020 5:00	141’420	8	0
08.04.2020 5:00 – 22.04.2020 14:25	50’965	8 - 25	0 – 0.06

10.5 Appendix E

The bed material was collected from different locations along the reservoir, at each measurement campaign. Figure 52 shows the sampled sediments in 2018. The name of the locations is based on Table 14. Larger gravels existed in upstream cross sections, cross sections 1 to 4, along the first 1’200 m of the reservoir, showing that these large particles were transported and deposited until this location. From there on, until cross section 7, which is upstream of the guiding wall close to the SBT inlet, small particles were deposited in the bed. In cross section 7 larger particles in the gravel size range were deposited on the bed. These particles were carried by the flow from previous floods and could not pass the guiding wall, so that they were deposited at this location, which shows the importance of the guiding wall to block large particles transported to the zone 3 region near the dam.

Figure 52: Bed material collected in October 2018.

The water flowing into the reservoir carries suspended sediments. To obtain *SSC*, samples were collected along the reservoir at different water depths. Due to small discharges to the reservoir and the dilution of particles, the measured *SSC*s were very low. Figure 53a shows the collected bottle samples from different locations as well as depths in 2018. Figure 53b shows that the concentration of suspended sediments is very low.

Figure 53: a) Bottle samples collected along the reservoir at different depths and b) very low *SSC* in one bottle because of dilution effect in 2018.

10.6 Appendix F

The *SSC* was measured using LISST in the 2021 field campaign. The vertical distribution of *SSC* at each location is presented in Figure 54.

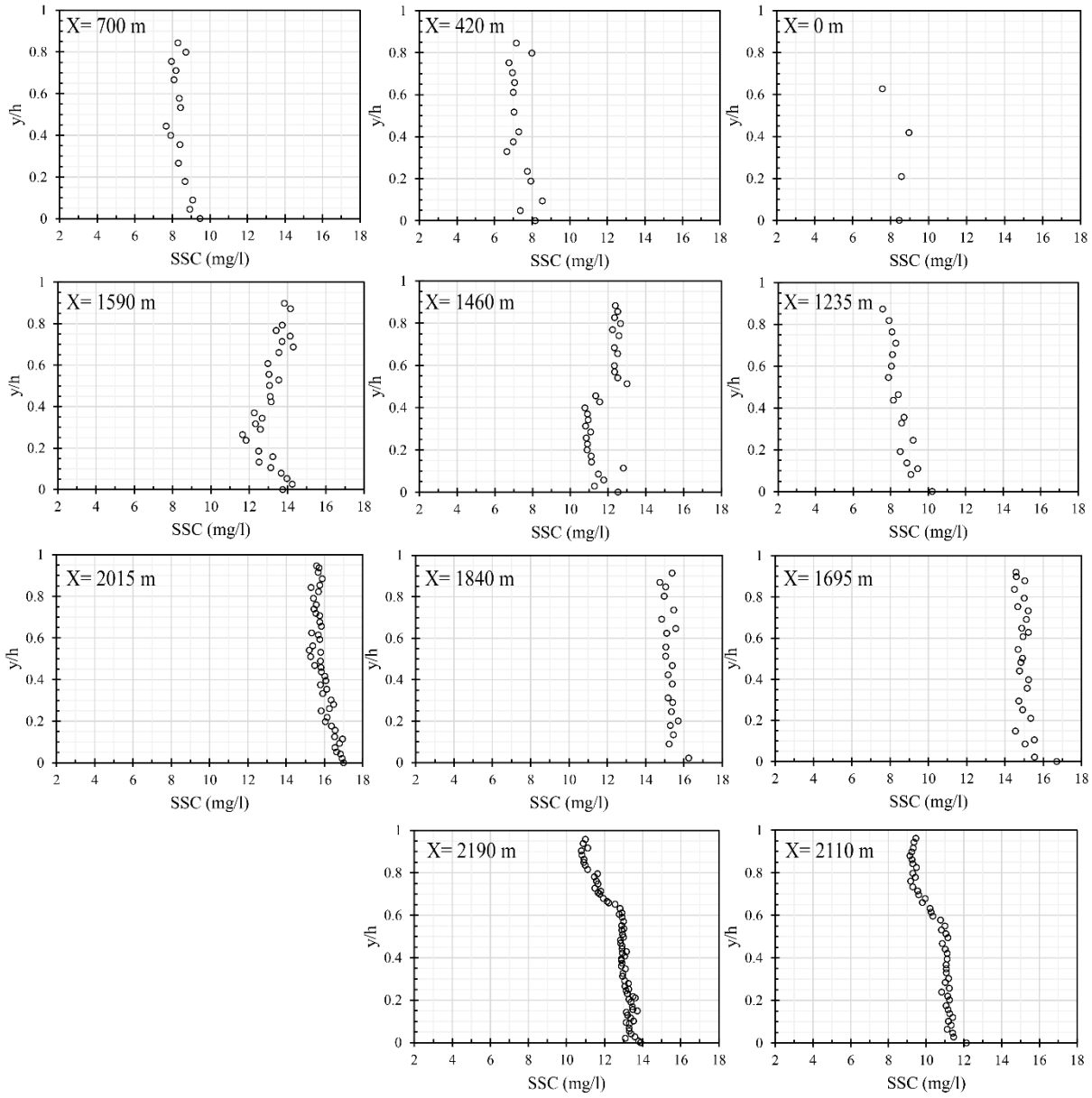

Figure 54: *SSC* profiles along the Solis reservoir measured in 2021 using LISST.